Fabrication and Structural Studies of Sequentially Adsorbed Polyelectrolyte Multilayers

Jeffery W. Baur

B. A. Physics/Chemistry Illinois Wesleyan University (1990)
B. S. Materials Engineering, University of Cincinnati (1992)

Submitted to the Department of Materials Science and Engineering and the Program in Polymer Science and Technology in partial fulfillment of the requirements for the degree of

Doctor of Philosophy

at the

Massachusetts Institute of Technology

June 1997

Signature of Author _____
Department of Materials Science and Engineering
May 2, 1997

Certified by _____
Professor Michael F. Rubner
TDK Professor of Polymer Science
Thesis Supervisor
Director, Program in Polymer Science and Technology

Accepted by _____
Professor Linn Hobbs
John F. Elliot Professor of Materials
Chair, Departmental Committee on Graduate Students

Fabrication and Structural Studies of Sequentially Adsorbed Polyelectrolyte Multilayers

Jeffery W. Baur

Submitted to the Department of Materials Science and Engineering and the Program in Polymer Science and Technology on May 2, 1997 in partial fulfillment of the requirements for the degree of Doctor of Philosophy in Polymer Science.

Abstract

This thesis has sought to understand the process of sequential adsorption of polyelectrolytes in terms of the effects that processing parameters have on the resultant film structure, to extend this technique's capability to include novel materials which have not previously been assembled, and to use sequentially adsorbed films in potentially useful applications such as light emitting devices (LEDs). Fundamental studies on the influence that polyelectrolyte molecular weight, solution ionic strength, and solution pH have on the resultant film structure were undertaken for films of poly(allylamine hydrochloride) (PAH) sequentially adsorbed films with either sulfonated polystyrene (SPS) or poly(methacrylic acid) (PMA). The molecular weight and the solution ionic strength of the SPS was varied for the SPS/PAH films. It was shown that under low ionic strength conditions ($\leq$ 0.1M NaCl) the bilayer thickness is independent of molecular weight, but that under high ionic strength conditions ($\geq$1.0 M NaCl) the bilayer thickness is significantly dependent on the molecular weight of the SPS. This was attributed to the transition of adsorbed molecules from relatively flat conformations at low ionic strengths to more loopy conformations at high ionic strengths. Analysis of the bilayer thickness for a given molecular weight of SPS as a function of the SPS solution ionic strength showed that for molecular weights of greater than 35K and ionic strengths of $\leq$1.0 M NaCl, the bilayer thickness scales with the square root of the ionic strength as predicted from the adsorption theory derived for a single adsorbed layer.

Analysis of PMA/PAH films assembled under varying pH conditions for solutions of both PMA and PAH showed an increase in the PAH layer thickness with an increase in the pH of the PAH solution due to the increase in surface charge of the previously adsorbed PMA layer, a decrease in PMA layer thickness with an increase in the solution pH of the PMA due to increased segment-segment repulsion, and an increase in PMA layer thickness with the thickness of the underlying PAH layer which was attributed to the presence of a contact-ion pair mechanism of sequential adsorption. Sessile drop contact angle measurements of these films taken as a function of the number of layers adsorbed indicated that at low number of layers ($\leq$ 10 adsorbed layers) the level of penetration of material from underlying layers to the outermost surface is dependent on the thickness of the last layered adsorbed. At higher numbers of layers ($\geq$ 20 adsorbed layers), the outermost surface layers of all of the films became more heavily penetrated by underlying layers. However, methylene blue adsorption studies indicated that the oscillation in surface charge with the adsorption of oppositely charged polymer molecules was maintained. This increase in layer mixing is believed to be linked to the increase in

surface roughness with increasing number of bilayers which was observed by SAXR. Cross-sectional TEM images of heterostructures consisting of blocks of PMA/PAH bilayers alternating with bilayers of ruthenium containing molecules also showed an increase in surface roughness with increasing number of bilayers in addition to a distinct layering of the assembled bilayer blocks.

Förster energy transfer studies between layers of derivatized poly(p-phenylene) (dPPP) and PPV separated by varying number of spacer bilayers of PMA/PAH, SPS/PAH, and poly(acrylic acid) (PAA) and PAH lead to estimations for the level of penetration into the spacer bilayers of between 15-53Å for the PMA/PAH spacer layers, over 50Å for the SPS/PAH spacer bilayers, and less than 80Å for the PAA/PAH spacer bilayers. Additionally, the technique of sequential adsorption was extended to include polyimide precursor which could be subsequently converted to the polyimide using either chemical or thermal means. Sequentially adsorbed films of dPPP with a variety of polycations were also investigated for use in blue light emitting devices with the overall result that the devices were dominated by the transport of holes and that further optimization is required to achieve balanced charge injection.

Thesis Advisor: Professor Michael F. Rubner
Title: TDK Professor of Polymer Science

Acknowledgments

I would like to thank first and foremost my wife, Sandy Baur, for her unwavering support of my academic and professional pursuits and to my children, Emily Baur and Adam Baur, for providing me with much needed breaks from the writing of this thesis. I would especially like to thank my thesis advisor and mentor, Prof. Michael Rubner, for his endless energy, constant encouragement, and helpful advice. I would also like to thank the other members of my Thesis Committee, Prof. Edwin L. Thomas and Prof. Kirk D. Kolenbrander, for their time and constructive input.

To both past and present Rubner Research Group members including Mike Durstock, Erika Abbas, Erik Handy, Ken Zemach, Dongsik Yoo, Bill Stockton, Augustine Fou, Marysilvia Ferreira, Cormac Lyons, Hedi Mattoussi, Bashir Dabbousi, Osamu Onitsuka, Pascal Besson, Anand Ragunathan, Mary Hamilton, Doug Howie, Wade Samec, and Sandy Schaefer-Ung, I would like to extend a sincere thank you for all of your support, friendship, and assistance during the past several years. Thanks also goes out to people outside of our group for collaborative work: Dr. Greg Kellog and Mike Fasolka for their help with SAXR measurements; Len Radzilowski for the excellent cross-sectional TEM images; John Martin, Libby Shaw, and Tim McClure for the help with the equipment in the Central Facilities.

I am extremely thankful to the United States Air Force's Palace Knight Program for funding my graduate studies and to my program mentor, Lisa Denny, who made sure the program actually worked. I thank my parents. Robert Baur and Sandy Baur-Orlando, who made sacrifices to provide me, as well as my 12 other siblings, with an excellent parochial education which helped lay the groundwork for my collegiate career.

Thanks also to the MIT Collegiate Rowing Program which provided a much needed retreat from the lab (college weigh 'nuf!).

Table of Contents

List of Figures

Chapter 1

Chapter 2

Chapter 3

Chapter 4

Chapter 5

List of Tables

CHAPTER 1. - INTRODUCTION AND BACKGROUND

1.1 General Background

The typical person cannot go through a day without coming in repeated contact with polymeric materials in a variety of shapes and sizes. Polymeric materials in thin films are one of the most common forms encountered and can be found on everything from computer circuit boards to our hair. However, some of the advanced applications of polymeric thin films which have been of intense research interest within the last decade make use of novel properties such as electrical conductivity, non-linear optical activity, and electroluminescence of specific polymers to make potentially useful devices. Sensors, transducers, optical switches, photovoltaics, and light emitting devices (LEDs) based on these films not only rely upon the electroactive properties of the specific polymer used, but also upon the ability of the device to be optimized by a desired film structure. Optimization typically includes creating arrays of molecules which have cooperative properties which are either different or better than what can be achieved without molecular manipulation. While biological polymers such as proteins optimize by self-organization into arrays of biological functionality which ultimately lead to living organisms, desirable arrays can also be achieved for synthetic polymers through such approaches as blending; phase separation of homopolymers, block copolymers, and/or segmented copolymers; photolithographic patterning; and sequential layering. In the past, sequential layering was achieved with multi-step processes such as spin-casting multiple layers of polymer from solution, undergoing a series of chemical reactions at a film surface (sequential chemisorption), and transferring a series of ordered organic monolayers from a water-air interface to a substrate (Langmuir-Blodgett film assembly). However, recently, a film fabrication technique known as layer-by-layer self-assembly, which is based on the sequential physisorption of positively and negatively charged molecules, has been shown to deliver high quality thin films of controllable thickness and to offer many advantages over other sequential layering techniques [1]. This thesis seeks to understand the relationship between processing conditions, film structure, and LED device operation of sequentially adsorbed polymeric thin films.

In order to provide a proper theoretical foundation in which to understand these relationships, a review of the polyelectrolyte solution properties and their subsequent adsorption to a surface will be made. To put this thesis' contributions in perspective with the field of sequentially adsorbed polymeric films, a brief review of the current field of sequential physisorption will also be made within this chapter.

1.2 Polyelectrolytes in Solution

A polyelectrolyte can be simply described as a polymer chain with ionized groups. However, it is these charged groups which often complicate the theory in regard to the chain's behavior in solution and the nature of their adsorption to a substrate. Excluding specific segment-segment interactions such as hydrogen bonding, the behavior of polyelectrolytes can be considered to be the supposition of non-charged polymer chain behavior and electrostatic interactions [2]. The conformations that a non-charged linear polymer adopts in solution are primarily dependent on the stiffness of the repeat units, the total length of the chain, and the interaction of the chain with the solvent. The root-mean-square distance of segments from the center of mass of a conformation of such an interacting polymer molecule, which is defined as the radius of gyration R_g, can then be written as

$$R_g = \frac{\alpha' q_o^{1/2} N^{1/2} \ell^{1/2}}{\sqrt{3}} \qquad (1.2.1)$$

where ℓ is the length of the polymer repeat segment, N is the number of segments in the polymer molecule (chain contour length = ℓ *N), q_o is the characteristic length along the chain over which the directional correlation between the segments decays to zero (also known as the persistence length), and α' is an expansion factor which takes into account the finite volume of the segments and the solvent-segment interaction. The expansion factor can be expressed as

$$\left(\alpha'\right)^5 - \left(\alpha'\right)^3 = q_o^{-3/2}(1-2\chi)N^{1/2}(3\ell)^{3/2} \qquad (1.2.2)$$

where χ is the energy change associated with the transfer of segment from pure polymer to pure solvent in units of kT [3]. The effects of having ionizable groups on the polymer molecule can then be expressed by rewriting the total persistence length (q_t) as the sum of the non-charged persistence length (q_o) and the electrostatic persistence length (q_e), given as [4]

$$q_t = q_o + q_e \qquad (1.2.3)$$

For a chain with the same type of charge along the polymer backbone, the electrostatic persistence length will be a function of the amount of repulsion between charged polymer segments. The amount of repulsion will, in turn, be dependent on the amount and location of charge along the polymer backbone as well as the amount of small ions present that can screen such charges. The charge along the polymer backbone can be expressed in terms of the distance between charges on a polymer chain (ℓ_e). The screening of a electrostatic potential by small ions can be quantified in terms of a characteristic length of decay known as the Debye length (κ^{-1}) which can be written as

$$\kappa^2 = \frac{2c_s N_A z^2 e^2}{\varepsilon kT} \qquad (1.2.4)$$

where c_s is the concentration of counterions in the equilibrium solution, N_A is Avogadro's number, z is their valence, e is the elementary charge, ε is the dielectric permittivity, k is the Boltzmann constant and T is the absolute temperature. While expressions for the equation relating the electrostatic potential and this decay parameter has been solved for flat geometries,[5,6,7] analytical solutions based on the cylindrical geometry used for polyelectrolytes suffer from the complication of divergence of the potential (very strong

non-linear screening effects at short distances) near the cylinder axis. Instead, two limiting cases of screening are outlined - one at high charge density and one at relatively low charge density [8,9,10,11]. In the case of a highly charged polymer where ℓ_e is small, counterions can be tightly held to a region close to the polymer backbone due to the high electrostatic potential. This counterion condensation decreases the effective charge along the backbone and increases the effective distance between charges (ℓ_{eff}). The amount of charge density required to cause counterion condensation is expressed in terms of the Bjerrum length (ℓ_B) which is the distance between two monovalent ions that have a Coulombic interaction energy just equal to kT and can be expressed as

$$\ell_B = \frac{e^2}{4\pi\varepsilon kT} \tag{1.2.5}$$

In water at room temperature, ℓ_B is approximately 7Å, which means that polyions having monovalently charged groups spaced closer together than 7Å along the polymer backbone should undergo counterion condensation. Thus, in the case of a highly charged polymer molecules, the effective distance between monovalent charges becomes the Bjerrum length ($\ell_{eff} = z * \ell_B$). In the case of weakly charged polymer molecules, counterion condensation does not occur and the real charge density is equal to the effective charge density ($\ell_{eff} = \ell_e$). While the transition between these two states is denoted here as being very sharp, experimentally the transition has been determined to be more gradual [12]. Additionally, the detailed nature of this counterion binding has been researched further in recent years to include both the non-specific binding denoted here and specific binding of certain counterions onto certain polyions [13]. However, using the simplified expression for non-specific binding, the electrostatic persistence length in the dilute regime can then be expressed as

$$q_e = \frac{\ell_B}{4}\left(l_{eff}\kappa\right)^{-2}. \tag{1.2.6}$$

Furthermore, when the non-electrostatic contribution to the excluded volume is small compared with the electrostatic contribution, the radius of gyration can then be expressed as

$$R_g = \frac{\alpha_e}{\sqrt{3}} q_t^{1/2} N^{1/2} \ell^{1/2} \tag{1.2.7}$$

where

$$(\alpha_e)^5 - (\alpha_e)^3 = q_t^{-3/5} \kappa^{-1} N^{1/2} \ell^{1/2}. \tag{1.2.8}$$

The above equations are derived for the dilute solution in which polymer molecules are largely isolated from one another. The transition from the dilute solution regime to the semi-dilute regime in which the molecules interact is typically discussed in terms of a critical polymer concentration c_p^* (expressed here in moles of monomer per liter) which can be expressed as

$$c_p^* \approx \left(\ell^3 N^2 N_A\right)^{-1} \tag{1.2.9}$$

in the upper limit of a highly charged polyelectrolyte in a low ionic strength solution. Above this concentration, segments of different chains interact and the conformational behavior become more concentration dependent and more difficult to model. It should be noted that the majority of the polyelectrolyte solutions used throughout this thesis are calculated to be within the dilute regime with the possible exceptions of very high molecular weight sulfonated polystyrene and precursor poly(phenylene vinylene) with concentrations above 0.001M. Thus, the conformation changes with solution and molecular parameters expressed in the preceding equations are considered to be good analogs of the solution behavior of most of the polyelectrolyte solutions used throughout

this thesis. However, because of the many simplifying assumptions made (the largest of which concerns the nature of the electrostatic screening [14]), the theoretically predicted radius of gyration values do not always strictly agree with experimental values. Yet, the trends predicted with variations in polymer charge density and ionic strength with respect to a reference situation usually agree well with experimental observations and can still be used as a guide for the understanding and manipulation of conformations in solution and in an adsorbed film [2]. The solution properties of poly(methacrylic acid) (PMA) which is known to undergo a transition from an extended coil to a globular form at acidic pH due to hydrophobic interactions may be the one exception to this statement [15].

An example of the manipulation of solution conformations using an accessible solution variable can be seen in the case of the electrostatic screening of the repulsive interaction between segments of a highly charged polyelectrolyte with added salt as illustrated in Figure 1.2.1. An example of such a highly charged polyelectrolyte is sulfonated polystyrene (SPS). One can expect that at very high ionic strength, κ^{-2}, q_e, and the electrostatic contribution to the excluded volume will all be small. This will, in turn, make the polymer conformations more compact (as $q_t \sim q_o$) and better described by non-charged polymer radius of gyration of Equation 1.2.A.1 which has only a small dependence on the salt concentration through χ as denoted in Figure 1.2.1 (case a). In fact, at very high ionic strengths (4.17 M NaCl in the case of SPS), the polymer molecule can reach the theta point where it will assume a conformation which can be described by simple gaussian statistics in which neither the electrostatic nor the non-charged expansion factor needs to be taken into account (χ = 0.5, $\alpha'=\alpha_e=1$) [16]. At intermediate salt concentrations (c_s), the polymer molecules are more extended as electrostatic contributions start to dominate. Both κ^{-1} and q_t will increase with decreasing salt concentration to give a R_g which varies as $(q_t/\kappa)^{1/5}(\ell N)^{1/2}$ for large values of α_e. For chains where q_e has increased to the point where it approximately equals q_t (small q_o), R_g will vary as $\kappa^{-3/5}$ and $c_s^{-3/10}$ (case b). With a further decrease in ionic strength, q_t (~ q_e for nearly all chains now) continues to increase, but now due more to the local stiffness of the charged segments than from the excluded volume of interacting segments ($\alpha_e \sim 1$). This causes R_g to vary as $(\kappa \ell_{eff})^{-1}(\ell N)^{1/2} \sim (c_s)^{-1/2}$ (case c). In the extreme limit of q_e, the

polymer molecule will take on the dimensions approximating that of a rod of length ℓN (the "rod limit") (case d) [17].

In addition to changing the "polymer conformation" by adding salt to the polyelectrolyte solutions, the "conformation" can also be manipulated by changing the charge density along the polymer backbone. In the case of weak polyacids and polybases, this can be done simply by changing the pH of the solution. The amount of charge along a polymer backbone is typically denoted by the degree of ionization α, which is different from the previously used expansion factors of α' and α_e. For acidic small molecules, the relationship between the degree of ionization α, the pH, and the negative log of the dissociation constant K (pK_o) is given by the Henderson-Hasselbach equation

$$pH = pK_o + \log\left(\frac{\alpha}{1-\alpha}\right) \tag{1.2.9}$$

However, for polymers, an additional term of δG_{el} is required to take into account the fact that it is increasingly harder to create more charged groups on a chain which already has charges. The ability to create more charged groups will also be dependent on the polymer concentration, the salt concentration, and the local environment of the chain which is all contained within this δG_{el} term [18]. The pK_a of a polyacid can then be defined as

$$pK_a = pK_{a,o} + 0.434\frac{\delta G_{el}}{RT} \tag{1.2.10}$$

and the extended Henderson-Hasselbach equation becomes

$$pH = pK_{a,o} + \log\left(\frac{\alpha}{1-\alpha}\right) + 0.434\frac{\delta G_{el}}{RT} \tag{1.2.11}$$

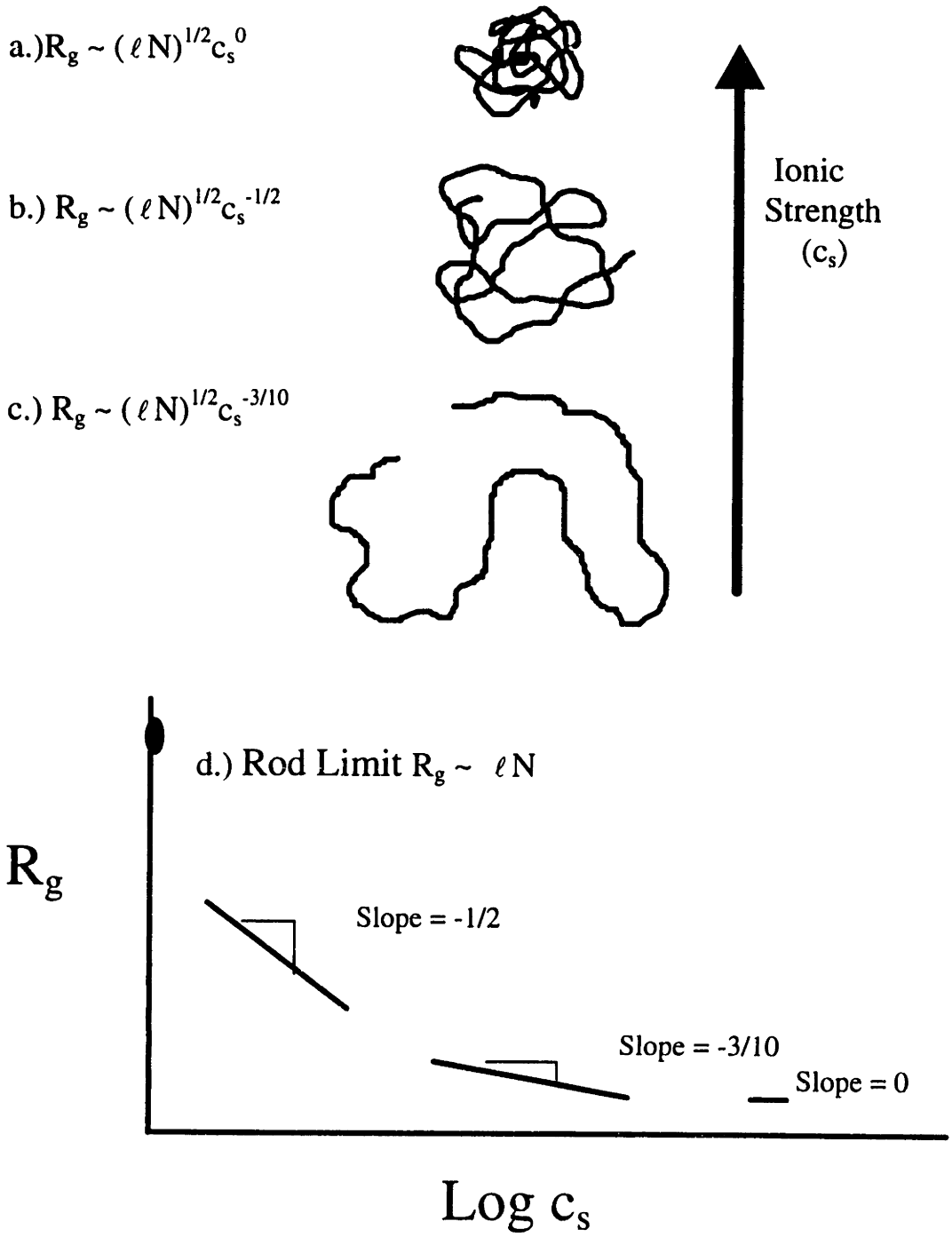

Figure 1.2.1 Polyelectrolyte solution conformations at various levels of solution ionic strength with the charges removed for clarity (top). Plot of the radius of gyration as a function of the log of the salt concentration in the three regimes discussed (bottom).

for polyacids and

$$pH = pK_{a,o} - \log\left(\frac{\alpha}{1-\alpha}\right) - 0.434\frac{\delta G_{el}}{RT} \qquad (1.2.12)$$

for polybases. Note that for very strong polyacids pK_a is very low and for very strong bases pK_a is very high such that at a moderate pH values, α will be very close to one.

For a weak polyacid, such as poly(acrylic acid) (PAA), the apparent pK_a is observed to increase with an increase in the degree of ionization α and to decrease as the amount of charge screening is increased through the addition of salt [2]. A comparison of this behavior with that of poly(methacrylic acid) which undergoes a conformational transition to a globular form in the range of 15-30% dissociation can be viewed in Appendix A [19]. However, because of the change in δG_{el} with various solution parameters for most polyelectrolytes, an accurate calculation of the amount of charge along a polymer backbone at a given pH is sometimes difficult to make.

Though simple and accurate predictions of polyelectrolyte behavior are often elusive due to the complexity of charged and non-charged effects, this same complexity can also provide multiple pathways in which the structure of a polyelectrolyte can be manipulated. If one considers that folded proteins not only use positively and/or negatively charged segments, but also secondary interactions involving hydrophobic, hydrophilic, and hydrogen bonding segments to obtain tertiary as well as primary structure, the multiple pathways for changing the structure of a molecule becomes apparent. This flexibility of manipulation of molecular conformations can also be realized in the vicinity of a solid interface through the process of adsorption. Thus, the solution interactions denoted above will provide a proper basis on which to understand the process of polyelectrolyte adsorption which is central to the fabrication of films using layer-by-layer sequential adsorption.

1.3 Adsorption at an Interface

Adsorption can be defined as the local enrichment (or depletion in the case of negative adsorption) of a material near an interface [20]. For polymers, this process typically attempts to balance the enthalpy of attraction to the surface against the loss in conformational entropy from the restriction of a solid surface. Even though the process may be thermodynamically driven, there are still debates as to whether the resulting film reaches a true equilibrium structure or simply a metastable kinetically "locked-in" structure [21]. Therefore, both the kinetic process of adsorption and the thermodynamically predicted film structure should be considered.

1.3.A Kinetics of Adsorption

As illustrated in Figure 1.3.1, the process of polymeric adsorption onto a solid surface is usually considered to take place in three steps - (1) mass transport of the chain to the surface, (2) initial attachment of the chain to the surface, and subsequent (3) spreading or rearrangement of the polymer segments [22]. In the initial stages of adsorption, all the polymer which is transported to the surface is immediately adsorbed and the overall kinetics are transport limited. The mass transport, or the flux, of polymer chains from the bulk to the surface proximity can be described in terms a diffusion coefficient, and a polymer concentration gradient between the bulk and the interface. For polyelectrolytes an additional term representing the additional driving force of the electrostatic surface potential should also be included into a diffusion expression.

In the dilute regime, the diffusion coefficient is typically inversely proportional to the effective size of the molecule which can be expressed in terms of the radius of gyration, R_g,as expressed previously in equation 1.2.7. For a polyelectrolyte of a given concentration, the diffusion coefficient can then be considerably influenced by such factors as solution pH (via l_e or α), solution ionic strength (via κ^{-1}), and polyelectrolyte molecular weight (N) with the overall trend that a short, contracted polymer will tend to give a higher diffusion coefficient than one that is long and swollen. Therefore, in an

(a.) Mass Transport

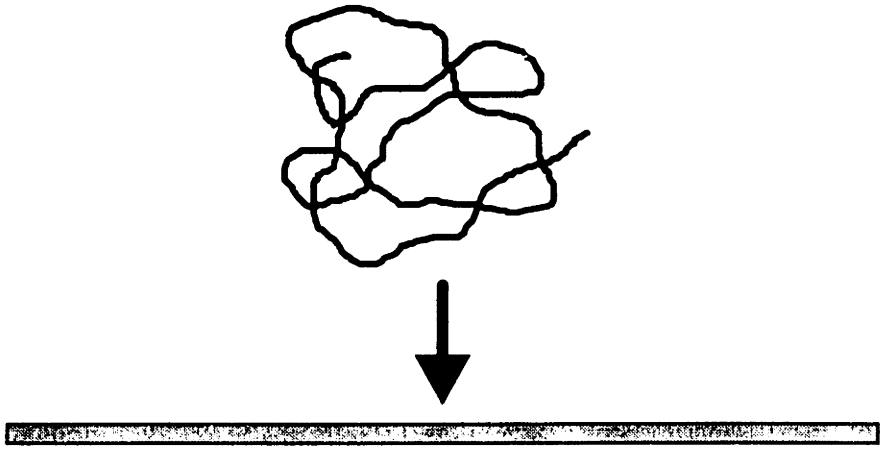

(b.) Initial Attachment

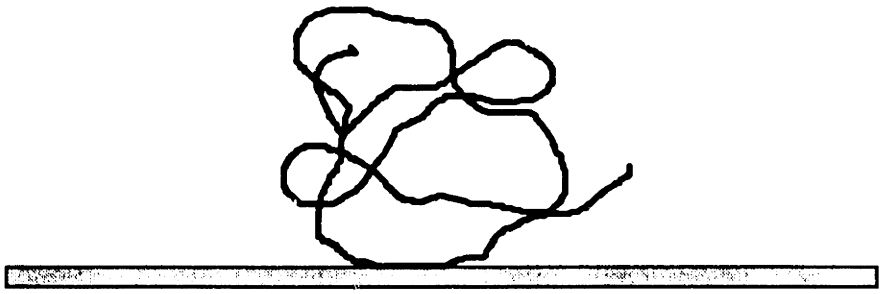

(c.) Rearrangement/Spreading

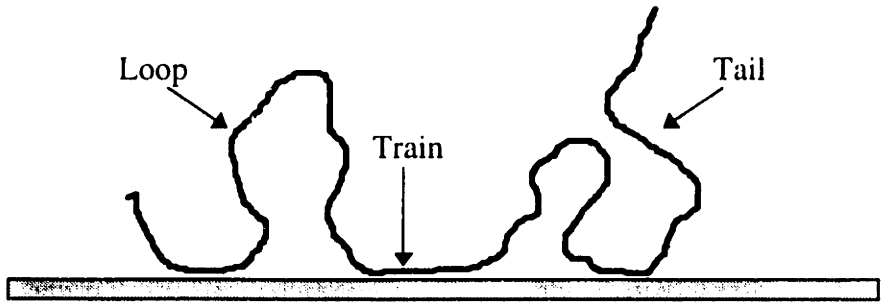

Figure 1.3.1 Kinetic stages of adsorption of an isolated polymer molecule onto a surface.

adsorption process which is mass transport limited, increasing the ionic strength of the solution and decreasing the molecular weight will increase the adsorption rate. The effect of adjusting the solution pH on mass transport limited diffusion will depend on the corresponding change it makes to the degree of ionization which, as denoted in equations 1.2.11 and 1.2.12, is dependent on the type and apparent pK_a of the polyelectrolyte. It would be expected that a change in adsorption rate would be observed when a change in pH corresponds to a significant change in the degree of ionization α, with lower values of α (higher values for ℓ_e) corresponding to higher adsorption rates provided that the more coiled polymers still have sufficient effective charge density to adsorb to the surface.

With more polymer surface coverage, the number of available surface sites decreases and further adsorption becomes hindered as the competition for attachment to the remaining sites becomes the rate limiting step. In comparison to uncharged polymer molecules, polyelectrolytes are much slower during this phase of adsorption due to the electrostatic repulsion encounter by the chains which are already adsorbed. In fact, because of this repulsive barrier, spontaneous adsorption under fixed solution conditions has been said to barely exceed the adsorbed amount corresponding to a complete exchange of the small counterions on the surface for the polyion segments [23]. Others have suggested that this repulsive interaction is so large that it causes a significant portion of the surface sites to remain uncompensated by polyion segments and leads to a kinetically hindered film structure with less adsorbed material than is thermodynamically predicted [24]. However, this self-limiting can be overcome for weak polyelectrolytes using a change in the solution conditions to produce an overall thicker layer [25]. Such a procedure usually involves changing the solution to a pH which will decrease the charge along the polymer backbone, allowing more adsorption to occur, and then returning the film to the original pH.

Because the adsorption at this stage is no longer simply dependent on the time at which molecules reach the surface, a competition between all available adsorbing molecules will occur which can cause preferential adsorption to occur. For polydispersed solution, this means that the lower molecular weight chains which were initially

adsorbed due to their quicker diffusion to the surface will now be in competition with higher molecular weight chains for the remaining sites. Though higher molecular weight chains are typically preferentially adsorbed due to their lower translational entropy penalty [26], a system involving strongly bound chains could also exhibit a preference for shorter chains due to steric restraints on the remaining unoccupied sites and the ability of smaller chains to more easily fill surface sites [27]. This competition will continue until a plateau adsorbed thickness is reached.

The final stage of adsorption involves the subsequent slow rearrangement of the polymer segments to achieve a more thermodynamically favored configuration. This rearrangement usually involves an unraveling of the polymer molecule from a "solution-like" coiled configuration which has only a few segments attached to the surface to a flat configuration with many attached segments [28]. Though the shape of the polymer molecule drastically changes during this molecular spreading, Monte Carlo simulations on an isolated chain have suggested that the overall conformational properties measured in terms of R_g are still very similar to what they would be in solution and that the shape change can simply be accounted for in terms of an anisotropic mean square end-to-end distance [29]. Experimentally, this temporal spreading has been observed for PAA, SPS, and poly(allyl amine) (PAH) via atomic force microscopy (AFM) [30,31]. But, depending on the kinetics involved and the barriers to spreading encountered, the resulting structure of the adsorbed film could involve coiled chains, flattened chains, or both [32].

One barrier to unraveling which is not encountered on a substrate which is sparsely populated is the interaction between adjacent unraveling chains. However, on substrates where adjacent adsorbed molecules are closely spaced, the competition for secondary attachment sites can lead to inhibition of spreading, an exchange of attachment sites, and/or desorption of material. The slow kinetics of this final step relative to the first two is the primary reason that macromolecular adsorption is often considered to be an irreversible, path-dependent process with a kinetically determined structure [33]. This is especially true for polyelectrolytes adsorbed on oppositely charged substrates which have relatively low mobility due to their electrostatic interactions [23]. The classic evidence sited for the irreversibility of polymer adsorption is the slow kinetics of

desorption or re-equilibration with a change in solution conditions. For example, according to typically observed high-affinity isotherm of polymer adsorption, when the polymer concentration is taken to zero through rinsing with pure water, thermodynamically, the polymer should desorb from the surface. Fortunately for the process of sequential adsorption which involves several rinses, desorption of the adsorbed films is hardly ever observed, even for very long times [34]

There are two main theories in regard to why polymer desorption is kinetically limited. The first is based on the large number of contacts that a high molecular weight polymer will make with the surface. If each of "n" contacts, are assumed to have an activation energy of 1 kT, then the energy required to completely desorb a polymer molecule will be prohibitively large at nkT and will have a probability of occuring of e^{-n} [20]. The other theory is based on the assertion that the adsorbed layer is rapidly equilibrated and it is the small concentration of polymer at the adsorbed surface that only provides enough driving force for a 10% desorption over the course of the next 300 years [23]. Though both of these theories lead to the same conclusion of effect irreversibility, the fact that a large energy savings of nkT is probably not realized through the initial process of adsorption would cause the latter theory to be more reasonable. Yet, the large number of contacts no doubt do play a vital role in kinetically inhibiting desorption. Similar tests for reversible readjustment to changes in solution composition, concentration, ionic strength, and pH have been made with the general result that whenever a desorption step is involved, a very slow and incomplete response of the adsorbed layer will be observed for systems with strong electrostatic interactions and a slightly faster, sometimes more complete, response will be observed with screened or weakened electrostatic interactions [23,35,36,37].

A slightly different post-attachment process which can be used to assess the level of reversibility involves an exchange of adsorbed lower molecular weight chains with higher molecular weight chains. High molecular weight chains are favored for adsorption both thermodynamically due to their lower translational entropy penalty upon adsorption and kinetically due to their lower probability of desorption from their higher number of contacts with the surface [38]. The exchange between the molecules differs from

desorption because it is believed to occur through a constant energy "zipping" process in which the detachment of a segment of the low molecular weight chain is followed by the immediate adsorption of a segment from a high molecular weight chain [23]. Thus, this process is diffusive in nature and has an overall lower barrier of activation. Whether or not a polyelectrolyte exhibits such an exchange of molecules appears to depend on the strength of the electrostatic interaction between the surface and the polymer. A specific example of this behavior has been observed for the adsorption of the highly charged SPS from a solution containing high and low molecular weight fractions onto a positively charged surface [39]. Under low ionic strength conditions the low molecular weight fraction is preferential adsorbed to the surface because it diffuses faster to the surface as predicted previously. At longer times, when the higher molecular weight chains are more accessible to the film, no exchange of the higher molecular weight chains with the lower molecular weight chains, or with themselves [40], was observed due to the high charge interaction. However, when salt is added to the solution, the interaction are shielded enough to let the high molecular weight fraction displace the adsorbed low molecular weight fraction. Similar trends have also been observed for other polymers and indicate some of the complex behavior which may occur for adsorption of polydispersed samples [23,41,42].

1.3.B Thermodynamic Theory of Adsorption

Despite the fact that, on the typical time scales examined, adsorbed films do not always respond to changes in solution condition in the manner to which a film in dynamic equilibrium is predicted, the agreement between theoretical predictions made on thermodynamic arguments and experimental observations is usually quite high [43,44,45,46]. While experimental agreement with a model does not constitute knowing the real nature of a system (especially when metastable states are known to exist), it does provide a means of visualizing , quantifying, and predicting system parameters in a manner which is clearly preferable to a table of empirical measurements. Therefore, the process of adsorption, and thus sequential adsorption, can be considered in terms of

thermodynamically derived equilibrium theories while, at the same time, realizing that kinetic factors can effect the structure of adsorbed layer or multilayers.

Similar to their solution properties, the adsorption of polyelectrolytes to an interface involves a convolution of polymeric and electrostatic behavior. This is especially apparent when it is considered that the first thorough treatments of polyelectrolyte adsorption involved the incorporation of electrostatic effects into existing theories of non-charged macromolecular adsorption [47,48]. The three main approaches to modeling polyelectrolyte adsorption behavior include analytical theories [34,49], Monte Carlo simulations [29,50,51,52], and numerical solutions to mean-field lattice models [53,54,55]. Regardless of which theory is used, the structure of the adsorbed film will typically be discussed in terms polymer chain segments that are either part of a train (segments directly bonded to the surface), a loop (segments not in the first layer which are bounded on either end by train segments), or a tail (segments not in the first layer which are bounded by a train segment on one side only). Figure 1.3.1(c) pictorially illustrates these segment types for an adsorbed polymer molecules. Of the three approaches, the last is the best developed and, therefore, will be used to describe the thermodynamically predicted conformations of an adsorbed polyelectrolyte.

Within this self-consistent field model, a polymer molecule is assumed to be adsorbed within a three dimensional lattice network in which the first layer contains those segments which are truly bonded to the surface. By differentiating a partition function with respect to the number of chains having a particular distribution of these segment types, the number of chains in a particular conformation can be determined at calculated [56]. Estimates of the amount adsorbed (Γ), the surface coverage (θ), and the bound fraction ($p= \theta / \Gamma$) can be solved for in terms of the non-electrostatic parameters which include the non-electrostatic interaction of the segments and the surface (χ_S), the interaction of the segment with solvent molecules (χ), the solution concentration (φ), and the molecular weight (r); and, in terms of the electrostatic parameters which include the salt concentration (c_S), the substrate surface charge density (σ_O), and the degree of dissociation (α) [57].

In the past discussion, the relative influence of the substrate was not mentioned. However, as expected, the nature of the substrate, which is expressed in terms of the surface charge density σ_0 and the non-electrostatic polymer-surface interaction parameter χ_S, will have a profound influence on the structure of the adsorbed film. First, the case of pure electroadsorption, in which there is primarily an electrostatic driving force for adsorption ($\chi_S \approx 0$), will be considered. For a surface which is neutral or has the same type of charge as the adsorbing polymer, adsorption will be inhibited because there is both no significant driving force for attachment and there is a repulsive barrier between the polymer segments and/or between the segments and the surface. A large depletion region may even form above the substrate due to these electrostatic repulsions. However, when the surface a charge opposite that of the polyelectrolyte, adsorption will be driven by electrostatic attraction between the surface charges and the polyion charges, while still experiencing mutual repulsion of the polymer segments and the entropic penalties of adsorption. In the limiting case of compensation where every polyion charge finds a surface charge, the adsorbed amount can be written as

$$\Gamma = \frac{-\sigma_0 \ell^2}{z\alpha e} \tag{1.3.1}$$

Thus, at a low degree of ionization, the ratio of non-charged segments to charged segments will increase and more overall material will be adsorbed for a given surface charge density [58]. However, the degree of ionization can not continue to decrease with out bound. At some point, the chain will become effectively neutral and there will be no electrostatic driving force for adsorption. The point at which this occurs will be dependent on the amount of counterions present to shield or displace the electrostatic segment of the chain. This critical salt concentration at which this occurs can be calculated as [59]

$$c_{s,crit.} = \frac{(\varepsilon kT)^{1/11}}{2N_A z^2 (e\ell)^{12/11}} (\alpha\sigma_o)^{10/11} \approx A(\alpha\sigma_o)^{10/11} \qquad (1.3.2)$$

Above this salt concentration, adsorbed films will become displaced by the counterions present and the adsorbed amount will decrease. The combination of the two interactions described in the above equations will then give rise to a maximum in the adsorbed amount at a certain degree of ionization under low ionic strength conditions. At higher ionic strength conditions, the peak will decrease in magnitude and shift to higher degrees of ionization until eventually it is no longer observed. The change in the amount adsorbed with decreasing degree of ionization or increasing ionic strength is expected to correspond with the change from flat chain configuration involving long trains and small loops and short tails to a more loopy structure consisting of only a few trains and many long loops and tails. In this and all subsequent discussions, the former conformation is not expected to have a molecular weight dependence on the layer thickness [$(N\ell)^0$] while the latter is expected to have a weak molecular weight dependence [up to $(N\ell)^{1/2}$] [60]. The effect of surface charge on adsorption for electroadsorption is summarized in Table 1.3.

The second case of polyelectrolyte adsorption to consider is the case were there is a non-electrostatic surface attraction contributing to the adsorption ($\chi_s>0$). For this case, the non-electrostatic surface attraction can work against the electrostatic interactions to cause adsorption on repulsively charged substrates, it can work with the electrostatic interaction to cause tighter binding of the adsorbed polymer to the oppositely charged surface, or it can work despite the electrostatic interactions to cause adsorption on neutral substrates. When the surface is neutral there is no electrostatic interaction with the surface force to promote or inhibit adsorption. But, there is repulsion between the polymer segments. This mutual repulsion causes a barrier to adsorption near the surface as the surface interaction parameter χ_s increases to $\chi_s^{eff.}$ (less attraction to the surface) and the solvency parameter χ, decreases to $\chi^{eff.}$ due to the swelling of the polymer (effectively becoming a better solvent), both of which inhibit adsorption. However, with the addition of salt, the mutual repulsion is screened both in the solution to make the solvent

effectively worse ($\chi^{eff.}$ increases) and at the surface to lower the barrier to adsorption to the surface ($\chi_s^{eff.}$ decreases). This gives an overall increase in the amount adsorbed which is predicted to scale with the square root of the salt concentration past a threshold amount of salt [53]. Such a trend has been observed for SPS on several neutral surfaces [43]. Because of the residual electrostatic repulsion of the segments at low ionic strength, the conformation of the adsorbed chains are expected to be very flattened with short loops, long trains, and very few tails in order to maximize the surface attraction and minimize the repulsion between the loops and tails. However, with increased ionic strength, the repulsion of loops and tails will be screened and the adsorption will approach that of an uncharged polymer which has many loops and tails. One would expect at low ionic strength that the adsorption onto a repulsively charged surface would occur only when the repulsion is small in comparison to the non-electrostatic surface attraction. But, with the addition of salt, both the segment-surface and the segment-segment repulsion will be screened and adsorption will become more likely. A similar chain conformation change as was predicted for the case of a neutral substrate should also occur.

For an oppositely charged substrate at low ionic strength, the adsorption behavior of a substrate with a non-electrostatic surface attraction is very similar to the case of pure electroadsorption described previously. In both cases, the amount of material adsorbed is primarily determined by the charge compensation between the surface and the polymer molecule and is observed to have a maximum at some low degree of ionization. However, due to the added attractive interaction, the substrates which have a non-electrostatic surface attraction are predicted to have slightly higher adsorption maximum at slightly lower degrees of ionization and to have better packed layers composed of molecules with flatter conformations [55].

At higher ionic strength conditions, the difference between pure electroadsorption and having a non-electrostatic surface attraction can become quite significant. In the former case, a high ionic strength caused displacement of the adsorbed polymer molecules. In the latter case there will be a critical value of χ_s , $\chi_s^{crit.}$, which marks the transition from the "screening-reducing" regime, in which adding salt decreases the amount of adsorption due to the competition for surface sites between the polymer

molecules and the more numerous salt ions, into the "screening-enhancing" regime, in which adding salt increases the amount of material adsorbed by screening the repulsion of the loops and tails of polymer molecules which now have enough preferential adsorption to compete with the more numerous salt ions and remain adsorbed. Considering that most of the sequentially adsorbed layers increase in thickness with the addition of salt, this case of adsorption is particularly relevant. Within this "screening-enhancing" regime the layer thickness should vary with the squart root of the salt concentration as was observed for a neutral substrate. These trends with surface charge and non-electrostatic surface attracction are also summarized in Table 1.3.

Other adsorption details which must be considered and which have relevance to sequential adsorbed films include the change in dissociation behavior of weak polyelectrolytes close to the surface, the influence of adsorbing onto a polymeric surface , and the level of charge overcompensation. The degree of dissociation of a weak polyelectrolyte will be dependent on the pH of the local environment which may differ widely between a surface and the bulk solution. Therefore, it has been theoretically predicted [53] and experimentally observed [61] that weak polyelectrolytes will readjust their level of dissociation (α) in an attempt to neutralize an oppositely charged surface because of the difference in local pH. This results in an adsorption maximum at roughly 1-1.5 pH units below the apparent pK_a for polyacids (above pK_a for polybases). The converse of this situation in which weak dissociating acidic groups are confined to a surface is even more complicated. While a decrease in dissociation relative to their dilute solution properties will be experience due the groups proximity to one another [62], an increase in dissociation relative to this decreased amount should still occur in the presence of an adsorbing polybase due to the change in local pH.

Up to this point adsorption has been assume to occur on a flat surface with uniform charge. However, for sequential adsorption the loops, tails, and trains of the preceding layer become the surface for the currently adsorbing film. While a rougher surface will lower the entropic penalty to adsorption [63], a comprehensive model which takes into account all the variables of sequential adsorption has not yet been presented. One of the challenges that will have to be dealt in producing such a model is the level of

Surface Charge Relative to the Polyion	Non-electrostatic Surface Interaction	Factors Promoting Adsorption	Factors Inhibiting Adsorption	Low Ionic Strength Behavior	High Ionic Strength Behavior
Same	None ($\chi_s = 0$)	Poor Solvent	Surface-Segment Repulsion Segment-Segment Repulsion Conformational Entropy Loss Good Solvent	No Adsorption (No driving force & repulsive barriers)	No Adsorption (No driving force & repulsive barriers lower)
Neutral	None ($\chi_s = 0$)	Poor Solvent	Segment-Segment Repulsion Conformational Entropy Loss Good Solvent	No Adsorption (No driving force, but fewer repulsive barriers)	Little to No Adsorption (No driving force & low repulsive barriers)
Opposite	None ($\chi_s = 0$)	Segment-Surface Attraction Poor Solvent	Segment-Segment Repulsion Conformational Entropy Loss Good Solvent	$C_s < C_s^{crit}$, Amount adsorbed determined by charge compensation with a maximum at low α High α - flat, Low α - loopy	$C_s > C_s^{crit}$, Amount adsorbed decreases with added salt from displacement of polyion at surface High α - loopy, Low α - desorbs
Same	Attractive ($\chi_s > 0$)	Non-electrostatic Surface Attraction Poor Solvent	Surface-Segment Repulsion Segment-Segment Repulsion Conformational Entropy Loss Good Solvent	Low χ_s - No Adsorption High χ_s - Flat, but more loopy at low σ & low α	Repulsion Screened Low χ_s - desorption possible Low driving force/Low Repulsion High χ_s - Loopy
Neutral	($\chi_s = 0$)	Non-electrostatic Surface Attraction Poor Solvent	Segment-Segment Repulsion Conformational Entropy Loss Good Solvent	Low χ_s - No Adsorption High χ_s - Flat Most surface interaction with least segment-segment repulsion	Segment Repulsion Screened Low χ_s - Very loopy, desorption possible High χ_s - less loopy do to surface attraction, thk ~ $c_s^{0.5}$
Opposite	($\chi_s = 0$)	Segment-Surface Attraction Non-electrostatic Surface Attraction Poor Solvent	Segment-Segment Repulsion Conformational Entropy Loss Good Solvent	Flatter more densely packed adsorbed film than without surface attraction	Segment Repulsion Screened Low $\chi_s < \chi_s^{Crit}$ - decreased amount adsorbed from displacement (like χ_s=0) High $\chi_s > \chi_s^{Crit}$ - increased amount adsorbed from segment screening, thk ~ $c_s^{0.5}$

Table 1.3 Summary of the adsorption behavior of a polyelectrolyte onto various surfaces under various solution conditions.

charge overcompensation. This factor is of extreme importance to the process of sequential adsorption and lack of consideration of it is probably the main reason that sequential adsorption was predicted to only occur for, at most, a few layers before the attraction decreased to the point where the process no longer occurred [20]. Instead sequential layering has been used for a large amount of different materials to produce films sometimes over two hundred layers thick.

Though overcompensation is discussed further in the next section, it is pointed out here that even in the case of a highly charged polyelectrolyte on a oppositely charged surface which has a relatively flat conformation, not all the charged segments will be paired with oppositely charged surface sites to completely neutralize the surface due to entropic and steric constraints. Therefore, a slight charge overcompensation could still occur on the adsorbed film surface even when the total number of surface charges and polymer charges are equal due to the undercompensation of the substrate surface. Such overcompensation has been experimentally measured to be as large as 50% and to be relatively independent of polymer molecular weight and charge density [64] In the self-consistent field lattice model, the theoretical overcompensation is expected to be very slight, to occur at low degrees of ionization when there is a significant non-electrostatic surface attraction, to be stabilized by the presence of salt ions, and to depend on the placement of charges along the polymer [55,65]. Further details of adsorption which have bearing on sequential adsorption will be discussed in the following section.

1.4 Layer-by-Layer Sequential Adsorption

Though the nature of the adsorption of a polyelectrolyte to a surface is dependent on a multitude of parameters which offer a high degree of processing flexibility, individual adsorbed layers are, on the whole, of limited practical use. However, one way that the adsorption process can be used to make thicker and more useful films is through the formation of multi-layered films. Having been first performed with colloidal particles of silica and alumina by Iler, multi-layered films can be fabricated by the alternate adsorption of positively charged species with negatively charged species [66]. Through this early work (1966), selective deposition of material onto an oppositely charged surface and the linear build-up of material as a function of each adsorption cycle was shown. The build-up was assumed to occur by the repeated reversing of the surface charge by adsorbed species. Once the charge is reversed through the formation of a monolayer, subsequent species of the same charge will be repelled. Thus, when the substrate is rinsed after the deposition, the repelled material will be removed while the adsorbed layer of material will be retained.

The extension of this technique to polyelectrolyte multilayers was not realized until over 20 years later. During that time, it was thought possible that a polyelectrolyte may expose sites at the surface of an adsorbed layer due to the conformational change undergone when adsorbed, but that the activity of such sites would diminish with each adsorbed layer [20]. However, Decher et al. disproved this concept when they showed that at least 100 consecutively alternating layers could be assembled with a linear increase in thickness by simply switching a rinsed substrate between a polyanion and a polycation solution [1]. Figure 1.4.1 shows a schematic of this sequential adsorption process for a substrate functionalized with positively charged amine groups. Note that while a thorough rinsing is typically required to build a uniform film, the drying step in between dipping the substrate into the polyelectrolyte solutions is not required.

Layer-by-Layer Sequential Adsorption

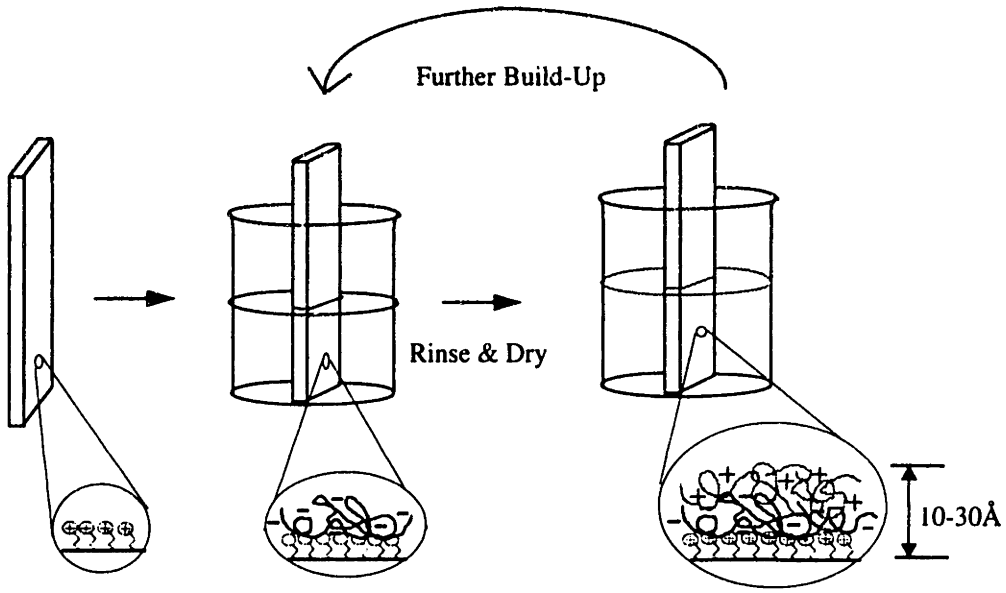

Figure 1.4.1 Schematic representation of the process of layer-by-layer sequential adsorption.

Since this initial work, the field of sequential adsorption has enjoyed a rapid growth as can be observed from Figure 1.4.2 which denotes the number of papers published in this field per year since 1991. The reason for this technique's popularity is that it allows one to build ultrathin films with supramolecular structure involving a wide variety of materials and to readily manipulate that structure by simply changing solution parameters. It also has the added advantages over other film-forming techniques such as spin-coating, Langmuir-Blodgett assembly, or solution casting, in that it can be applied to any geometry of substrate, that the deposition time is independent of substrate area, that it is usually performed with non-toxic aqueous-based solutions, and that it requires no specialized equipment (though an automatic dipper is highly recommended!). The papers denoted in Figure 1.4.2 represent the efforts (1) to understand the structure of sequentially adsorbed multilayered films, (2) to extend this techniques capabilities to new classes of

materials, and (3) to use such films in specific application which make use of their unique properties.

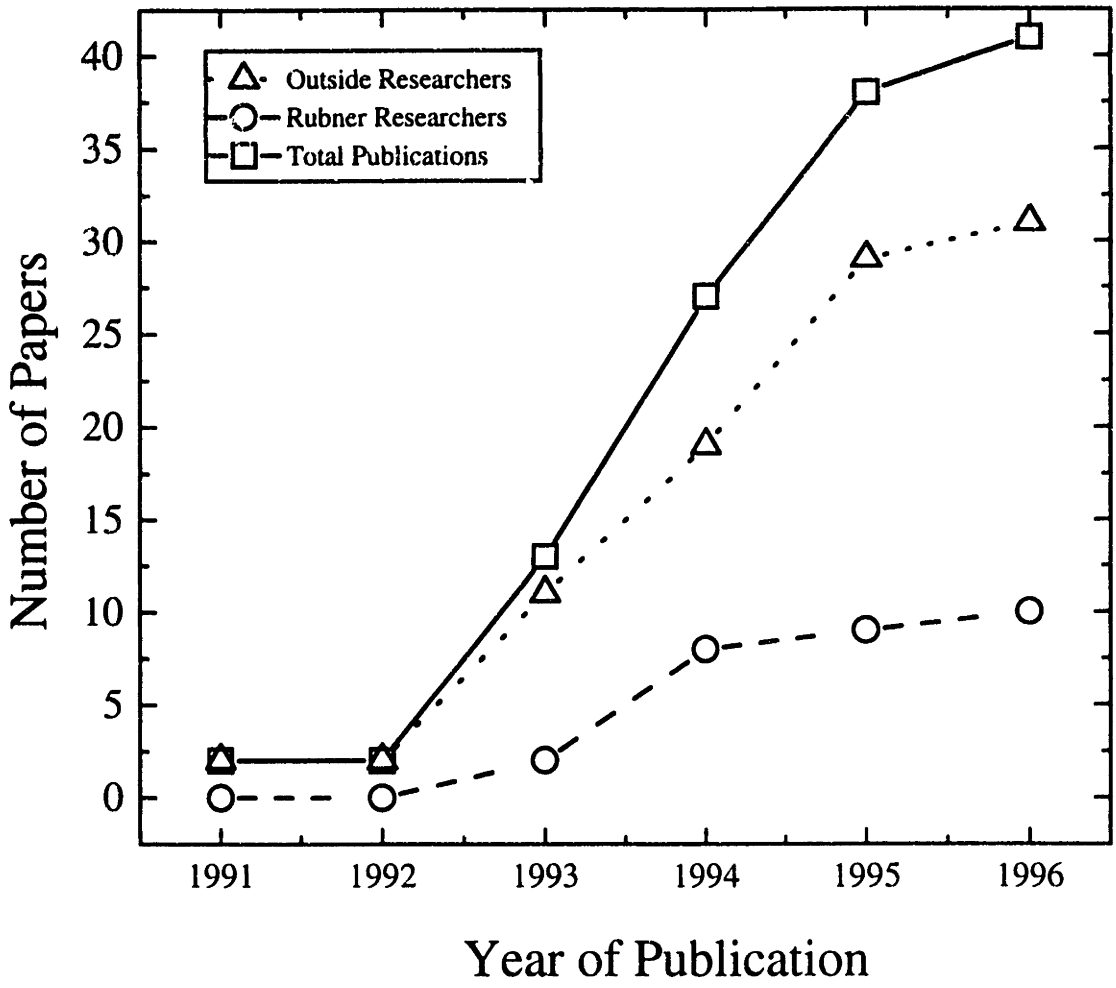

Figure 1.4.2 Number of collected papers on the subject of Sequential Adsorption published each year since 1991.

As mentioned in the preceding section, the process of sequential adsorption requires a renewal of the interacting groups at the surface to produce the multilayer film structure. While sequential adsorption based on hydrogen bonding [67] and biospecific interactions [68,69] have been observed, we will limit the discussion to sequential adsorption based primarily on electrostatic interactions. With these interactions, early researchers considered layer-by-layer sequential adsorption to occur through an

overcompensation of the surface charge due to ion-exchange of surface counterions with a polyion which had steric or kinetic restraints which leads to exposed charged groups on the surface [1]. Early measurements of such forces using a Surface Force Apparatus (SFA), indicate that the charge reversal only occurs at a sufficiently high polyion concentration (0.002M for SPS) [70]. However, more recent work has suggested that the average surface charge is reversed simply by adsorbing an oppositely charged polyion due to the presence of loops and tails which extend far into the solution [71]. This same work suggests that the surface sites will not be completely filled due to the large activation barrier imposed by the electrostatic repulsion of adsorbing more polyions and that the process of sequential adsorption may be more accurately thought of in terms of the formation of contact-ion pairs between a polyion and an oppositely charged site on a surface which may contain both types of charged groups. Such a heterogeneous surface is not considered in the Self-Consistent Field (SCF) lattice theory discussed in the previous section. Currently it is not entirely clear which representation of sequential adsorption is the most accurate. Therefore, the molecular mechanism of sequential adsorption will continue to be an active research area.

As could be predicted from the previous discussion on single layer adsorption, the solution parameters play a significant role in the structure of a sequentially adsorbed multi-layered film. The solution parameter which is varied most often for strong polyelectrolytes is the salt concentration. For example, when the amount of salt added to a solution of poly(vinyl sulfate) (PVS) was increased, the resulting multi-layered film assembled with poly(allyl amine) (PAH) significantly increased in bilayer thickness and in roughness due to the electrostatic shielding promotion of loops and tails [72]. While a few polycation-polyanion combinations require a small amount of salt to form a multilayered film and others will stop building with such an addition, usually increasing the salt concentration is used as a way to fine tune the bilayer thickness [73]. The other variable which can have a large effect on bilayer thickness for weak polyelectrolytes is the solution pH. Because the majority of the field of self-assembly has focused on strong polyelectrolytes, this parameter has not been manipulated often in the past. However, recently, the Rubner group has taken a comprehensive approach into determining the

effect of solution pH on the structure of multilayered films of weak polyacids. Results of this study indicate remarkable flexibility in changing individual layer contributions and will be discussed in the Chapter 2 of this thesis.

Early structural analysis of sequentially adsorbed films of strong polyelectrolytes investigated by x-ray and neutron reflectivity revealed that continuous molecular layers could be achieved with well defined supramolecular structure. For the system of poly(allyl amine) (PAH) and poly(styrene sulfonate) (SPS) deposited under high ionic strength conditions (2M NaCl), it was determined that the deposition starts off with much thinner layers near the substrate, but quickly reaches an equilibrium thickness that persist for the rest of the deposition. The thickness of the individual layers was estimated and the level of mixing between them was estimated to represent only 20% of the total bilayer thickness [74]. Subsequent structural studies on the same polyion combination using other analytical techniques have yielded vastly different estimates of the level of mixing. The details of these studies will be discussed in more detail in Chapter 4 in a comparison of my own estimates of the level of interpenetration made through energy transfer experiments for a variety of polyion combinations.

Another structural attribute of multilayered films which early researchers highlighted was the incredible smoothness of these films. Claims of being able to smooth out an 18Å rough air/glass interface to a 4.5Å rough film/air interface through sequential adsorption [74] called into question whether the fit to the X-ray data was accurate, especially in light of the higher roughness values obtaine by AFM. However, despite the absolute value of the roughness and/or the level of interpenetration, this early work was successful in putting forth the general concept of a sequential adsorbed film as having thinly deposited first bilayer(s), followed by bilayers of uniform thickness characterized by a certain volume percent of each component with a certain level of interpenetration at their interface.

The components used for sequential adsorption have been extended well beyond simple polycations and polyanions. Some of the classes of materials which were sequentially adsorbed outside our research group include positive and negatively charged inorganic colloids [66], bipolar amphiphiles and polyelectrolytes [75], anionic

amphiphiles and cationic amphiphiles (no polyelectrolytes) [76], layered protein structures held together with polyelectrolyte "glue" [77], DNA-polyelectrolyte layered structures [78], polypeptides with charged dyes [79], charged viruses with polyelectrolytes [80], dendrimers with re-activated dendrimers [81], semiconducting nanoparticles with polyelectrolytes [82], semiconducting nanoparticles with bipolar bolaforms [83], clay platelets with polyelectrolytes [84], exfoliated zirconium phosphate with polyelectrolytes [85], metal colloids with polyelectrolytes [86], cross-linkable amphiphiles [87], and silicate sheets with polyelectrolytes [88]. Some of the applications of sequentially adsorbed films which have been pursued outside our research group include optical limiters [79], immobilized active enzymes for increased catalytic efficiency [89], protein-based electronic devices (biosensors) [90], sequentially adsorbed polymer waveguides [91], humidity detectors [92], asymmetric gas separation membranes [93], and non-linearly optically active films [94].

Within the Rubner group, work on self-assembly has focused on electroactive polymers and dyes for applications which include organic light emitting diodes, photovoltaics, ultra-thin devices utilizing conducting polymers, and surface property manipulation. It has been shown that p-doped underivatized conjugated conducting polymers can be assembled with non-conjugated polyelectrolytes [95,96], with non-conjugated non-ionic hydrogen bonding polymers, or with derivatized conjugated polymers [97]; that derivatized conjugated polymers can be assembled with themselves or with ordinary polyelectrolytes [98,99,100]; that precursor polymers can be assembled with non-conjugated polyelectrolytes, underivatized p-doped conjugated polymers, derivatized conjugated polymers, and other precursor polymers [101]; that charged dye molecules can be assembled with polyelectrolytes [102]; that thin films with a conductivity as high as 300 S/cm can be fabricated [103]; that heterostructures of alternating blocks of conducting layers and insulating layers can produce conduction anisotropy of 10^{10} (in-plane vs. through plane) [104]; that films can easily be assembled onto a complex, non-planar geometry [105]; that light emitting diodes (LEDs) can be made with self assembled films [106,107]; that heterostructures can be built to optimize the LED operation and efficiency [108], that there can be excited state interactions

between layers [109], and that the properties of the film surface can drastically and consistently be change through the adsorption of single layer several angstroms thick [110].

The objective of this thesis is (1) to relate the molecular parameters and the solution processing parameters to the structure of the resultant sequentially adsorbed film, (2) to extend the process of sequential adsorption to include new and novel materials, and (3) to then use these sequentially adsorbed films in electroactive devices. Chapter 2 will highlight fundamental studies undertaken to relate molecular parameters, such as the ionizable functional group type and the polymer molecular weight, and polyelectrolyte solution parameters, such as solution concentration, pH, and ionic strength, to the resultant structure of the sequentially adsorbed film. Chapter 3 will extend the types of materials used for sequential adsorption to include polyimide precursors and discussed their properties. Chapter 4 will estimate the level of penetration between adsorbed layers using non-radiative energy transfer. And, Chapter 5 will discuss the electroactive properties of these sequentially adsorbed when they are incorporated into light emitting devices.

Chapter 2. - The Effect of Molecular Parameters and Solution Conditions on the Sequential Adsorption

2.1 Introductory Remarks

As mentioned in Chapter 1 of this thesis, the technique of sequential adsorption has been used on a variety of materials for a diverse set of applications. Within this thesis, sequential adsorption is used primarily for polyelectrolytes which can be distinguished from one another in terms of their charge type, their relative dissociation of their ionizable functional groups, and their chemical rigidity. The chemical structures of some of the polymers assembled within the Rubner research group are displayed in Figure 2.1.1 in relative terms of these variables. These polymers include flexible non-conjugated polyions, precursor polymers, p-type doped conducting polymers, and derivatized conjugated polymers. Within this chapter, the effect of molecular weight, solution pH, and solution ionic strength on the multilayered structure of sequentially adsorbed films of flexible, non-conjugated polyions will be examined. More specifically, the sequential adsorption of the strong polycation of poly(allylamine hydrochloride) (PAH) with the weak polyanion of poly(methacrylic acid) (PMA) and with the strong polyanion of sulfonated polystyrene (SPS) will be studied. The chemical structures of these polymers can be viewed in Figure 2.1.2.

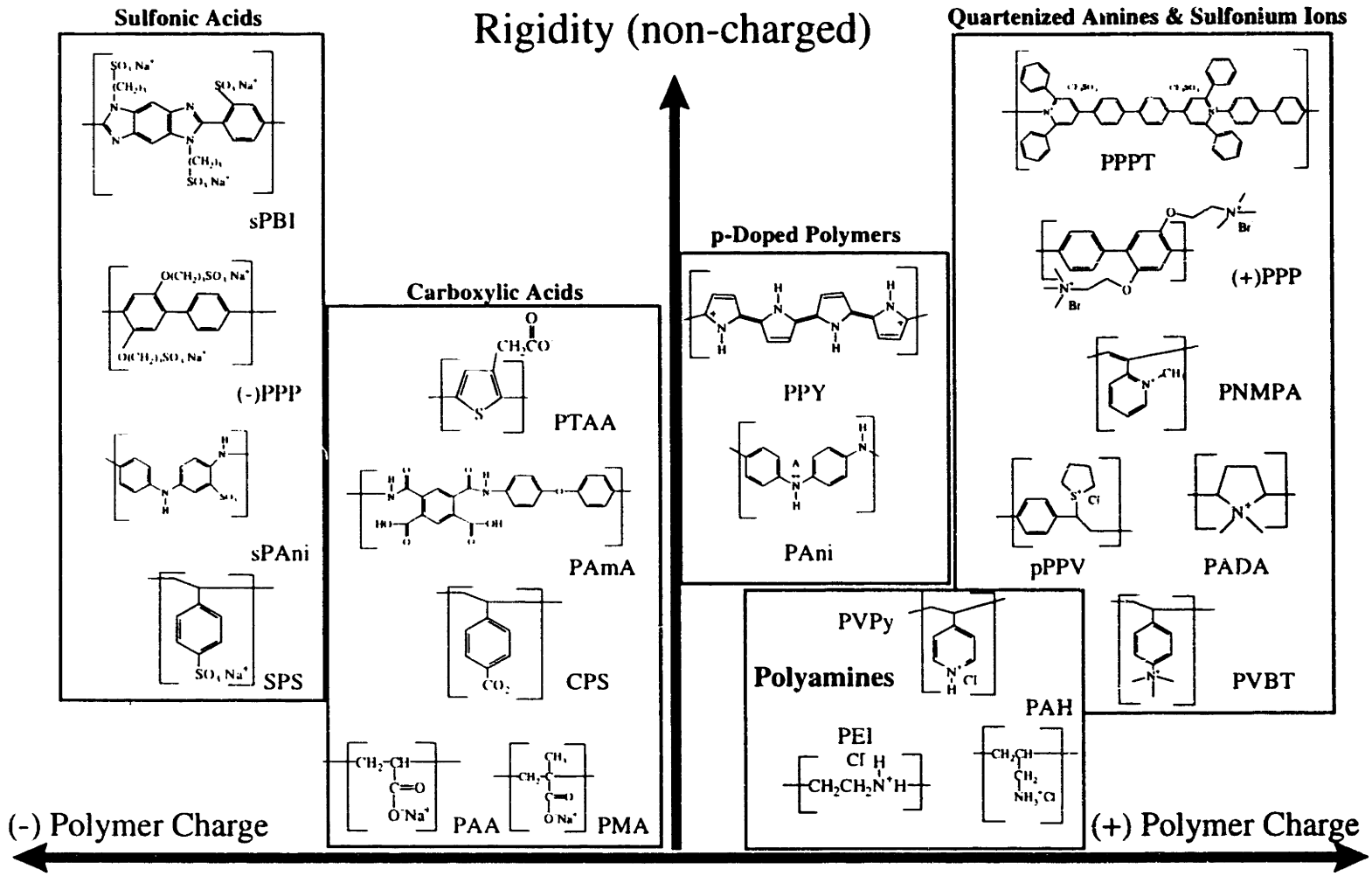

Figure 2.1.1 Various charged polymers which have been sequentially adsorbed

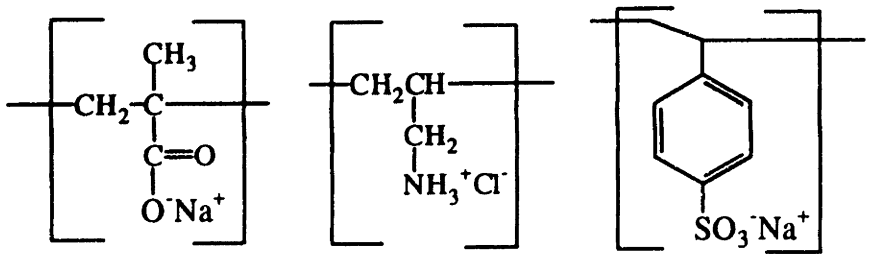

PMA PAH SPS

Figure 2.1.2 Chemical structures of poly(methacrylic acid sodium salt) (PMA), poly(allyl amine hydrocloride) (PAH), and poly(styrene sodium sulfonate) (SPS).

2.2 Experimental

The poly(methacrylic acid sodium salt) with a molecular weight of 15K was received from Aldrich as a 30% aqueous solution. The poly(styrene sodium sulfonate) with a molecular weight of 70K and the poly(allyl amine hydrochloride) with a molecular weight of 50-65K were received from Aldrich in powder form. The poly(methacrylic acid) with a molecular weight of 100K, the poly(styrene sodium sulfonate) with a molecular weight of 500K, and all low polydispersity (M_w/M_n = 1.10) poly(styrene sodium sulfonate) samples were received from Polysciences as powders. All sulfonated polystyrene (SPS) solutions were diluted with 18 MΩ Milli-Q water to a concentration of 0.01 M (monomer moles per liter), pH adjusted to 2.0-2.5, and syringe filtered through a 0.45 μm membrane. The poly(methacrylic acid) (PMA) and the poly(allylamine hydrochloride) (PAH) solutions were made through dilution with 18 MΩ Milli-Q water to a concentration of either 0.01M or 0.005M, were pH adjusted to 3.5 (unless otherwise noted), and vacuum filtered through a 1 μm membrane. All solutions were filtered immediately prior to use.

Substrates used for sequential adsorption included hydrophilic glass slides and hydrophilic single crystal silicon wafers. The hydrophilic glass slides were prepared by submerging standard microscope glass slides in a 7:3 solution of concentrated sulfuric acid and 30% hydrogen peroxide (a piranha solution) for one hour, rinsing in Milli-Q water, and then placing them in a boiling solution of 5:1:1 Milli-Q water: concentrated ammonium hydroxide: 30% hydrogen peroxide for 30 minutes. [Special care should be

taken in making and using the piranha solution due to its exothermic and highly reactive nature.] The slides were thoroughly rinse with Milli-Q water, dried with filtered compressed air, and then stored in air until used. The silicon substrates were cleaned and rendered more hydrophilic though submersion into a saturated solution of chromium trioxide in concentrated sulfuric acid for at least 4 hours. Immediately before use, the silicon substrates were taken out of the cleaning solution, thoroughly rinsed with Milli-Q water, and then dried with compressed air. To promote film build-up, preparatory layers of PMA and PAH were sometimes adsorbed to the substrate surface prior to use from 0.005M solutions with a pH of 3.5 and no added salt.

Using a modified sample holder, the substrates were dipped into the proper polyelectrolyte solutions and rinsed with Milli-Q water using an Zeiss HMS Programmable Slide Stainer purchased from Fisher Scientific. The substrates were dipped into the polyelectrolyte solution for 15 minutes followed by rinses in three separate static water baths for 2 minutes, 1 minute, and 1 minute each with slight agitation. The water in the rinse baths was typically changed after every five rinses. Occasionally, a gradient approach for the rinse baths was used in which the second and third rinse baths of the first series of five rinses was used as the first and second rinse baths of the second series of five rinses with a fresh bath used for the third rinse. No difference between the first method and the gradient method of rinsing was observed. Occasionally, the rinse water was pH adjusted to the pH of the solution to minimize the solution pH drift which is sometimes observed. Additionally, the "Flow Through" bath, in which deionized water continuously flowed, was occasionally used for the third rinse for both polycations and polyanions. When used, the substrates were submerged in the "Flow Through" bath for 10 minutes - a time calculated to be more than adequate for the removal of any rinsed polyelectrolyte from the bath.

Once assembled onto the substrates, the polymeric films were characterized using profilometry, ellipsometry, contact angle measurements, and UV-Visible spectroscopy. A Sloan Dektak 8000 profilometer with a 2.5 μm stylus with a weight of 10 mg and a medium scan rate was used to determine the step heights of scratched films on hydrophilic glass and silicon substrates. A Gaertner multiple wavelength ellipsometer was used to

determine the index of refraction and film thickness of the films assembled on silicon. An index of refraction of 1.550 was assumed for films below 200Å due to the fact that the ellipsometer had trouble converging to consistent values for both the film thickness and index of refraction for such thin films. A VCA2000 contact angle measurement system with camera and measurement software obtained from Advanced Surface Technology was used to determine the hydrophilicity of the film surface through the measurement of the angle that a drop of water made with the surface. An Oriel Multispec multi-channel analyzer with a halogen source, a spectral range of 300 - 800 nm, and a resolution of 0.2 nm was used to measure the relative amount of methylene blue, a positively charged dye molecule, that was adsorbed onto a surface after assembly as will be described below.

2.3 The Effect of Molecular Weight and Solution Ionic Strength on Sequentially Adsorbed Films of Strong Polyelectrolytes

2.3.A Introductory Remarks

As mentioned in Chapter 1 for the case of single layered adsorption on a flat impenetrable surface, the expected dependence of the adsorbed film thickness on the molecular weight (M) will be dependent on the conformations found in the film. For example, an adsorbed film with a relatively flat structure involving many directly adsorbed segments and only a few short loops and tails would be expected to show no molecular weight dependence (M^0) because both short and long chains can cover the surface equally well. However, when the structure of the chains changes to one with fewer directly adsorbed segments and many long loops and tails, a molecular weight dependence would be expected because the long chains are better able to make long loops and tails than are short chains. If the adsorbed chains, are extremely coiled with only a few directly adsorbed segments, then the conformations are similar to those found in solution and the film thickness would be expected to vary as $M^{0.5}$ near theta conditions as has been experimentally observed for SPS on platinum [16]. In an even further extreme where a polymer "brush" is created, in which only one end segment is attached to the surface, the molecular weight dependence on the film thickness approaches $M^{1.0}$ [60].

In the case of sequential adsorption, where adsorption occurs on top of a previously adsorbed polymer molecule, rather than on a flat uniformly charged substrate, the adsorption process can be more complicated. In addition to the strict definitions of trains, loops, and tails being confused due to the three dimensional porous nature of the surface, additional factors need to be considered. For example, a change in the thickness contribution of one polyelectrolyte layer might cause a corresponding change in the thickness of the oppositely charged polyelectrolyte. Likewise, the molecular weight of the polymer molecule may affect the bilayer thickness by changing the extent of penetration into adjacent layers. Penetrated segments would be expected to contribute to the molecular weight dependence of the thickness in a manner similar to that of the tails and loops of a single adsorbed layer. However, penetrated segments have the distinct difference that they would be burrowed into adsorbed material instead of dangling at the surface and therefore should be more dependent on the nature of the adjacent layers. Finally, in the case of films where low molecular weight chains have difficulty building due low surface overcompensation and/or a higher probability of desorption, an increase in molecular weight could simply cause an increase in bilayer thickness through a stabilization of the sequential adsorption process.

2.3.B. The Effect of Polyanion Molecular Weight on Bilayer Thickness

Within this section, a study of the effect of varying the molecular weight and polydispersity of sulfonated polystyrene (SPS) on the bilayer thickness of sequentially adsorbed films of SPS with poly(allylamine hydrochloride) (PAH) is made under several different SPS solution ionic strength conditions. This polyanion/polycation combination was chosen based on the availability of literature data on both single layer SPS adsorption and SPS/PAH bilayer sequential adsorption from which a comparison will be made to the results obtained here. Each SPS/PAH film was built on cleaned silicon and hydrophilic glass substrates which had at least one preparatory bilayer of poly(methacrylic acid) (PMA) and PAH - an amount which has previously been shown to provide a good surface for the adsorption of highly charged polyelectrolytes. Both the PMA and PAH layers were adsorbed from solutions with a concentration of 0.005M (based on the monomer repeat

unit) and a pH of 3.5 with no added salt. These same PAH solution parameters were also used to build-up bilayers with SPS. No build-up was observed at basic SPS solution pH values (pH>7) for substrates both with and without "prep" layers. This lack of build-up is believed to be due to the lower charge density of the adsorbed PAH when placed into the basic SPS solution. Therefore, each 0.01M SPS solution was adjusted to a pH of 2.0 and the bins of rinsing water were matched to the pH of their respective polyelectrolyte solutions. Films were built-up to a final thickness of around 200Å with low polydispersity SPS molecular weights of 35K, 100K, 400K, and 1 M and higher polydispersity SPS molecular weights of 70K and 500K. Films were also assembled with low polydispersity SPS with a molecular weight of 4.6K, but will not be included in the data presented here because of their tendency to stop building. This is believed to be due to their higher probability for desorption.

As can be seen in Figure 2.3.1 for the case of low polydispersity SPS with no salt, the bilayer thickness, as measured by ellipsometry at 630 nm, is generally low with a constant bilayer thickness of 6 to 8 Å. The lack of a molecular weight dependence ($M^{0.06}$) was expected for films with such flat conformations and the measured bilayer thickness differs only slightly from the literature value of 10.9Å which was achieved for films built on aminosilane functionalized surfaces and measured by Small Angle X-ray Reflectivity (SAXR) [111]. The fact that the bilayer thickness measured by ellipsometry of 6 to 8 Å is less than the summation of the molecular cross-sections of the two polyions implies that either full surface coverage was not achieved or that the sites left empty by previous adsorption steps are filled in by subsequent adsorption steps.

When 0.1 M NaCl was added to the SPS solution and the conditions were kept constant for the PAH, thicker bilayers were obtained with a molecular weight dependence similar to the "no salt" case. The relatively constant bilayer thickness of 9-11Å was more consistent with the full substrate coverage, but the molecular weight dependence was still negligible at $M^{0.09}$. With another increase in NaCl concentration of the SPS solution to 1.0 M, the bilayer thickness increased to 10-19Å and began to show a slight molecular weight dependence of $M^{0.18}$. When the amount of NaCl added to the SPS solution was increased even further to 2.0 M, the lower molecular weight samples were unchanged in thickness

while the higher molecular weight samples continued to increase, to give an overall expanded bilayer thickness range of 10-22Å and a molecular weight dependence on the bilayer thickness of $M^{0.23}$. If the films made with a SPS molecular weight of 1 million are excluded from consideration due to concerns over being close to the semi-dilute solution regime, of having a much larger range of molecular weights for the same measured polydispersity (M_w/M_n = 1.10), and of requiring more time to rearrange into a thermodynamically favored conformation, then the dependence of the bilayer thickness on the SPS molecular weight goes from $M^{0.00}$ under conditions where no salt was added to the SPS solution to $M^{0.30}$ under condition where 2.0 M NaCl was added to the SPS solution.

While the molecular weight exponents should not be taking as definitive values due to the large scatter between the limited number of data points, the increase in molecular weight dependence with increasing ionic strength does appear to be a real trend. This trend can most clearly be observed through consideration of films made with a SPS molecular weight of 35K and 400K. Under conditions where no additional salt was added to the SPS solutions, the bilayer thickness of the 35K and 400K SPS films are the same (7Å). However, when 2M of NaCl are added to the SPS solutions, the bilayer thickness of the 400K SPS films (21 Å) is over double that obtained for the films made with a SPS molecular weight of 35K (9Å). This clearly demonstrates a negligible dependence of the bilayer thickness on the molecular weight for conditions which lead to flat conformations and a significant dependence for conditions which lead to loopy conformations.

The bilayer thickness values measured here by ellipsometry for a SPS molecular weight of 100K (7Å at no salt, 16Å at 1.0 M NaCl, and 15Å at 2.0 M NaCl) are thinner than those reported for SPS/PAH on aminosilane functionalized surfaces as measured by SAXR (11Å at no salt, 18Å at 1.0 M NaCl, and 23Å at 2.0 M NaCl). The small disagreement between these two sets of values can likely be attributed to differences in substrate type, processing procedure, and/or the technique used for thickness measurement. Despite these differences, an increasing SPS molecular weight dependence would still be predicted for the increasingly thicker SPS/PAH bilayers. However, a thicker bilayer does not necessarily always imply a stronger molecular weight dependence. For

example, a similar SPS molecular weight study for sequentially adsorbed films of p-doped polyaniline and SPS showed no molecular weight dependence for films with an average bilayer thickness of 41Å made under low ionic strength conditions [112]. This suggests that the molecular weight dependence has more to due with the SPS chains adopting a more loopy configuration through an increase in the ionic strength of the SPS solution than with the resultant bilayer thickness.

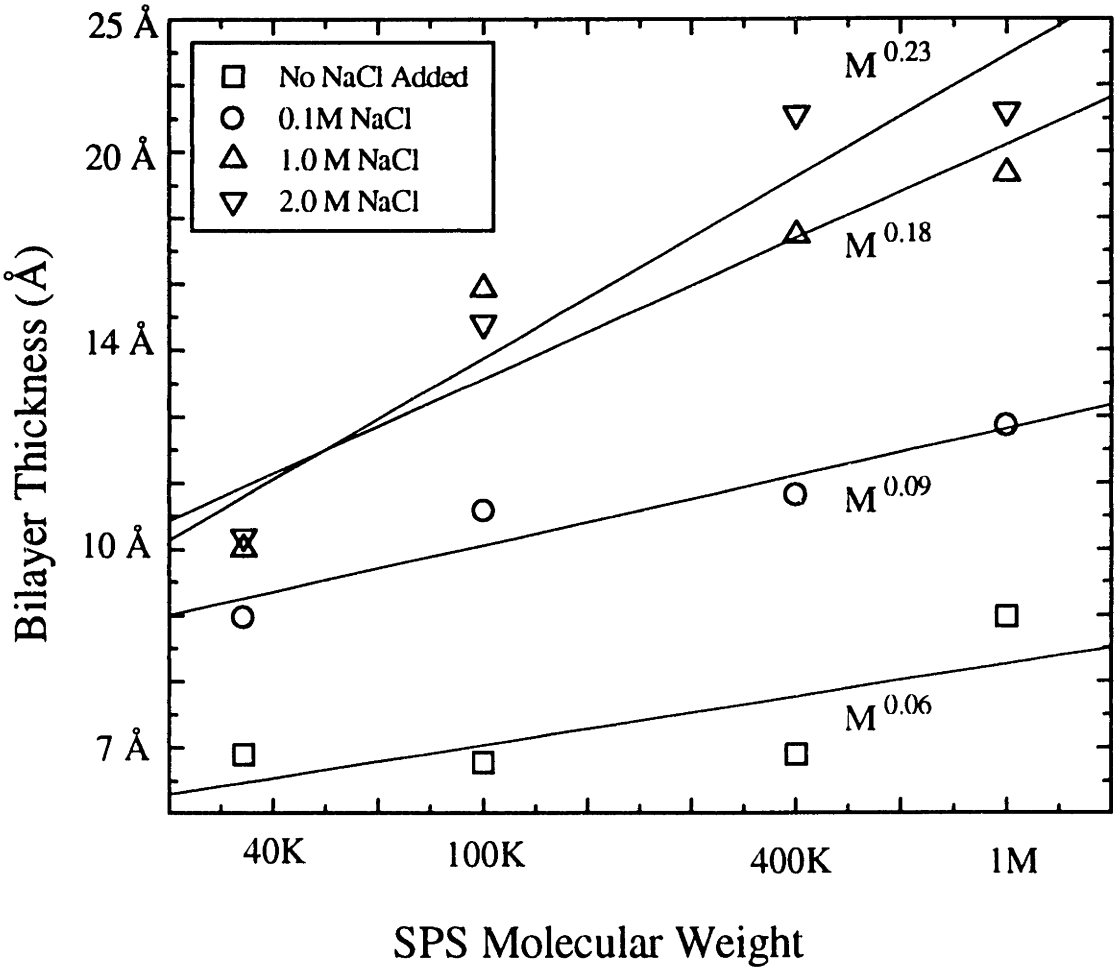

Figure 2.3.1 Log-Log plot of the SPS/PAH bilayer thickness as a function of the SPS molecular weight (low polydispersity) for NaCl concentrations in the SPS solution of 0 M (no added salt), 0.1 M, 1.0 M, and 2.0 M.

Not unexpectedly, similar behavior to that observed in SPS/PAH bilayers has been exhibited for the single layer adsorption of SPS on various substrates under a variety of solution conditions. Aside from results of SPS adsorption on platinium which gave a $M^{0.4}$ at only 0.1M NaCl [113], a negligible molecular weight dependence on the amount adsorbed is observed for films adsorbed onto both neutral and oppositely charged substrates under low ionic strength solution conditions (≤0.5 M NaCl) [17,43]. At higher ionic strength levels, SPS films on neutral surfaces, such as poly(oxymethylene) and isoelectric silica, showed an increase in the amount adsorbed with SPS molecular weight corresponding to a molecular weight dependence of $M^{0.37}$ at a NaCl concentration of 2 M [114,115]. Little information is present in the literature regarding the molecular weight dependence of SPS on oppositely charged surfaces. However, because an electrostatic attraction to the surface tends to decrease this molecular weight dependence, the exponent value for the neutral substrate can be considered to represent an upper limit for the case of an oppositely charged substrate. This is in good agreement with the results obtained for sequentially adsorbed multilayered films.

When more polydispersed SPS samples are sequentially adsorbed under identical conditions, a slight variation to the behavior exhibited by the low polydispersity samples is observed. At low ionic strength, the more polydispersed samples stop building or give a significantly lower bilayer thickness than the low polydispersity samples as indicated in Figure 2.3.2. However, at higher ionic strengths they become comparable to, or even slightly thicker than, the predicted low polydispersity bilayer thickness. This behavior is consistent with a transition from a mass transport limited kinetic regime to an attachment limited kinetic regime. For example, at low ionic strength, the adsorption process is mass transport limited with the smaller chains adsorbing to the surface first because they can diffuse to the surface faster. Once adsorbed, no exchange with higher molecular weight chains occurs due to kinetic barriers. However, when salt is added to the adsorbing solution, the molecules in solution are less swollen and the diffusion rates increase to the point that mass transport is no longer the rate limiting step. Either the process of attachment to the surface or rearrangement of the adsorbed polymer molecules will then dominate the kinetics. The fact that larger bilayer thickness values are obtained for the

SPS samples with higher polydispersity under high ionic strength conditions suggests that the molecular weight exchange reactions which are characteristic of rearrangement dominated kinetics may be occurring on the time scale examined. Though this is a subtle effect for the case examined, it could be much larger for polymers with an even broader or bimodal molecular weight distributions.

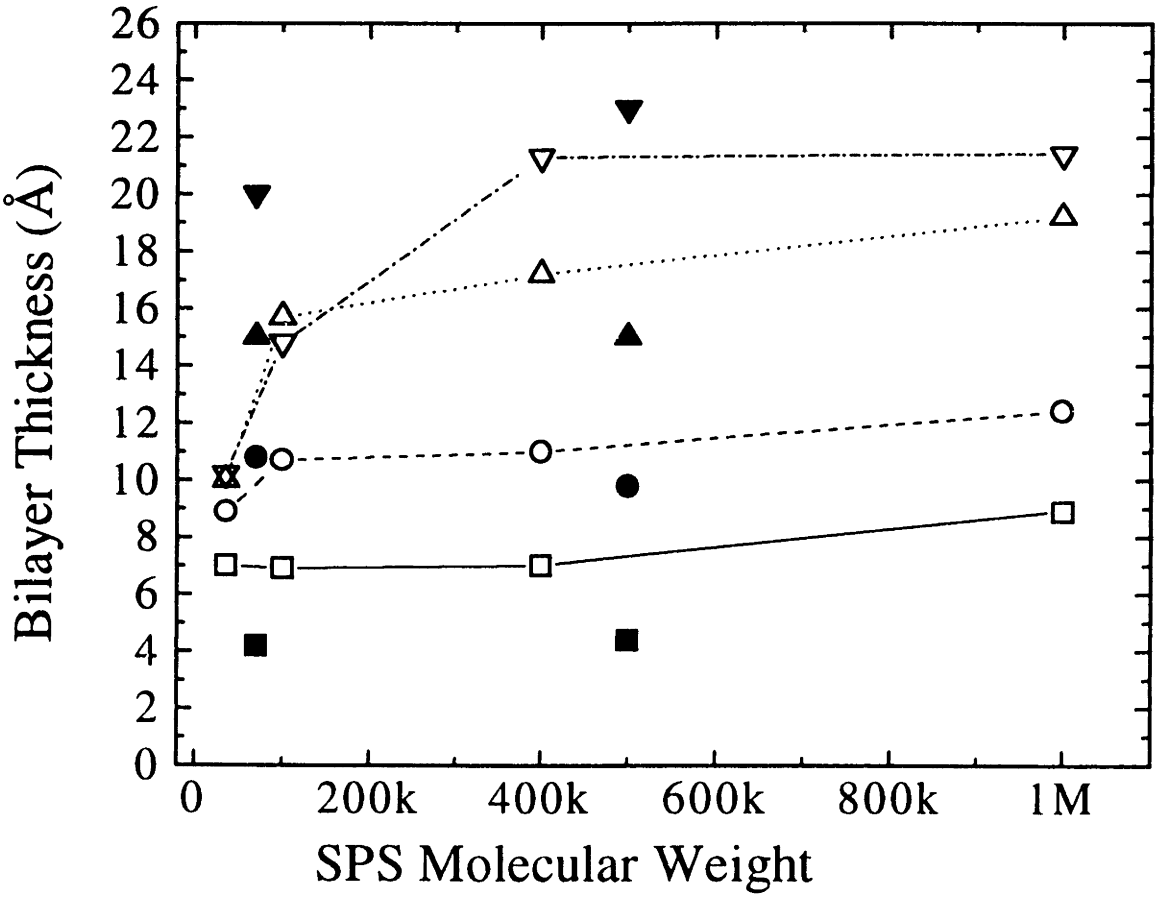

Figure 2.3.2 SPS/PAH bilayer thickness as a function of SPS molecular weight and polydispersity (solid symbols = high poydispersity, hollow symbols = low polydispersity) for concentration of added NaCl in the SPS solution of 0M (—□—), 0.1M (- ○-), 1.0 M (·· △··), and 2.0 M (-· ▽-·).

2.3.C. The Effect of Polyanion Solution Ionic Strength on Bilayer Thickness

Up this point the above data has been interpreted in terms of the molecular weight effects for a given solution ionic strength. However, the same data can be recast to give information regarding the influence of ionic strength on the film thickness for a given molecular weight polymer. From the single layer adsorption theory discussed in Chapter 1, the SPS layer thickness is expected to increase with the square root of the ionic strength ($thk \sim Kc_s^{0.5}$). From Figure 2.3.3, it can be observed that such a trend is present for films made with a SPS molecular weight above 35K and an ionic strength less than 2M NaCl to give K=9-12. Films made with SPS solutions containing 2M of NaCl appear to have a weaker dependence on the solution ionic strength. This is similar to the decreasing ionic strength dependence observed for the radius of gyration of polyelectrolytes in solution at increasingly higher ionic strength values which was discussed in Chapter 1 and can be linked to the approach of a saturation in the shielding effect of the salt ions. The plateau bilayer thickness achieved for SPS/PAH films fabricated with a SPS molecular weight of 35K and a solution ionic strength of $\leq$ 0.1M NaCl can likely be attributed to reaching a limit to the average length that loops and tails can form.

It should also be noted that these results are very different from those reported by Decher and Lvov for a SPS molecular weight of 100K which gave an ionic strength dependence on the SPS/PAH bilayer thickness which was proportional to the ionic strength squared ($thk \sim K_1 c_s^2$) rather than to the square root of the ionic strength that was predicted by single layer adsorption theory [111]. In addition, they also suggested that strong polyanions and polycations at low ionic strength have a stoichiometry which approaches 1:1 in charge, but assumed that the layer thickness ratio and charge stoichiometry could simply be varied by increasing the thickness of one polyion independently of the other through the addition of salt to just one solution. [111]. The linear increase in bilayer thickness with the square root of the ionic strength exhibited for SPS molecular weights of above 35K is consistent with that assumption.

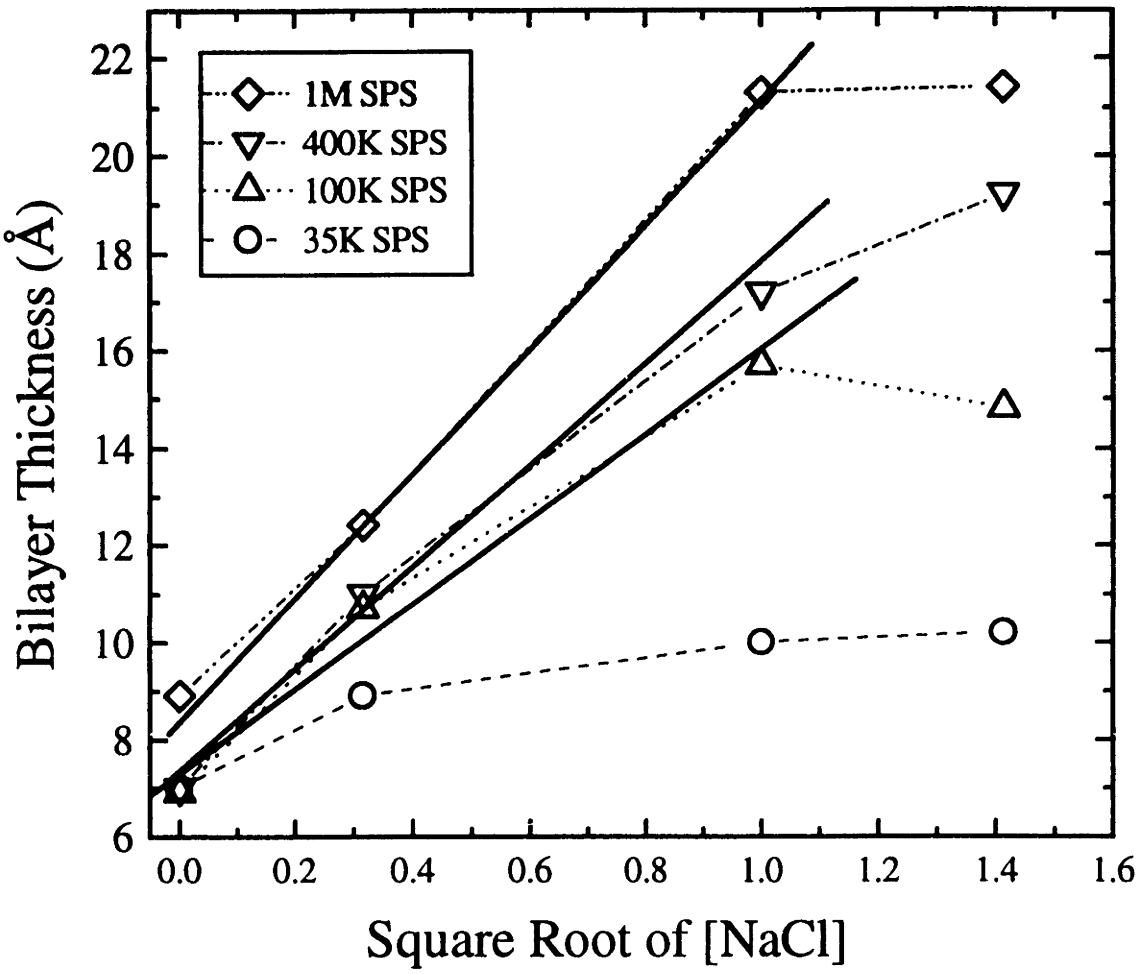

Figure 2.3.3 SPS/PAH bilayer thickness as a function of the square root of the NaCl concentration in the SPS solution for SPS molecular weights of 35K, 100K, 400K, and 1M.

Recently, McCarthy and coworkers confirmed that the layer thickness ratio could be changed through the addition of salt to one solution for SPS/PAH films on a neutral substrate [116]. In contrast, Fleer and coworkers have concluded that the charge stoichiometries of highly charged polyelectrolytes are dictated by the polycation/polyanion pair and that the layer thickness ratio will remain constant with changes in surface charge, the order of layer adsorption, or the ionic strength [117]. However, Fleer and coworkers used relatively low ionic strength conditions and simultaneously changed the ionic strength of both polyanion and polycation solutions. Therefore, this study may still be consistent with the others. Taken together, these studies seem to imply that when the ionic strengths of the polycation and polyanion solutions are equal, a certain stoichiometry exists between

the thickness of the layers and between the charges. But, the stoichiometry can be significantly changed when the ionic strength of one polyelectrolyte significantly differs from the other. This change in the layer thickness ratio with a change in the "realized" charge density of a molecule by electrostatic screening is analogous to the case considered in the next section of changing the layer thickness ratio with a change in polymer charge density through solution pH.

Overall, this section illustrates that for the sequential adsorption of strong polyelectrolytes, no significant molecular weight dependence of the film thickness occurs at low ionic strengths conditions, but that a significant molecular weight dependence exists at higher ionic strengths. This measured molecular weight dependence was shown to be similar to that observed for single layer adsorption. Moreover, the increase in bilayer thickness for high molecular weight SPS was shown to scale with the square root of the salt concentration, as also predicted from single layer adsorption theory.

2.4 The Effect of Solution pH on the Structure of Films Containing a Weak Polyacid

2.4.A. Introductory Remarks

While the structure of sequentially adsorbed films of strong polycations and polyanions can be manipulated through variation of the solution ionic strength and molecular weight as discussed in the previous section, weak polyelectrolytes have the additional capability of manipulating their structure through a change in solution pH. Within this section, the sequential layering of the weak polymer acid, poly(methacrylic acid) (PMA), with poly(allylamine hydrochloride) (PAH) under a variety of different pH conditions will be discussed. In this particular case, values for both the individual layer and the bilayer thickness will be measured in an effort to fully understand the complex behavior that changing the solution pH has on the structure of the multilayered film. The resultant structure can than be compared to a prediction made from theoretical models to gain insight into the molecular mechanism of sequential adsorption.

2.4.B. Mechanisms of Sequential Adsorption

Two types of limiting behavior can be imagined for sequential adsorption. Firstly, the adsorption of a molecule onto an oppositely charged adsorbed molecule could be similar to the single layer SCF thermodynamic adsorption theory and be primarily determined by the charge density (σ_o) and non-electrostatic attraction (χ_s) of the outermost surface. Or secondly, the adsorption process could be considered to occur through the formation of acid-base contact-ion pairs as described by Lowack and Helm [71]. As shown schematically in Figure 2.4.1, the major differences between surface charge dominated and contact-ion pair dominated sequential adsorption are that while surface charge dominated behavior is based on assumptions of thermodynamic adsorption to a surface layer of uniform charge density with little penetration into the underlying layer, contact-ion pair dominated behavior in based on assumptions of "kinetically hindered" adsorption driven by the formation of contact-ion pairs on a potentially heterogeneously charged surface. Furthermore, the "kinetically hindered" nature of contact-ion pair dominated adsorption allows for the possibility that many binding sites which would have been filled under thermodynamic considerations, are left empty, and, therefore, available for binding when additional layers are adsorbed which can result in an overall structure which is very interpenetrated. Additionally, the level of charge overcompensation at the film surface of the kinetically determined structure could potentially be much higher than what is predicted under thermodynamic considerations.

One way to probe which behavior is controlling the adsorption process is to observe the response that an adsorbing layer has to an increase in the thickness of the underlying layer. For contact-ion pair dominated adsorption, a change in the thickness of the underlying layer results in more binding sites for the formation of contact-ion pairs with the incoming adsorbing molecules and thus to a thicker adsorbed layer as the system tries to maintain charge stoichiometry (a constant ratio of positive to negative charged functional groups). However, for surface charge dominated sequential adsorption, the amount adsorbed will remain relatively constant as long as the outermost surface charge does not significantly change. Of course, these predictions are only simplified notions of very complex behavior, but they may still serve as a preliminary attempt to decipher the

details of sequential adsorption which, as of now, are still unknown. For example, this approach does not take into account any changes to the electrostatic repulsion between the molecules trying to adsorb and the molecules already adsorbed which should play a major role in determining the thickness of the final adsorbed layer for both of these behaviors.

While no in-depth study relating changes in polymer charge density to layer thickness ratio has been published for sequentially adsorbed films, such a change could possibly be consistent with both surface charge dominated and contact-ion pair dominated sequential adsorption. For example, with a change in the degree of ionization of one of the polyelectrolytes under contact-ion pair dominated sequential adsorption, the charge stoichiometry will attempt to be maintained, but the ratio of the thickness of the positively charged layer to the negatively charged layer will vary with the difference in the degree of ionization between the two polyelectrolytes. For surface charge dominated sequential adsorption, the layer thickness ratio will also change as the thickness of the polymer which undergoes a variation in the degree of ionization responds to that change independently of the other polymer layer. However, the main difference between the two mechanisms is that contact-ion pair dominated adsorption attempts to achieve charge stoichiometry between the layers while surface charge dominated adsorption does not.

One way to change the degree of ionization in order to cause such changes in the layer thickness ratio is to synthetically tailor the number of fully ionized groups along the backbone of a strong polyelectrolyte. However, a much easier way to change the number of charged groups along a polymer backbone is to use a polyelectrolyte containing ionizable functional groups with dissociation equilibriums and vary the solution pH. While some consider both PAH and PMA to be weak polyelectrolytes because they both have functional groups with ionic dissociation equilibriums [118], under the experimental conditions used for his study, the PAH can be considered to be a strong polyelectrolyte which is fully charged and pH independent. In fact, PAH is rather unique in comparison to other polyamines, such as poly(ethyleneimine) (PEI) and poly(vinyl amine), in that it is nearly fully charged ($\alpha \approx 1$) all the way up to a neutral pH [119]. The dissociation of PMA,

Surface Charge Dominated Sequential Adsorption

Contact-Ion Pair Dominated Sequential Adsorption

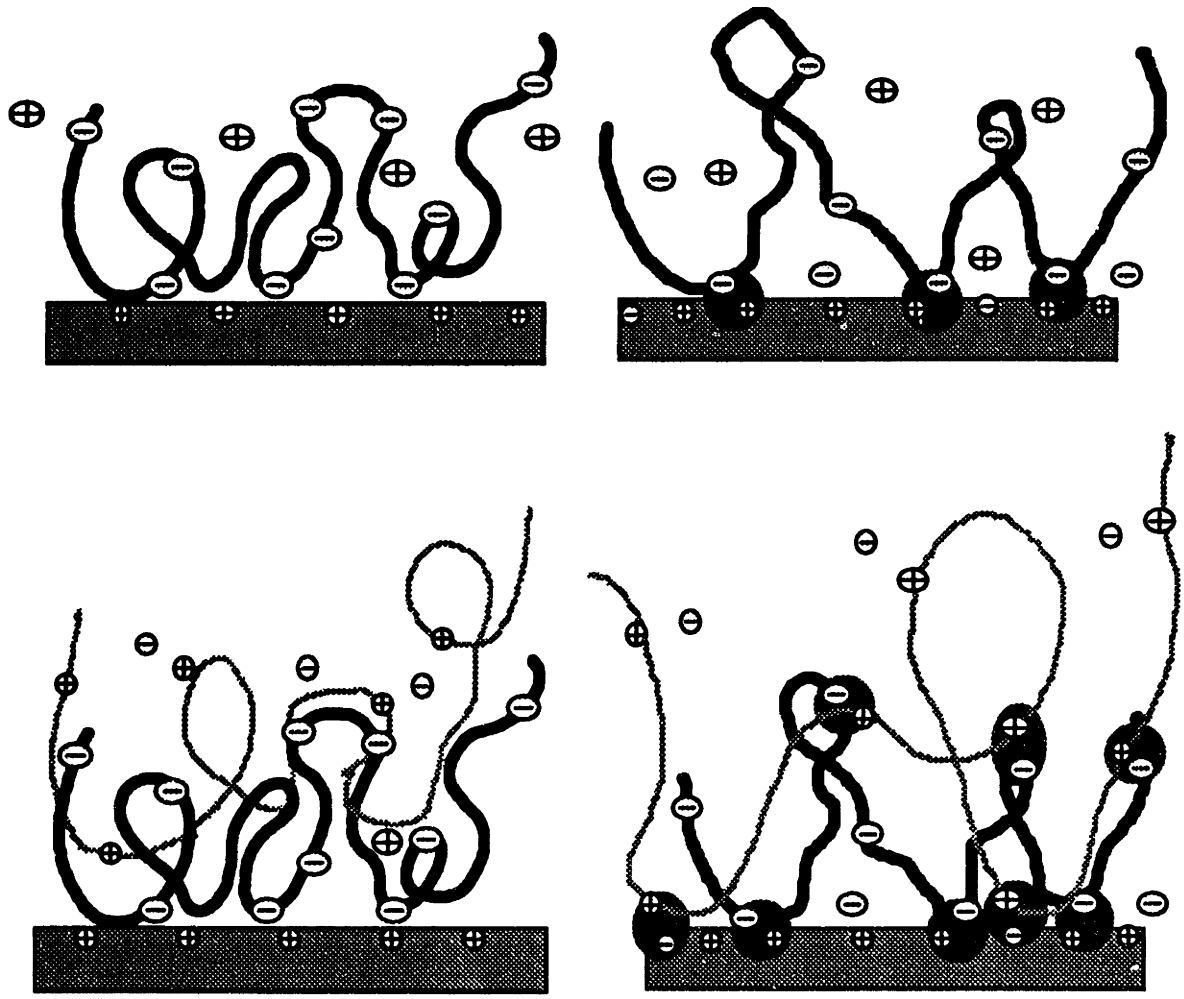

Figure 2.4.1 Surface charge dominated and contact-ion pair dominated sequential adsorption. Contact-ion pair dominated sequential adsorption allows for the possibility of adsorption on heterogeneously charged substrates and extensive layer penetration. Surface charge dominated adsorption is affected by surface properties only. The ellipses on the right hand schematic denote contact-ion pair formation.

however, is complicated by a strongly varying apparent pK_a [19] and by a transition to a globular form at α=0.15 to 0.30 which is due to either hydrophobic interactions [120] or preferred conformations for hydrogen bonding [121]. From titration curves of PMA in solution, the degree of ionization is extrapolated using the extended Henderson Hasselbach equation of the previous chapter (Eq. 1.2.11) to be 5% or less ($\alpha \leq 0.05$) for the pH values used in this study [122]. According to Fleer and coworkers, polymer charge density below 5% can not even cause complexation for one bilayer [113], much less provide a means for continued sequential adsorption for over a hundred bilayers as has been personally achieved. However, it is not clear whether Fleer and coworkers took into account the local pH increase which can occur in the proximity of a fully charged polymer like PAH.

2.4.C. The Effect of Solution Concentration and PMA Molecular Weight on Adsorbed Layer Thickness

Despite the predictions of others to the contrary, sequential adsorption of PMA with PAH has been achieved under a variety of different solution conditions on many different substrates. Studies examining the effect of dipping time, polyelectrolyte concentration, and molecular weight on film structure have been undertaken. Dipping time studies reveal that a self-limiting amount of PMA and PAH are adsorbed within 15 minutes and that no significant increase in thickness is observed for films dipped at longer times. Therefore, polyelectrolyte dip times of 15 minutes were used for all of the films mentioned here. The results of varying the solution concentration of both PMA and PAH from 0.005M to 0.01M for a constant PMA molecular weight of 15K and the result of changing the PMA molecular weight from 15K to a 100K at a constant concentration of 0.01M are shown together in Figure 2.4.2 for films on silicon assembled with the PMA, PAH, and rinse solutions all pH adjusted to 3.5. The measurements of total bilayer thickness (dashed line) were calculated from the slopes of the lines fitted to all of the thickness data as a function of the number of bilayers, while the individual layer thickness values (the bars in the bar chart) represent the average of measurements made before and after the adsorption of a single layer. Using both measures of thickness, a weak

concentration dependence can be observed from Figure 2.4.2. But, within the error of the measurement (~3Å), no PMA molecular weight dependence of the thickness is observed. It is interesting to note that according to the experimental data taken, the 4Å increase in bilayer thickness with solution concentration is due to a 4Å increase in the thickness of the PAH layer and not the PMA layer. Though this increase is still small, it may indicate that only the adsorption of PAH is sensitive to the solution concentration. Much larger and statistically more significant changes in layer thickness can be made through varying the backbone charge density though solution pH to both manipulate the resultant film structure and to understand the nature of sequential adsorption.

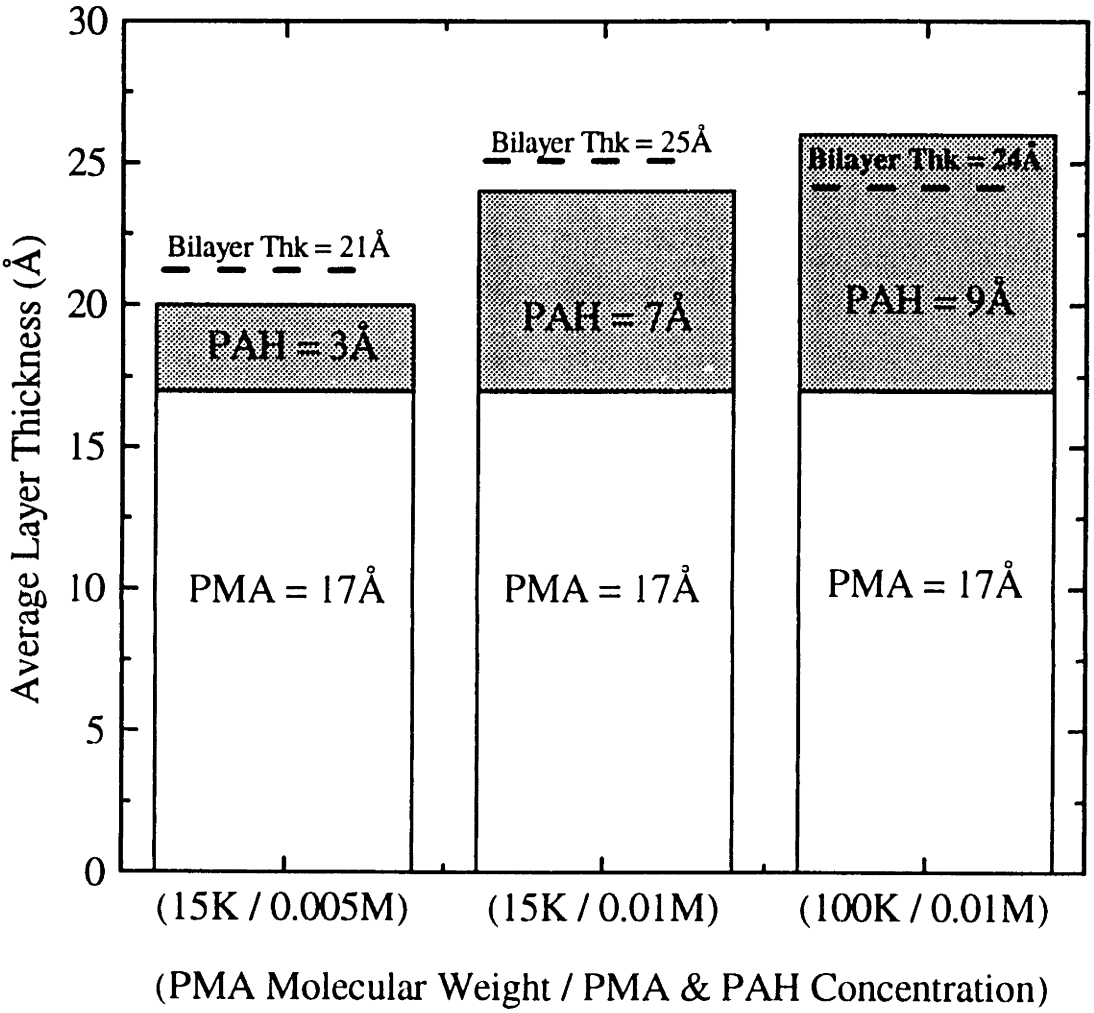

Figure 2.4.2 Layer thickness measured by ellipsometry for PMA and PAH assembled at pH 3.5 on silicon as a function of polyelectrolyte concentration and PMA molecular weight.

2.4.D. The Effect of Solution pH on the Sequential Adsorption of PMA/PAH

In an attempt to understand the factors that dominate the sequential adsorption of PMA with PAH, the thickness contributions of the individual layers of PMA and PAH were measured by ellipsometry for films built on cleaned silicon as the pH of both the PMA solution and the PAH solution were varied. The molecular weight of the PMA and the PAH were held constant at 100K and 50-65K, respectively. Additionally, the solution concentrations of both PMA and PAH were held constant at 0.01M. For films with a PMA pH of 3.5 and a PAH pH of 3.5, the rinse solution was pH adjusted to 3.5 to avoid pH drift. There were no significant thickness differences between these films and those assembled earlier under identical conditions which did not use pH adjusted rinse water. All other pH combinations of PMA and PAH used unadjusted rinse water (pH~5.5). All films except those made with a PMA pH of 2.5, built up with a linear increase in thickness and were very uniform and optically clear. The films made with a PMA pH of 2.5 became cloudy and had a nonlinear build-up above 10 bilayers likely due to the excessively low charge density along the polymer chain.

For each pH condition used, ellipsometry measurements were made on several different silicon substrates for films built to varying thickness. The thickness of individual layers were calculated based on film thickness measurements made before and after the adsorption of a single layer. No significant film thickness difference was observed between films which had been dried after several adsorption steps to obtain single layer thickness data and those which remained wet until they reached their final film thickness. Ellipsometry measurements made on films below 200Å were made by fixing the index of refraction to 1.55 - the average index of refraction found for thicker films. The thickness of the films on both silicon and hydrophilic glass which had been built up to 20 or 30 bilayers were also measured by profilometry. The bilayer thickness of films measured on silicon and on hydrophilic glass by profilometry were an average of 32% and 25% thinner, respectively, than those measured by ellipsometry on silicon. This disagreement can be attributed to combination of the difference in experimental technique used (optical vs. mechanical) which in the past has been measured to be as large as 20% and to the capability of these films to shrink by more than 20% through water loss, independent of

the film structure [123]. To ensure that the films measured here had similar degrees of hydration when measured, ellipsometry measurements were made immediately after the films were pulled out of the last rinsing solution and dried with compressed air. The thickness measurements made by profilometry were taken after all the films were stored at room temperature in ambient humidity for several weeks and, therefore, are also assumed to have similar degrees of hydration. The fact that the same bilayer thickness trends are observed by both ellipsometry and profilometry further supports these assumptions.

The pH response of both the bilayer and the individual layer thickness as measured by ellipsometry can be viewed in Figure 2.4.3. The dashed lines in Figure 2.4.3 denoted the bilayer thickness as calculated from the slope of all of the individual thickness measurements as a function of the number of bilayers. The individual layer thickness contributions from PMA and PAH represent the average of 4 or 5 measurements made at different values of the total film thickness, but in no way imply the existence of discrete layers. The typical standard deviation of the single layer thickness values was measured to be approximately 3Å. Though the agreement between the sum of the average single PMA and PAH layer thickness and the bilayer thickness as measured by the slope of the thickness plot is acceptable, even better agreement can be found for films with 5 bilayers or less as displayed in Figure 2.4.4. This seems to suggest that the structure of the multilayered film may be perturbed at higher numbers of bilayers. Further experimental evidence supporting this assertion will be discussed in the next section of this chapter. However, such effects do not change the overall trends exhibited in Figure 2.4.3.

As can be seen from Figure 2.4.3, there is an overall increase in bilayer thickness, PMA layer thickness, and PAH layer thickness with a decrease in the PMA solution pH as well as with an increase in the PAH solution pH. This trend can be interpreted as being the result of three influences; (1) the variation of the charge of the previously adsorbed PMA layer with changes in the pH of the PAH solution, (2) the increase in PMA adsorption though a decrease in the PMA polymer charge density at decreased PMA pH, and (3) a tendency for more PMA to adsorb onto thicker PAH layers.

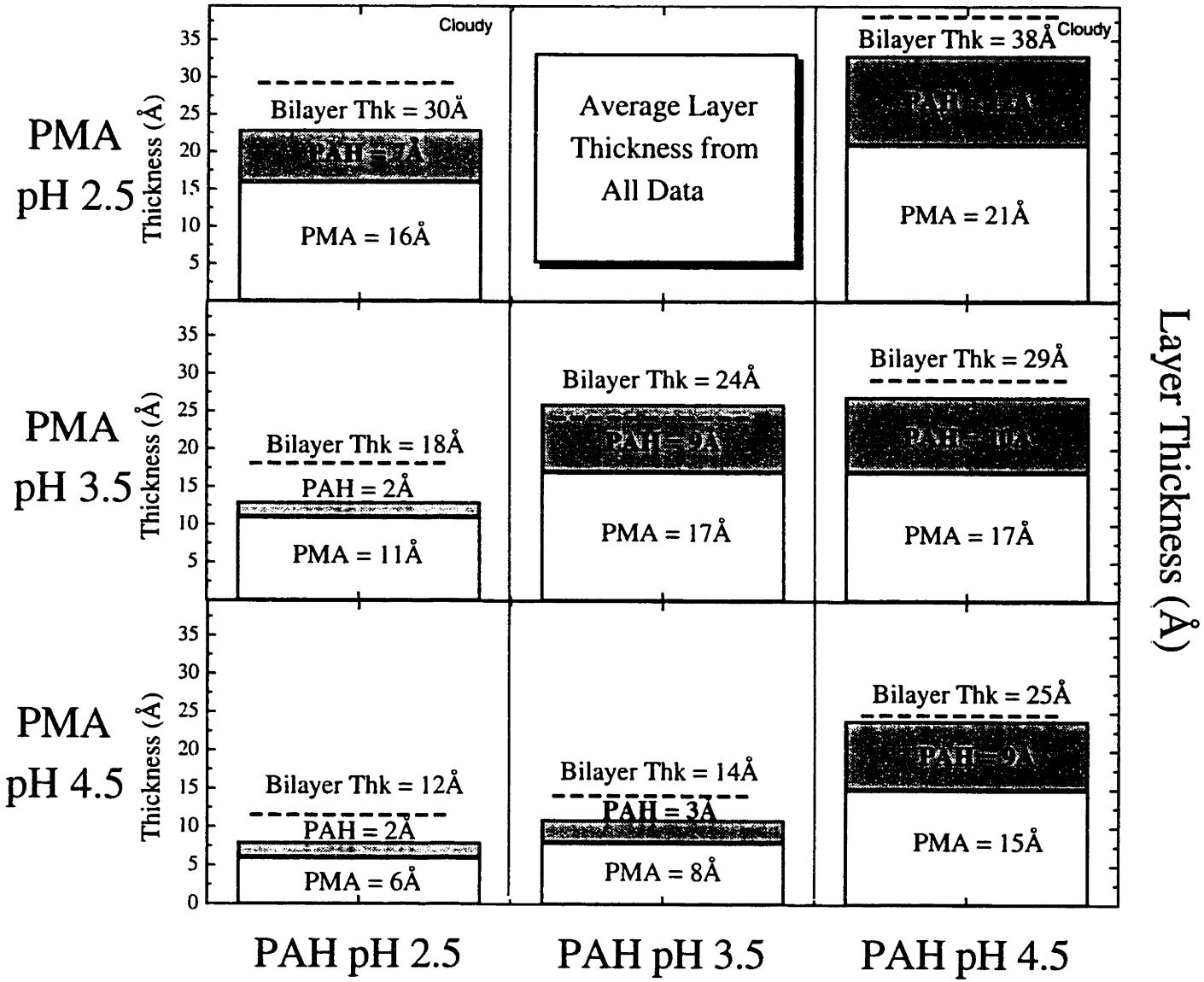

Figure 2.4.3 Average PMA and PAH layer thickness measured for films up to 30 total bilayers by ellipsometry for various values of solution pH.

First the adsorption of PAH onto an adsorbed layer of PMA is considered. For both contact-ion dominated and surface charge dominated sequential adsorption, an increase in the amount of PAH adsorbed with increasing PAH pH can be understood in terms of the promotion of adsorption through a change in the degree of dissociation of the adsorbed PMA segments. From the data in Figure 2.4.3 taken for films up to 30 bilayers thick, it can be observed that the film structure is relatively the same when the PAH pH is either the same or higher than the pH at which the PMA was adsorbed. This corresponds to the case where the surface charge produced from the adsorption of PMA is either maintained (cells along the plot diagonal) or increased (cells in the upper right) when placed into the PAH solution. The films which have a PAH pH lower than the pH at which the PMA was adsorbed (cells in the lower left) correspond to the case where the PMA charge is decreased when placed in the PAH solution. Therefore, these films show significantly lower amounts of adsorbed PAH. Because there was no consistent trend of increased adsorption with increased underlying layer thickness for films which have the same difference between PMA and PAH solution pH, it appears that this is a surface charge dominated effect.

Secondly, the adsorption of PMA onto a layer of PAH is considered. Because the charges of the PAH segments are pH independent in solution for the conditions examined, they are also assumed to be pH independent when part of an adsorbed molecule. Therefore, for surface charge dominated adsorption on a monolayer of PAH, the thickness of the PMA layer should only depend on the pH of the PMA solution with a lower pH leading to a lower degree of dissociation and consequently a larger thickness. However, for contact-ion pair dominated adsorption, the amount of PMA adsorbed should depend on both the thickness of the underlying PAH layer and on the pH of the PMA solution whereby a thicker PAH layer provides more sites for the formation of contact-ion pairs with the charged PMA segments. It can be observed from either Figure 2.4.3 or 2.4.4 that the amount of PMA adsorbed is dependent on both PMA pH and PAH layer thickness which implies that the adsorption of PMA onto PAH is dominated by the formation of contact-ion pairs.

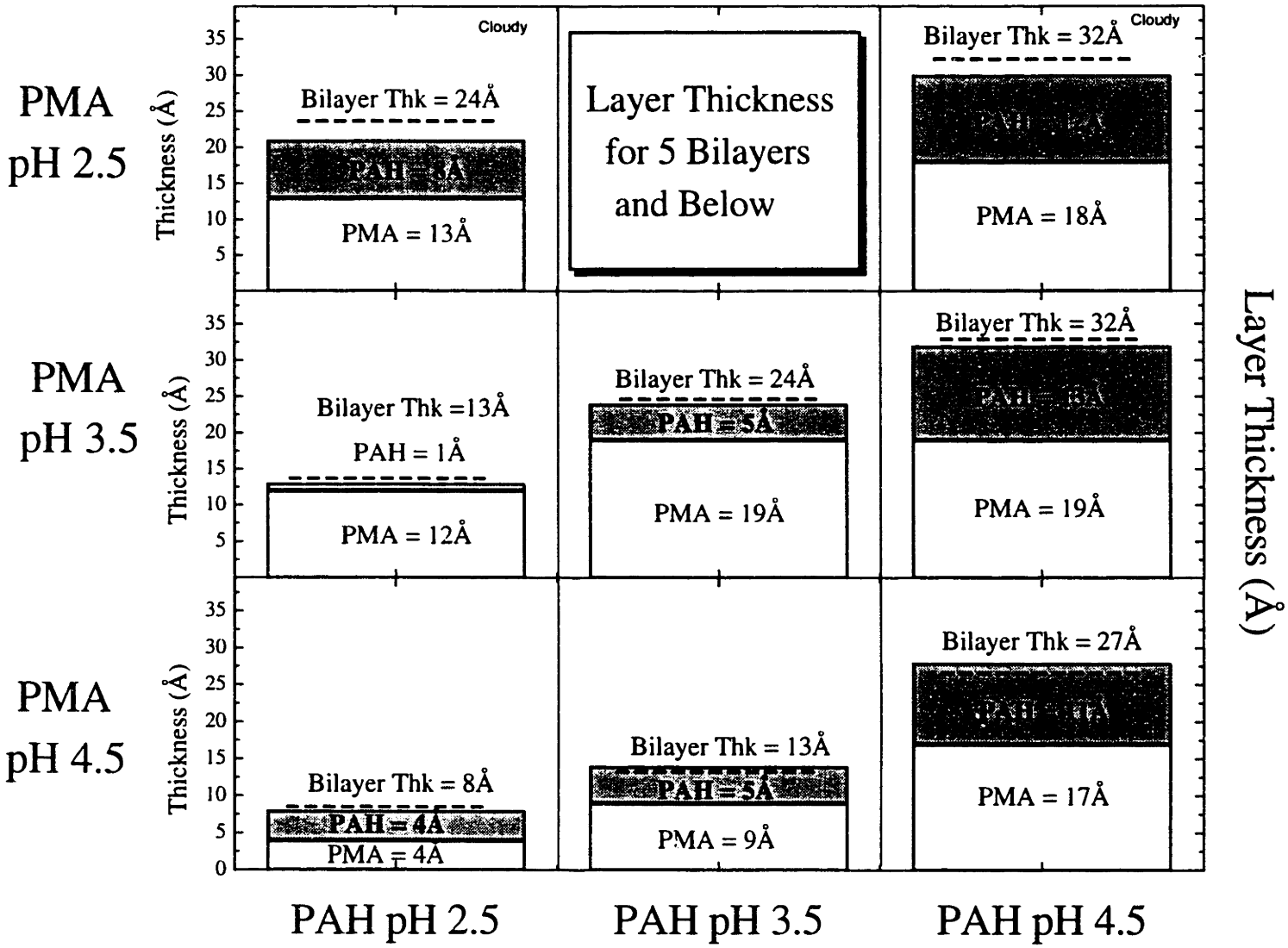

Figure 2.4.4 Average PMA and PAH layer thickness measured for films of 5 bilayers and below by ellipsometry for various values of solution pH.

In comparison, preliminary results for PAH and poly(acrylic acid) (PAA) have shown surface charge dominated adsorption with roughly the same thickness of PAA adsorbed at a given pH for PAH surfaces with varying thickness [124]. The likely reason for the difference between PMA and PAA, which chemically differ only in the substitution of a methyl group for a hydrogen, is the dissociation differences of the carboxylic acid due to this local environment effect. From the titration curve, it can be observed that in addition to the globular transition that PMA undergoes, the solution dissociation of PAA is much higher than the PMA. At pH values were PMA in solution is calculated to have only a degree of ionization of 5%, PAA is calculated to have a degree of ionization of 10%.

Instead of concluding that the adsorption of PMA onto PAH is driven by the formation of contact-ion pairs, one could argue that the trends displayed in Figures 2.4.3 and 2.4.4 are the result of going from incomplete PAH coverage of 2-5Å to complete coverage of 5-12Å. However, sessile water drop contact angle measurements of the films on silicon suggest that all the films have roughly the same surface coverage. A more likely explanation to account for the variation of PMA thickness with surface charge dominated adsorption is desorption of the weakly bonded molecule when placed in the PAH solution with a lower pH. While rapid desorption is usually not observed for well adhered polyelectrolyte films, it can occur for weakly charged polymers on weakly charged surfaces. It is interesting to note that the decrease in PMA thickness scales with the estimated amount of decrease in PMA charge density while in the PAH solution. Correspondingly, the thinnest measured PMA layer is obtained for a PMA layer adsorbed at pH 4.5 which is then placed in a solution of PAH at a pH of 2.5.

For contact-ion pair dominated sequential adsorption, the system is assumed to approach a constant charge stoichiometry which can be related to the layer thickness ratio with proper assumptions regarding the size and degree of dissociation of the polymers used. However, because the layer thickness ratio (PMA thk :PAH thk) can be made to fluctuate drastically when the thickness of the individual layers are varied by only one standard deviation (±3Å), this experimental data may not be precise enough to discern whether a constant charge stoichiometry exist. A more sensitive measurement technique

would be needed to provide more accurate estimates of both the layer thickness ratio and the charge stoichiometry. Taken as a whole, the pH response of the sequential adsorption of PMA with PAH appears to be somewhere in between pure contact-ion pair dominated behavior and pure surface charge dominated behavior. The adsorption of PAH onto PMA is more consistent with surface charge dominated adsorption while the adsorption of PMA onto PAH is more consistent with contact-ion pair dominated adsorption. Regardless of which adsorption process ultimately dominates, changing the pH of the polyelectrolyte solutions still provides an easy and effective way to manipulate the structure of sequentially adsorbed films containing weak polyelectrolytes in a manner which, up to this point, has not been fully realized in the literature.

An even more versatile way to change the structure of a sequentially adsorbed film containing a weak polyelectrolyte, is to vary both the solution pH and the solution ionic strength. A systematic study exploring these parameters has not been made. From the limited data which has been taken, it appears that at higher pH values (~4.5) salt could be added to the PMA and PAH solutions to increase the bilayer thickness to over 100Å, but that at lower pH values salt causes lack of assembly. This again shows the extremely flexible nature of sequential adsorption.

2.4.E. Introduction to the Use of Contact Angle Measurements and Methylene Blue Adsorption as Molecular Surface Probes of PMA/PAH Films

Further structural information on the PMA/PAH films made with various solution pH values can be obtained through sessile water drop contact angle measurements and the adsorption of the positively charged methylene blue dye. The use of contact angle measurements is widespread both in research and industry to assess the wettability of a surface. The technique usually involves placing a small drop of deionized water (~ 5µl) onto a relatively flat surface and measuring the "recently advanced" angle the drop makes with surface as depicted in Figure 2.4.5. Young describes this contact angle, θ, as the result of balancing the forces resulting from the air-solid surface energy (γ_s), the solid-liquid interfacial energy (γ_{sl}), and the air-liquid interfacial tension (γ_l) in the following expression [125]:

$$\gamma_s = \gamma_{sl} + \gamma_l \cos\theta \,. \qquad (2.4.1)$$

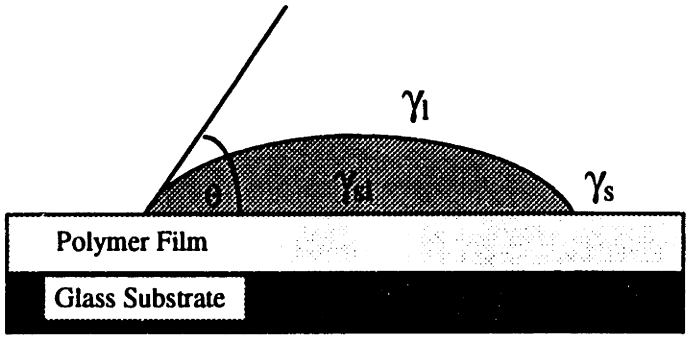

Figure 2.4.5. Schematic of a sessile water drop on a flat polymer surface. The water drop forms a contact angle of θ due to balancing of the interfacial tensions of the air-solid (γ_s), the solid-liquid (γ_{sl}), and the air-liquid (γ_l) interfaces.

This equation shows that for water (γ_l = constant), the wettability will decrease and the contact angle will increase as γ_s is decreased and/or γ_{sl} is increased. However, it has been shown that these two parameters, γ_{sl} and γ_s, are related. For apolar liquids and solids the previous expression can be simplified to [126]

$$\gamma_s = \gamma_l (1+\cos\theta)^2 / 4 \,. \qquad (2.4.2)$$

However, for polar liquids and surfaces which also have acid-base interaction, the expression will have additional contributions to the interfacial energy from the Lifshitz-van der Waals interactions (γ^{LW}) and the acid-base interactions ($\gamma^{A\text{-}B}$) to give

$$\gamma_l (1+\cos\theta) = 2\left[\sqrt{\gamma_s^{LW}\gamma_l^{LW}} + \sqrt{\gamma_s^{A}\gamma_l^{B}} + \sqrt{\gamma_s^{B}\gamma_l^{A}}\right] \qquad (2.4.3)$$

From this more complicated expression, it can still be observed that the contact angle θ will decrease as the terms for the solid-air surface energy (γ_s^{LW}, γ_s^{A}, and γ_s^{B}) are increased and the terms for the liquid-air interfacial energy (γ_l^{LW}, γ_l^{A}, and γ_l^{B}) remain constant. Through this formalism, the contact angle becomes more than the balance between air, liquid, and solid interfacial energies as expressed by Young's equation. It becomes a true measure of the surface energy of the solid material as probed by a specific liquid, which in this case is water. Because the above expressions assume a flat solid surface with no roughness, a correction factor, which assumes that the primary effect of surface roughness is to increase the actual surface area, has been put forth which results in a measured contact angle which is less than the "flat" contact angle for angles below 90° and greater than the "flat" contact angle above 90° [127]. Given the typical low roughness values of sequentially adsorbed films, the roughness correction is disregarded in the analysis of the films presented here. Overall, sessile drop contact angle measurements provide a simple, yet powerful means to assess the surface energy of a material. Within this thesis, contact angle measurements will be made to characterize the nature of the surface following the adsorption of polyelectrolytes which potentially differ in hydrophobicity as well as in charge from the underlying adsorbed polymer.

It should be kept in mind that contact angle measurements probe approximately the top 5-10Å of a film surface which has been collapsed from the hydrated solution structure after drying [127]. Therefore, a surface which is collapsed and is indicated by contact angle measurements to be a homogenous layer of one material may, in fact, have different properties when hydrated in solution. However, probing the collapsed surface structure using contact angle still provides a powerful means to characterize the properties of a polyelectrolyte surface.

Another characterization technique which does not suffer from this limitation to the same extent because it is performed in the hydrated state is the adsorption of the positively charged molecule of methylene blue. The preferential adsorption of the methylene blue to negatively charged species has been widely used in biology as a selective stain [128] and in industry as a quality control test [129]. Here we use methylene blue as a relative gauge of the surface charge. Further work, including taking into account

the effects of all solution variables and non-electrostatic interactions, would be necessary to make this technique into a truly quantitative measure of the surface charge.

Contact angle measurements of all the PMA/PAH films made with the various pH combinations denoted in the previous pH study were made with increasing number of layers deposited on separate substrates. The reported contact angles represent the average of 3 to 4 drops measured on both ends of the drop after a thermal treatment of one hour at 92° C in air and storing at room temperature in ambient humidity for 2 days. The thermal treatment was performed in an effort to keep the level of hydration in all the films the same. The standard deviation of the measurements was typically lower than 3° and measurements below 10° were all set to 10° due to the low resolution below this value. The contact angle measurements on the hydrophilic glass slides were made in the center of the substrate to allow the bottom region to be used for the adsorption of methylene blue. The measurements made at PAH pH 2.5 / PMA pH 4.5 and at PAH pH 4.5 / PMA pH 3.5 were made on glass which, while still clean, had a higher bare-surface contact angle (not shown). According to work on PAA/PAH, this difference does not significantly change the contact angle of subsequent layers.

The methylene blue adsorption was performed by submerging the substrate into a 0.005 M methylene blue solution at pH 4.0 for 10 minutes, dipping the substrate into a static rinse bath of pH 4.0 water for 1 minute, gently rinsing with water also at pH 4.0, and then blowing the substrate dry with compressed air. The absorbance of the film was then immediately measured by UV-Visible spectroscopy. The reported values are the absorbance peak maximum, but the same trends can be obtained when the area under the absorbance curve is used. The chemical structure of methylene blue and a typical absorbance curve can be viewed in Figure 2.4.6.

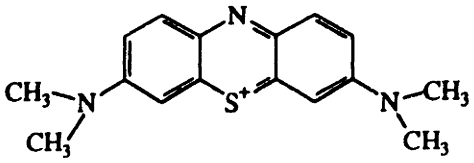

Methylene Blue Dye

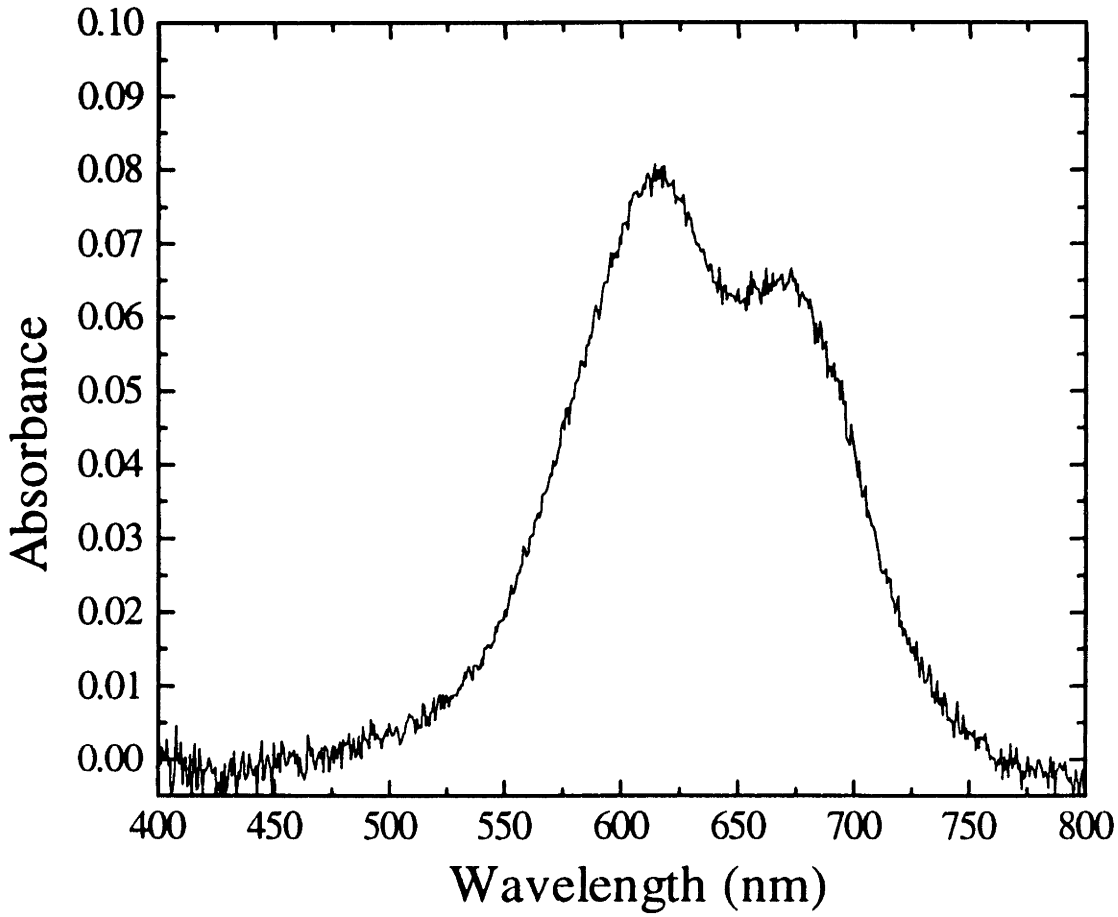

Figure 2.4.6. Visible absorbance spectrum of adsorbed methylene blue dye.

2.4.F. Experimental Results of Contact Angle Measurements and Methylene Blue Adsorption Studies

Figure 2.4.7 displays the results of the contact angle measurements of each layer up to 8 layers (4 bilayers) on glass for the pH conditions previously considered. The interpretation of this data is based on the wetting differences between the hydrophilic PMA, which contains one polar carboxylic functional group per repeat unit, and the more hydrophobic PAH which contains a less hydrophilic amine functional group. The oscillation observed in nearly all the cells of Figure 2.4.7 is caused by the alternation between a PAH rich outermost layer and a PMA rich outermost layer, which is central to the process of sequential adsorption. For example, it can be observed from the data with PMA as the last polymer adsorbed (whole numbers of the bilayers), that under all pH conditions, hydrophilic surfaces could be achieved with contact angles of 20° or less. The fact that some data points are higher than the self-imposed wettability measurement limit of 10° suggests that the more hydrophobic PAH segments may have penetrated to the surface of the more hydrophilic PMA layer. The likelihood of penetration, in turn, would be expected to increase when the PMA is thin relative to the PAH layer. Using the measured layer thickness values displayed in Figure 2.4.4 for films with a total thickness of 5 bilayers and less, experimental confirmation of this expectation can be obtained by considering the two films with the thinnest PMA layers (4 and 9Å) which both show deviation from complete wetting with the larger deviation coming from the thinner PMA layer. With the exception of a few fluctuations for the films assembled with a PAH pH of 4.5 and a PMA pH of 3.5, all of the films with a thick PMA outermost layer showed complete wettability.

When PAH is the outermost layer (data at half integer values for the number of bilayers), the wettability appears to be even more dependent on the film structure. For example, considering the values at 3.5 bilayers which have the smallest influence of surface for the data displayed, the films which have an average PAH thickness of 5Å and below (PAH pH/PMA pH = 3.5/3.5, 3.5/4.5, 2.5/3.5, 2.5/4.5) typically gave relatively low contact angles of between 20° and 35°. The contact angle data taken at PMA pH 3.5 /

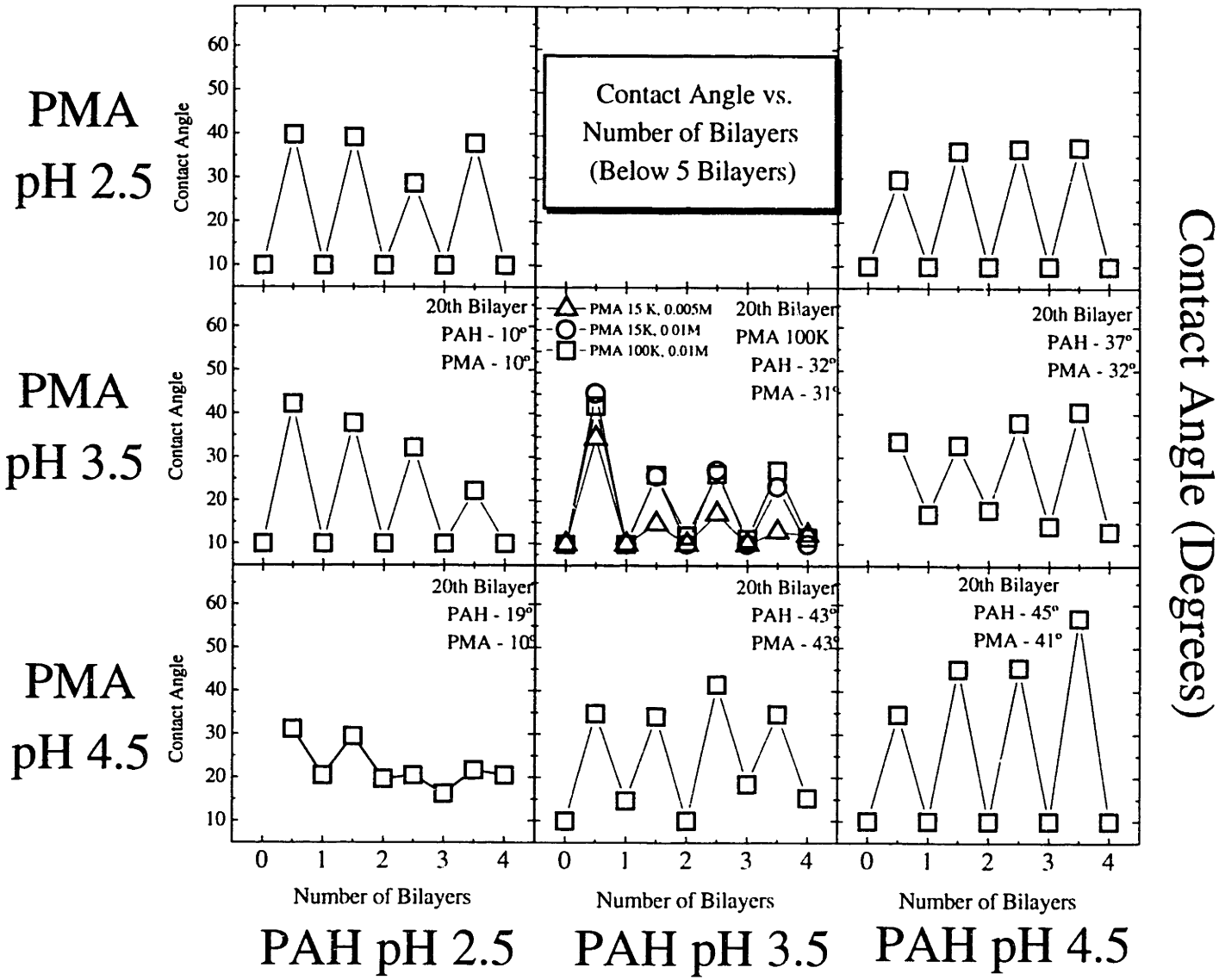

Figure 2.4.7 Sessile water drop contact angle measurements made on PMA/PAH films sequentially adsorbed on glass at various pH conditions for increasing number of bilayers. Interger represent PMA as the last layer adsorbed.

PAH pH 3.5 for varying PMA molecular weight and polyelectrolyte concentration show similar trends. In contrast, films with thicker PAH layers had average contact angles at 3.5 bilayers which were greater than 35° and individual film averages which reached as high as 55°.

Additionally, trends in the contact angle measurements with increasing number of bilayers for films with PAH as the last polymer adsorbed can be observed in Figure 2.4.7. For the two thinnest PAH layers (PAH pH/PMA pH = 2.5/3.5, 2.5/4.5), the contact angle decreases with increasing number of bilayers which implies that the layers become more interpenetrated as the film increases in thickness. For thicker PAH layers (all other data), the contact angle either remains relatively constant or increases with increasing number of bilayers. Further evidence for mixing with increasing number of bilayers was observed from the additional data which was taken for the 10^{th} and 20^{th} bilayer. The contact angle measurements for the 20^{th} bilayer are summarized in the upper right hand corner of each cell. The contact angles of the thicker films made with a PMA pH of 2.5 were excluded from consideration because of their tendency to build non-linearly and become cloudy at a higher numbers of bilayers. From this additional data, it can be observed that the decrease in contact angle for the thin PAH layers persists with increasing number of bilayers. It can also be seen that most of the films which gave either constant or increasing PAH contact angles over the first 4 bilayers, gave higher contact angle values as the number of bilayers was increased further. Moreover, all of the films with thicker PAH layers showed a substantial decrease in the wettability of the PMA outermost surface from being nearly complete wettability (~10°) at low number of bilayers to being nearly indistinguishable from the PAH outermost layers (32-43°) at 20 bilayers. While there was more scatter in the thickness data at higher numbers of bilayers, no systematic increase or decrease in the individual layer thickness which could account for this response was observed. Therefore, these changes in wettability are believed to be due to an increase in the mixing of the layers to form a relatively heterogeneous surface. Though the collapsed surfaces may be different from the hydrated surfaces, the continued linear build-up implies that sequential adsorption can still occur on a heterogeneous surface containing both PMA and PAH

segments as has been previously discussed in the description of sequential adsorption through contact-ion pair formation [71].

To further characterize the structure of the sequentially adsorbed films of PMA and PAH in terms of the surface charge, experiments involving the adsorption of methylene blue, a positively charged dye molecule, to the outermost surface of the same films mentioned above was undertaken. The amount of dye adsorbed to the surface was characterized by UV-Visible spectroscopy and assumed to be proportional to the amount of negative charge present on the surface. Therefore, the absorbance of the adsorbed dye is expected to oscillate between very little on the PAH outermost surfaces and significantly more on the PMA outermost surfaces. The results of these experiments are summarized in Figure 2.4.8 as a function of the PMA and PAH solution pH used during assembly. The general trend observed in this figure is that relatively small oscillations are observed at PMA pH 4.5, larger oscillations, which appear to scale with the thickness of the PMA layer, are observed at PMA pH 3.5, and at PMA pH 2.5 very large oscillations are observed.

The trend with PMA solution pH can be understood in terms of the difference between PMA dissociation in the methylene blue solution at pH 4.0 and the PMA dissociation in the PMA solution during adsorption. For example, when a PMA layer is adsorbed at pH 4.5, it obtains some self-limiting thickness which is not only dependent on the surface charge, but also on the segmental repulsion of the dissociated PMA segments. When the film is then rinsed, dried, and placed in the methylene blue solution at pH 4.0, the PMA is collapsed, re-hydrated, and partially re-equilibrated to the new solution conditions. However, because of the lower pH of the methylene blue solution, the adsorbed segments have lower charge than they did during their initial adsorption and the amount of methylene blue adsorbed is small. For the case when the PMA layer is adsorbed at a lower pH (2.5 and 3.5) than the methylene blue solution, the negative charge of the adsorbed segment is much higher than it was during adsorption and therefore the amount of methylene blue adsorbed will increase to give an overall larger oscillation. Therefore, an increase in the level of oscillation with a decrease in the PMA pH is predicted.

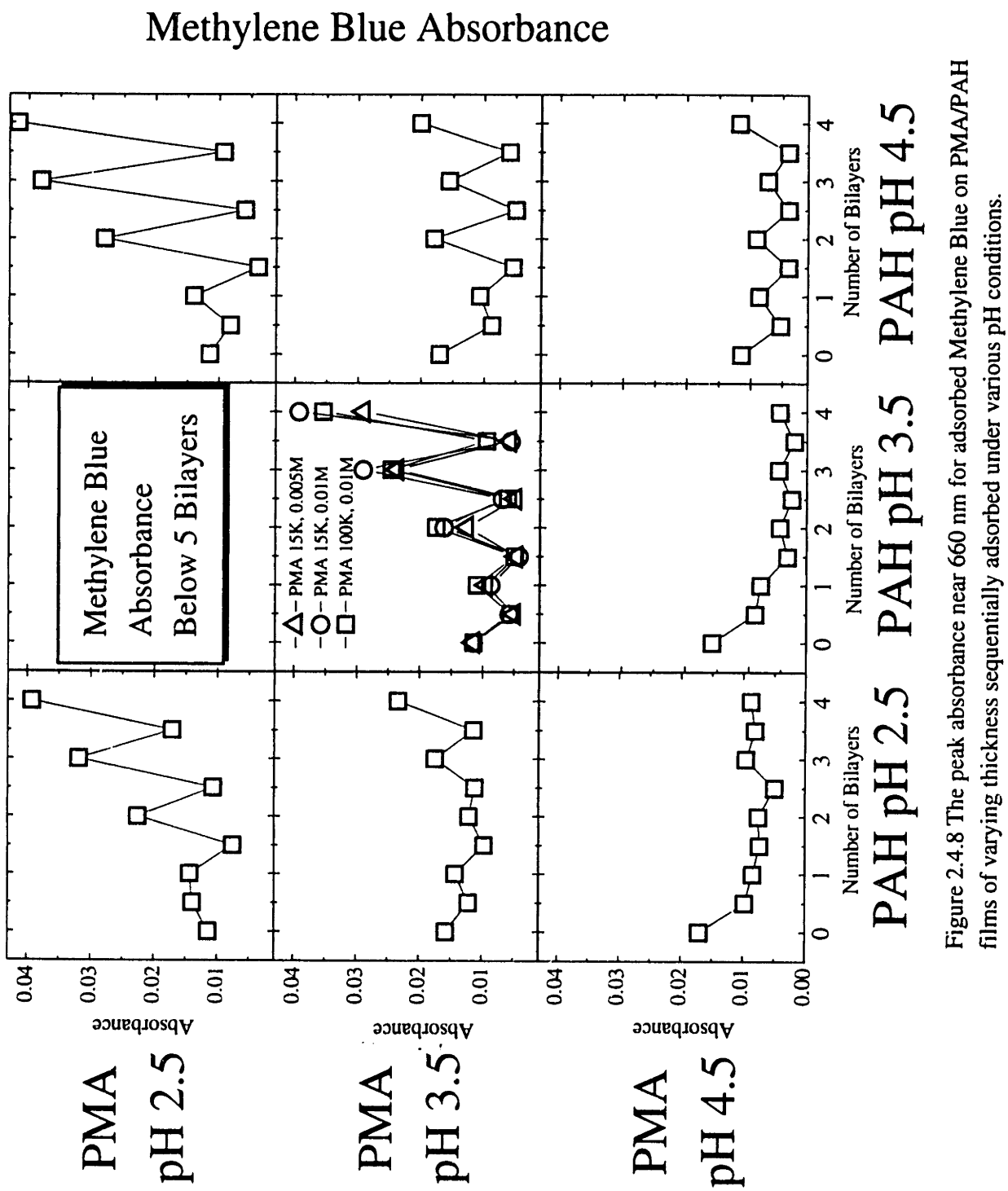

Figure 2.4.8 The peak absorbance near 660 nm for adsorbed Methylene Blue on PMA/PAH films of varying thickness sequentially adsorbed under various pH conditions.

Also predicted is an increase in methylene blue adsorption which scales with the thickness of the PMA layer due to an increase in the number of negatively charged sites near the surface. While these trends are observed in Figure 2.4.7, additional increases in the amount of dye adsorbed both on the PAH and PMA surfaces with an increasing number of bilayers can be observed under several different pH conditions. From the additional data taken at 10 and 20 bilayers (not shown), it was observed that the dye absorbance reached a maximum for both PAH and PMA surfaces at a total thickness of 200-300Å for all films except those with a PMA pH of 2.5 which turned cloudy. For films with a total thickness larger than this, a decrease in dye adsorption followed the maximum. However, in all cases, the oscillation between the dye adsorbed on a PAH and PMA layer was maintained. From the fact that a maximum is observed on both the PAH and PMA surfaces and at the same thickness for films made under a variety of processing conditions, it is concluded that the increase in dye absorbance with increasing number of bilayers is likely due to the penetration of the dye into the bulk of the film rather than to any changes which occur on the film surface. The decrease in absorbance observed after the maximum is reached, however, is likely due to an increase in the amount of positive charge from PAH segments on the outermost surface with increasing number of bilayers. This is consistent with the increase in contact angle also observed for these same films.

In comparison to the results taken on bilayers of PAA and PAH, the amount of methylene blue adsorbed for the PMA/PAH system is much lower [124]. A typical methylene blue peak absorbance of 0.1 units was observed for the adsorption on a top layer of PAA at 4 bilayers, but only a maximum of 0.04 was observed for a top layer of PMA at 4 bilayers. This difference can be attributed to the fact that at a given pH, PAA is more dissociated than PMA (as has been previously discussed) and that the methylene blue adsorption has been optimized for sensitivity to the case of PAA. It is believed that if the pH of the methylene blue solution was increased above 4.0, the magnitude of the adsorption on PMA would become more comparable to that on PAA at pH 4.0.

Overall, characterization of the PMA/PAH sequentially adsorbed films via contact angle measurements and methylene blue adsorption indicate that for a small number of total bilayers, the amount of surface penetration from the underlying layers depends on the

thickness of the top layer relative to the underlying layer. At higher numbers of total bilayers, the film surfaces become better mixed and both types of surfaces are dominated by one component, as determined by contact angle measurements. However, an oscillation in the surface charge, as measured by methylene blue adsorption, and a linear build-up, as measured by ellipsometry, still occurs. Taken together, this implies that the sequential adsorption of PMA with PAH is better characterized by contact-ion pair dominated adsorption.

2.4.G. Experimental Results of Small Angle X-ray Reflectivity and Cross-Sectional Transmission Electron Microscopy Studies

In addition to the characterization of layer thickness and surface properties of the sequentially adsorbed films of PMA/PAH mentioned previously, further characterization has been done using the techniques of Small Angle X-ray Reflectivity (SAXR) and cross-sectional Transmission Electron Microscopy (TEM) through collaborations with other researchers [130]. Both techniques were used to analyze films of PMA and PAH layers which were both adsorbed from 0.005M solutions at a pH of 3.5 with no added salt.

Figure 2.4.9 displays the scattering curves of PMA/PAH films, built to a thickness of 20 and 40 bilayers on silicon, as measured by SAXR. From the characteristic Kessieg fringes, which result from the interference of waves reflected from the film-substrate and the film-air interfaces, an average film thickness which corresponds to a bilayer thickness of 21Å was measured. This agreed well with the thickness measurements of 20Å and 21Å per bilayer made by profilometry and ellipsometry, respectively, on the same films. The line indicates the fit made to the experimental data from which the air-film r.m.s. roughness was estimated to increase from 18Å for the 20 bilayer film to 29Å for the 40 bilayer film. An increase in roughness was also observed for films which were dried for 5 minutes after each rinse with air heated to 80° (17Å for 20 bilayers and 21Å for 40 bilayers), but with an overall lower roughness and a slightly lower bilayer thickness of 19Å. The observation that the layers of PMA and PAH become better mixed with increasing number of bilayers may be linked to this increase in surface roughness. However, a comprehensive series of experiments would need to be performed to truly

substantiate this relationship. Additional details regarding the internal structure of these films could not be obtained by SAXR due to the low electron density contrast between the polymer molecules.

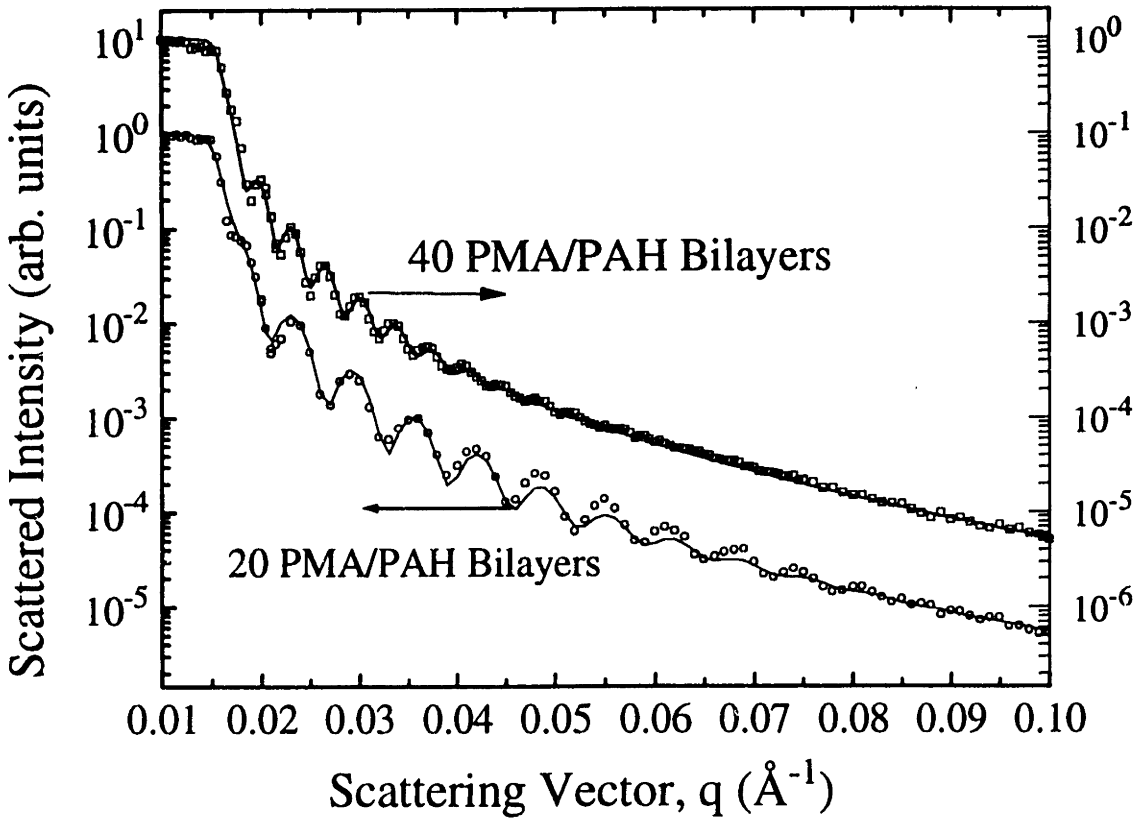

Figure 2.4.9 Small Angle X-ray Reflectivity data taken on sequentially adsorbed films of PMA/PAH with a thickness of 20 and 40 bilayers on silicon.

In order to increase the contrast between layers, studies have been undertaken to incorporate molecules containing high atomic mass elements, such as ruthenium, into sequentially adsorbed film heterostructures. The first such film which was fabricated involved a heterostructure consisting of a "high atomic number" block of five bilayers of the ruthenium containing molecules shown in Figure 2.4.10 [a negatively charged dye and a positively charged polyester oligomer (~7 repeat units)] alternating with a "low atomic number" block of four bilayers of PMA/PAH. By analyzing this film with cross-sectional TEM, a distinct layering of the individual blocks could be observed as shown in Figure 2.4.11. This represented the first time that such cross-sectional images of sequential adsorbed films have been obtained.

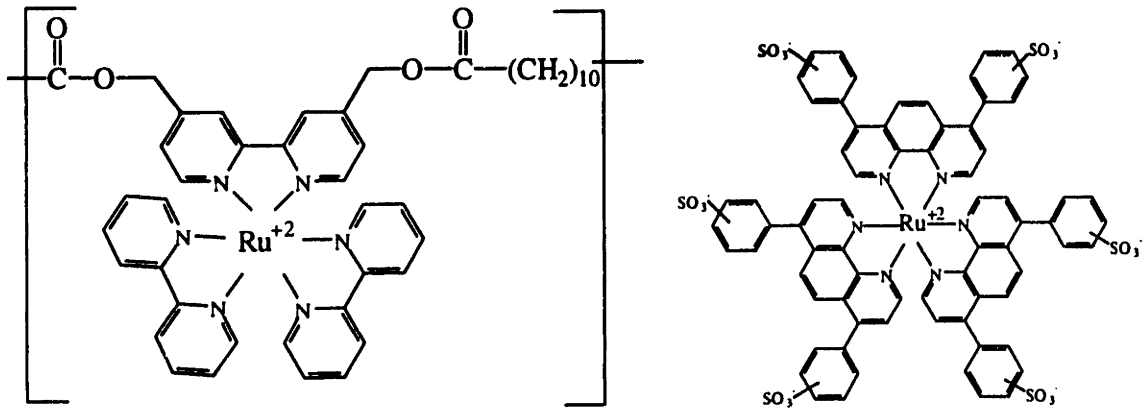

Ruthenium containing Polyester
(Ru Polyester)

Ruthenium Containing Dye
(Ru Dye)

Figure 2.4.10 Chemical structure of ruthenium containing polyester and dye

Based on measurements made by ellipsometry for films on silicon which were dipped with the epoxy substrate used for TEM, the thickness values of the two different blocks were estimated to be 80Å for the $(PMA/PAH)_4$ block and 45Å for the $(Ru\ Dye/Ru\ Polyester)_5$ block for a total film thickness of 625Å. However, by TEM the total film thickness is estimated to be approximately only 500Å which may indicate a difference in build-up between the epoxy substrate and the silicon substrate. It can also be observed from this image that the PMA/PAH block which was first deposited onto the epoxy appears dark while the next Ru containing block appears light. This is the opposite of what was predicted from the electron density argument given above and is currently the subject of continued research. Possible explanations for the reversed contrast are differences in each layer's susceptibility to damage by the electron beam and a preferential enrichment of the PMA/PAH block layer with high electron density impurities during the sample preparation. Assuming that the contrast is still a true representation of the layering of the assembled blocks, the estimated block thickness values measured from this image are 40Å for the $(PMA/PAH)_4$ (dark) block and 30Å for the $(Ru\ Dye/Ru\ Polyester)_5$ (light) block. This difference from the ellipsometry data taken

A subsequent ruthenium containing heterostructure which used 10 bilayer blocks of PMA/PAH and a decreasing number of Ru containing bilayers (10,6,3,1), gave thicker and more easily distinguished block layers as shown in Figure 2.4.12 [130]. It can be observed from the bottom image within this figure that the blocks could conformally coat large features left by previous adsorption steps. A slight decrease in thickness of the ruthenium containing (light) blocks with increasing numbers of blocks could be observed in the top image with the last ruthenium block, which consisted of only one bilayer, being nearly indistinguishable. The lower contrast for this last ruthenium containing block is no doubt linked to the thinness of the layer, but it may also be affected by what appears to be an increase in roughness with increasing number of bilayers as was previously observed for films of PMA/PAH (no ruthenium containing layers) assembled under identical conditions. Further interpretation of these images can only come after more is known about the origins of the layer contrast and these observations are substantiated by the examination of other films. Nevertheless, from this preliminary work, it does appears that, at least with blocks of bilayers, true layering can be obtained on the order of 50Å.

Figure 2.4.11. Cross-sectional TEM image of a sequentially adsorbed heterostructure composed of five alternating blocks of (PAH/PMA)$_2$ [dark layers] and (Ru Polyester/Ru Dye)$_2$ [light layers], assembled on an epoxy substrate. The thickness of the light Ru-containing layers is approximately 3.0 nm and the intervening dark (PAH/PMA)$_2$ is approximately 4.0 nm thick.

Figure 2.4.12. Cross-sectional TEM image of 5 blocks of (PAH/PMA)10 alternating with 4 Ru Polyester/ Ru dye blocks with a decreasing number of bilayers of 10, 6, 3 and 1 (as denoted) on an epoxy substrate. The measured average PAH/PMA block is 17 nm and the measured thicknesses of the Ru-containing blocks are 8.5, 6.5, 6.0, and 5.0 nm (±0.5 nm) for blocks consisting of 10, 6, 3, and 1 bilayers, respectively.

2.5 Concluding Remarks

Within this chapter it has been shown that the structure of a sequentially adsorbed film can be manipulated through variation in the solution ionic strength, pH, and polymer concentration, as well as through selection of the type of polyelectrolyte used. For the combination of a strong polyanion and a strong polycation (SPS/PAH), the bilayer thickness is characterized by a weak molecular weight dependence which increases with solution ionic strength and which scales with the square root of the salt concentration for higher molecular weight polyanion chains with solution ionic strengths of 1M NaCl and below. For the combination of a weak polyanion and a strong polycation (PMA/PAH), the bilayer and single layer thickness of both the polyanion and polycation decreases when the pH of the polycation solution is lower than the pH of the polyanion solution. When the pH of the two solutions are either matched or the polycation solution pH is greater than that of the polyanion, the thickness of both the single layers and the bilayer are nearly constant. The resulting structures of these films are characterized by increased mixing of the layers with an increasing number of bilayers. However, even at higher numbers of bilayers, the surface charge oscillates with adsorption of the oppositely charged polyelectrolytes and the films continue to increase linearly in thickness.

Chapter 3. - Sequential Adsorption of Precursor Polymers: Poly(amic acid) with Various Electroactive Polymers

3.1 Introductory Remarks

Because of their tailorability, thermal stability, and low dielectric constant, polyimides have wide uses in the microelectronics industry for such applications as circuit board coatings and dielectric layers. Typically, polyimides are processed by spin-coating a polyimide precursor, poly(amic acid), in polar aprotic organic solvents, and then thermally converting the poly(amic acid) into a robust, intractable polyimide. While spin coating is a mechanically simply process and produces films of uniform thickness, it is limited to nearly planar substrates and usually results in large losses of material. Film fabrication using sequential adsorption of the poly(amic acid) overcomes some of these obstacles. Furthermore, because the chemical structure of polyimides can readily be synthetically altered, the layer-by-layer assembly of polyimide precursors could represent a means of incorporating new and novel materials into robust ultra-thin films with designed supramolecular structures. In this chapter, we specifically present the fabrication of thin films of poly(4,4'-oxydiphenylene pyromellitimide) (PMDA-ODA) through sequential adsorption of a precursor poly(amic acid) with three different charged molecules - poly(allylamine hydrochloride), polyaniline, and a poly(p-phenylene vinylene) precursor.

3.2 Experimental

The poly(amic acid) (PAmA) was obtained as a 11% by weight solution of poly(4,4'-oxydiphenylenepyromellitamic acid), the precursor to poly(4,4'-oxydiphenylene pyromellitimide) (PMDA-ODA), in dimethyl acetamide from Dr. Anne K. St. Clair of NASA Langley Research Center. The polyallylamine hydrochloride (PAH) (MW~28,000g/mole) and poly(styrene sulfonate) SPS (MW ~ 70,000 g/mole) were obtained from Aldrich Chemical and used without further purification. The poly(vinylpyrrolidone) (PVP) was obtained from American Polymer Standards Corp. (M_w = 125,400, M_n = 45,900) and used without further purification. The poly(phenylene

vinylene) precursor, was synthesized by the tetrahydrothiophene (THT) route and was provided by Dr. B. R. Hsieh of the Xerox corporation as an aqueous, ~10^{-3} moles/liter solution (based on repeat unit molecular weight) [131].

The polyaniline (PAni) was synthesized chemically by the direct oxidation of aniline as has been previously described [132]. The resultant PAni powder was then dissolved in dimethyl acetamide (DMAc) at 18 mg/ml by stirring overnight, sonicating for 8-10 hours, and filtering through a 2 μm and a 0.45 μm filter. The aqueous solution used for dipping was prepared by slowly adding one part (by volume) of the PAni solution to nine parts water, adjusting the pH to 2.5-2.6 with methane sulfonic acid (MeSA), and syringe filtering through a 0.45 m filter [133] . From results of similar syntheses, the number average molecular weight is estimated to be 20-25K with a polydispersity of about 2.5 [134,135]. The overall result is a 10% DMAc: 90% H_2O, ~10^{-2} moles/l dipping solution [based on a two aniline (181g/monomole) repeat unit] of the partially oxidized emeraldine base form of PAni. This PAni can be rendered conductive through the generation of stable, positive charge carriers along the polymer backbone by protonic "doping" at the nitrogen atom [136].

The typical PAmA aqueous solution was prepared by first diluting the 11 wt. % solution to a 1 % solution in DMAc, and then further diluting with water until a concentration of approximately 10^{-3} moles/l (based on the repeat unit molecular weight) with 3-7% DMAc and a typical pH of 3.8 was obtained. Other aqueous PAmA solutions which contained larger amounts of DMAc were made in a similar manner using the same DMAc stock solution. The PAH and SPS solutions were prepared by diluting the appropriate amount of material with deionized water to a concentration of 10^{-3} moles repeat unit/l and then adjusting the pH to 4.0 and 3.8, respectively. The PVP solution was diluted with deionized water to a concentration of 10^{-2} moles repeat unit/l and used at a pH of 2.5. The PPV precursor was used as received at a pH of about 5.0. All solutions except the viscous PPV precursor solution were syringe filtered through a 0.45 μm Millipore filter prior to use.

Hydrophilic glass substrates were prepared as previously noted in Chapter 2. Aminosilane functionalized (positively charged) glass slides were prepared through

reaction of the hydrophilic glass substrate with the silane coupling agent, N-2-aminoethyl-3-amino propyl trimethoxysilane. This was accomplished by sequentially rinsing the substrates with methanol, a methanol : toluene (1:1) mixture, and toluene; and then placing them in a 2 volume percent solution of N-2-aminoethyl-3-amino propyl trimethoxysilane in toluene for 11 hours. The substrates were then transferred to a solution of boiling toluene for 1 hour and rinsed in the opposite order as before (toluene, a methanol : toluene (1:1) mixture, methanol and deionized water). The net objective of this treatment was to anchor molecules to the substrate which had surface exposed amine groups that could be protonated to create a positively charged surface. To maintain stability, the silanized substrates were submerged in to a $1x10^{-3}$ solution of the polyanion poly(styrene sulfonate) [131]. The zinc selenide plates were used as received (Wilmad).

Each hand-dipped multilayer film was assembled by first dipping the substrate into the dilute aqueous polycation solution for 10 minutes, thoroughly rinsing with water to remove unbound material, drying with filtered compressed air, and then placing the substrate into the PAmA solution for 10 minutes, rinsing, and drying. This entire cycle was repeated until the desired number of layers were achieved. The films were characterized by UV-visible spectroscopy, infrared spectroscopy, ellipsometry, profilometry, and atomic force microscopy (AFM). In the case of ellipsometry, a manual fit of intermediate optical parameters Δ and Ψ was performed to arrive at the index and thickness of the assembled films. All other characterization techniques were employed in the usual manner. Each auto-dipped multilayered film was assembled as previously mentioned in Chapter 2 with the exception that the substrates were dipped in to the polyelectrolyte solution for only 10 minutes. Electrical conductivity of PAni containing films was made using the Vander Pauw measurement technique in which a 2.5 x 2.5 cm^2 square region at the center of the film was patterned and contacted at the corners with gold wire using silver paint [137].

Polyimide Conversion

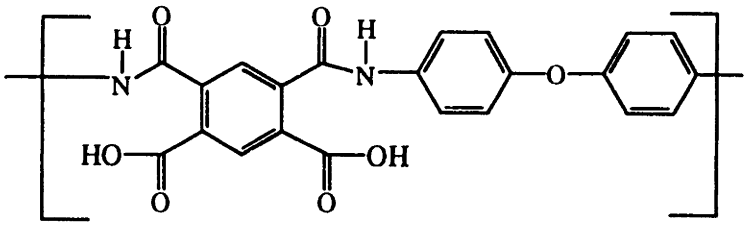

Poly(amic acid) (PAmA)

Chemical or Thermal Imidization

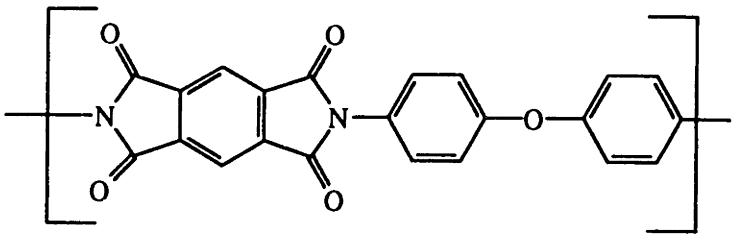

PMDA-ODA

Polycations

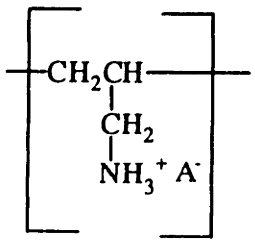

Poly(allyl amine) (PAH)

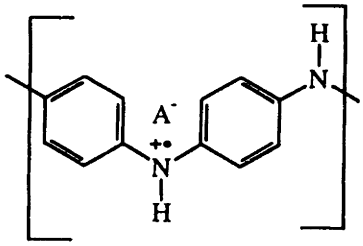

Polyaniline (PAni)
(doped emeraldine salt)

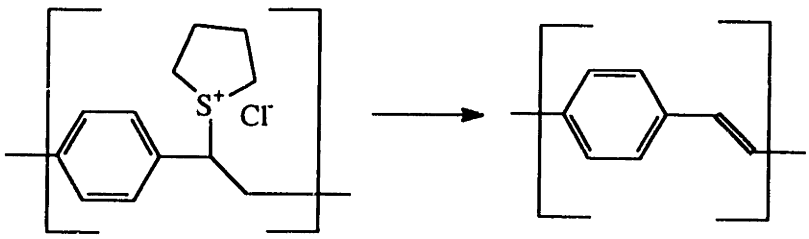

Precursor PPV (pPPV)

Poly(p-phenylenevinylene) (PPV)

Figure 3.2.1. Chemical structures of the polymers which were sequentially adsorbed to make multilayered films.

3.3 Experimental Results and Discussion

Using the experimental parameters discussed above, assembled films of poly(amic acid) and three different polycations, polyallylamine (PAH), polyaniline (PAni), and a precursor to poly(p-phenylenevinylene) (PPV), were fabricated and characterized. The chemical structures of these polymers can be viewed in Figure 3.3.1. A variety of multilayer films containing the simple linear polycation of PAH have been assembled both within and outside our laboratory[78,100,104]. This polycation is therefore an ideal material to use for comparison. Multilayered films containing p-type doped electrically conducting polymers such as PAni have also been previously fabricated to produce highly conducting thin films [95,96,100,105]. The conductivity of such films can be used as a relative probe of film morphology. Similarly, multilayered films containing PPV have also been used for electroactive applications including organic light emitting devices [106,107]. In this work, the sequential adsorption of the precursor to PPV (pPPV) with PAmA, a precursor to PMDA-ODA, was used to make ultra-thin films of two completely non-charged molecules through processing and conversion of their polyelectrolyte precursors.

3.3.A. Sequentially Adsorbed Films of PAmA and PAH

Because both PAH and PAmA are optically clear, infrared spectroscopy was used to monitor the build-up of PAH/PAmA films on substrates of ZnSe (IR transparent plates). Spectra were recorded after the deposition of each layer up to a final thickness of 10 bilayers for films adsorbed from PAmA and PAH polyelectrolyte solutions with a concentration of 10^{-3} M, a pH of 4.0, and no additional added salt. Because the ZnSe is a planar transparent substrate and measurements were made in transmission, substrates which had undergone 10 dip cycles were actually measurements of a front and back film each with a thickness of 10 bilayers for a total of 20 bilayers. Figure 3.3.2 shows the IR spectra of a film after 1, 5, and 10 dip cycles (2, 10, and 20 bilayers of deposition) with the inset displaying the maximum absorbance near 1500 cm^{-1} as a function of the number of dip cycles. As expected, this peak, which is associated with the aromatic groups of the PAmA, primarily increases after being placed in the PAmA solution. As can also be

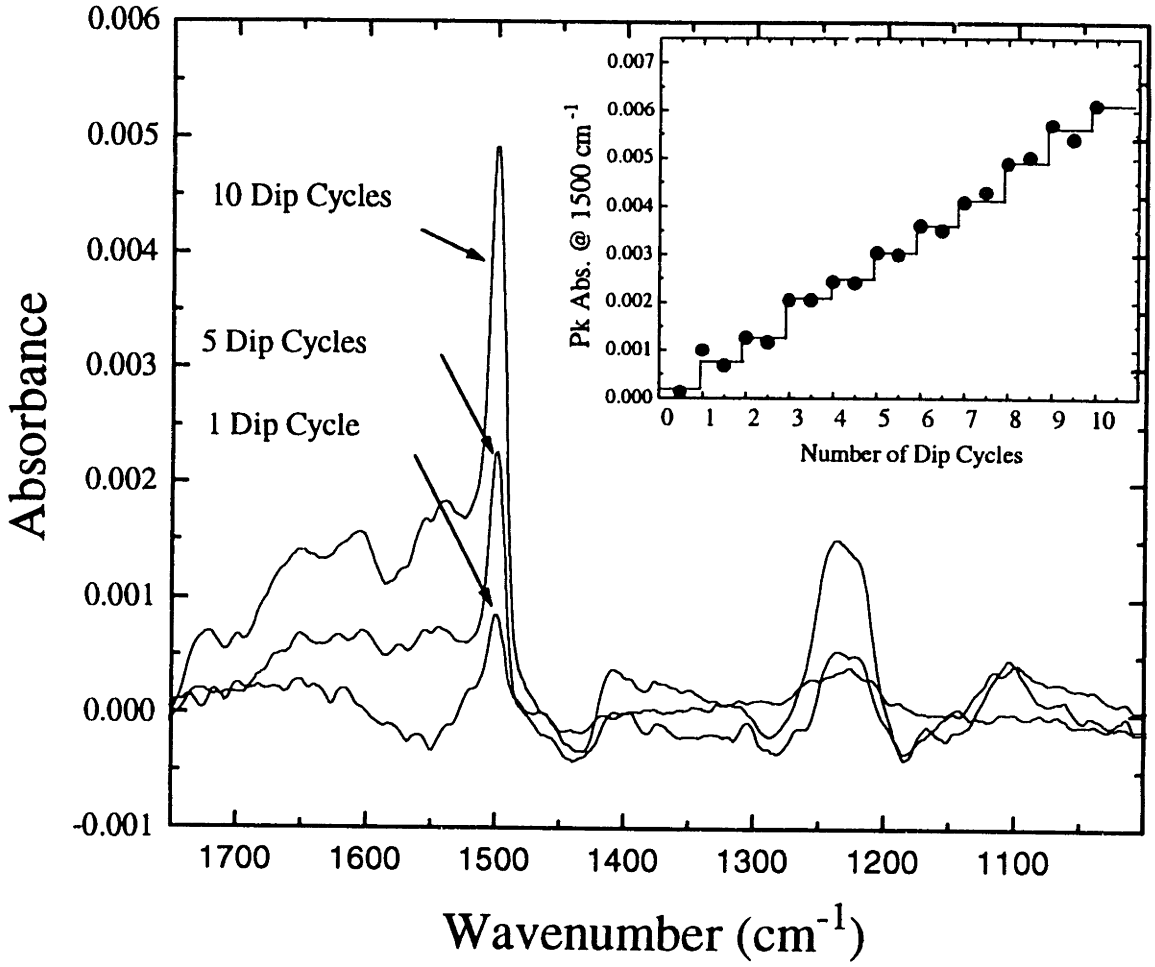

Figure 3.3.2 Infrared spectra taken during build-up of a PAmA/PAH on ZnSe. Absorbance values are the sum of the contributions of the films deposited on both sides of the substrate (i.e. "10 dip cycles" = 10 bilayers on front + 10 bilayers on back film = 20 bilayers). The inset plot shows the peak absorbance at 1500 cm^{-1} as a function of the number of dip cycles.

observed from this figure, the growth is linear which indicates that the same amount of absorbing material is being deposited in each bilayer cycle.

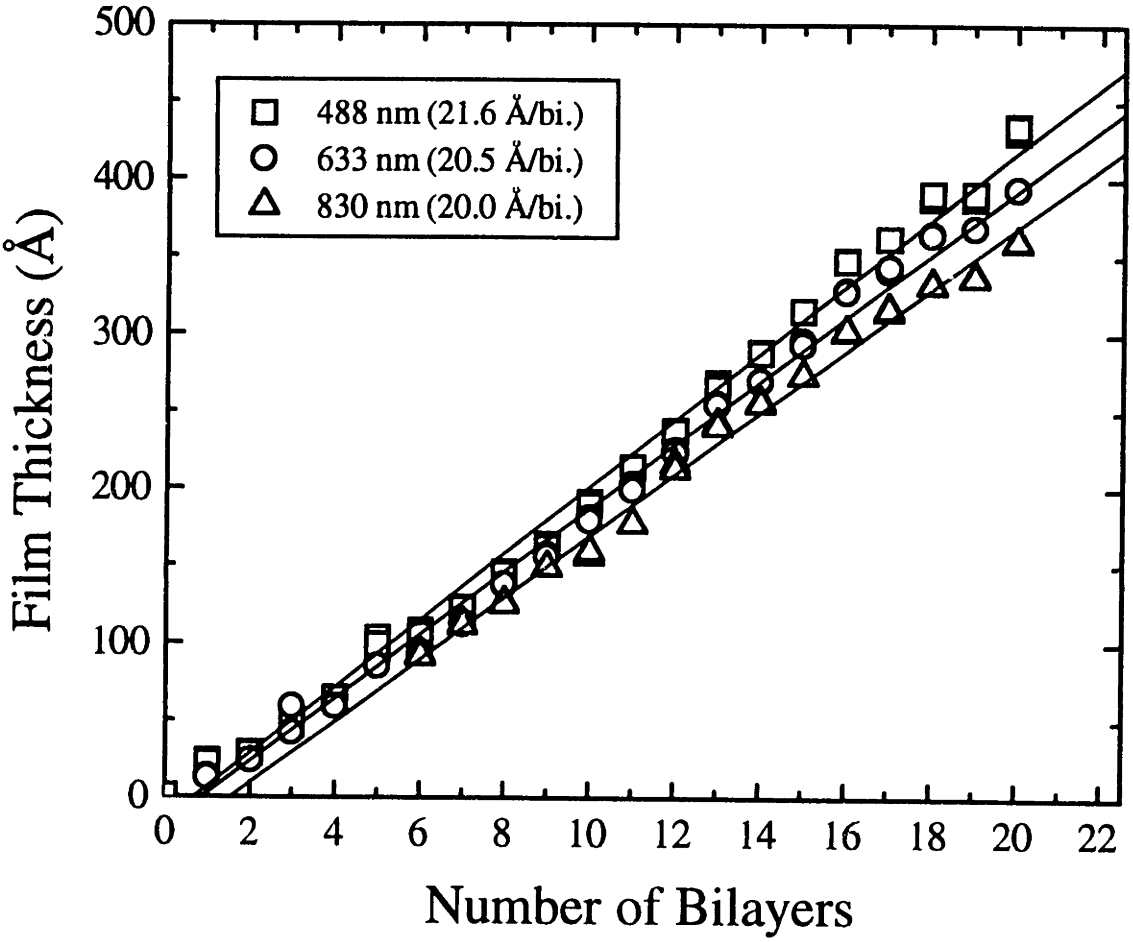

Figure 3. Film thickness vs. number of bilayers for a sequentially adsorbed film of PAmA/PAH with a final thickness of 20 bilayers (20 dip cycles) on a silicon wafer as measured by ellipsometry at three different wavelengths.

As another means to monitor the assembly process, a Gaertner rotating ellipsometer was used to track the thickness during build-up of a PAH/PAmA film on a bare silicon wafer. Using a manual fitting approach for three different wavelengths (488, 633, and 830 nm), a linear build-up was again found for all three wavelengths as shown in Figure 3.3.3. However, the average bilayer thickness measured by the ellipsometer of 21Å/bilayer did not agree with the value of 10 Å/bilayer that was measured by profilometry on the same films. Considering that the ellipsometer also gave very low

values for the index of refraction (1.26-1.35), this discrepancy was believed to be linked to a high film roughness. The roughness of similar films on glass was measured by Atomic Force Microscopy (AFM) over a 1 μm^2 area and gave a high r.m.s. surface roughness of about 90Å both before and after conversion of the PAmA. This high roughness is likely caused by having the mixed DMAc/water solvent of the PAmA solution so close to solubility limit of the PAmA that the molecules tend to form nano-aggregates which then adsorb onto the surface as larger particles rather than as individual polymer molecules. The slight decrease in solution clarity observed with the addition of water to the DMAc-based PAmA solution during preparation supports this idea. The fact that the final solution is readily passed through a 0.45 μm syringe filter further suggests that the aggregates are on the order of nanometers in size. Attempts to increase the amount of DMAc to 10 or 20% with no ionic strength adjustment resulted in lack of build-up which can likely be attributed to the decrease in driving force for adsorption due to the increase in polymer solubility with increasing amounts of DMAc.

In an effort to increase the bilayer thickness and perhaps, simultaneously, decrease the roughness, the ionic strength of the PAmA solution was varied. As can be observed in Figure 3.3.4, the bilayer thickness scaled with the square root of the added salt concentration as predicted from single layer adsorption theory [138]. Though the "hand-dipped" films tended to deviate from linearity at high salt concentrations, this same basic trend was observed for 10 bilayer "hand-dipped" films on both hydrophilic glass and on silane treated glass and for 32 bilayer "auto-dipped" films on hydrophilic glass at a solution pH of 4.0 for both PAmA and PAH. Poly(amic acid) solutions made with 0.3 M NaCl precipitate within 24 hours. Therefore, 0.3M NaCl was considered to be the polymer's solubility limit.

The ability to increase the bilayer thickness from 10 to 60 Å/bilayer is typically attributed to a shielding of the repulsion between the negatively charged carboxylate groups which allows the adsorbed polymer chains to assume a more looped conformation on the surface. However, if aggregates of chains are being formed, it is also reasonable that the layer thickness would likewise increase with increased ionic strength. This thickness increase could occur through an increase in the number of aggregates adsorbed

or an increase in the size of the aggregates both of which could be due to the shielding of the repulsive charges and/or the decrease in PAmA solubility. Though adjustment of the ionic strength was successful in controlling the bilayer thickness, the roughness of films built from PAmA solutions containing 0.2 M NaCl showed a slight increase in the r.m.s. roughness to 96 Å.

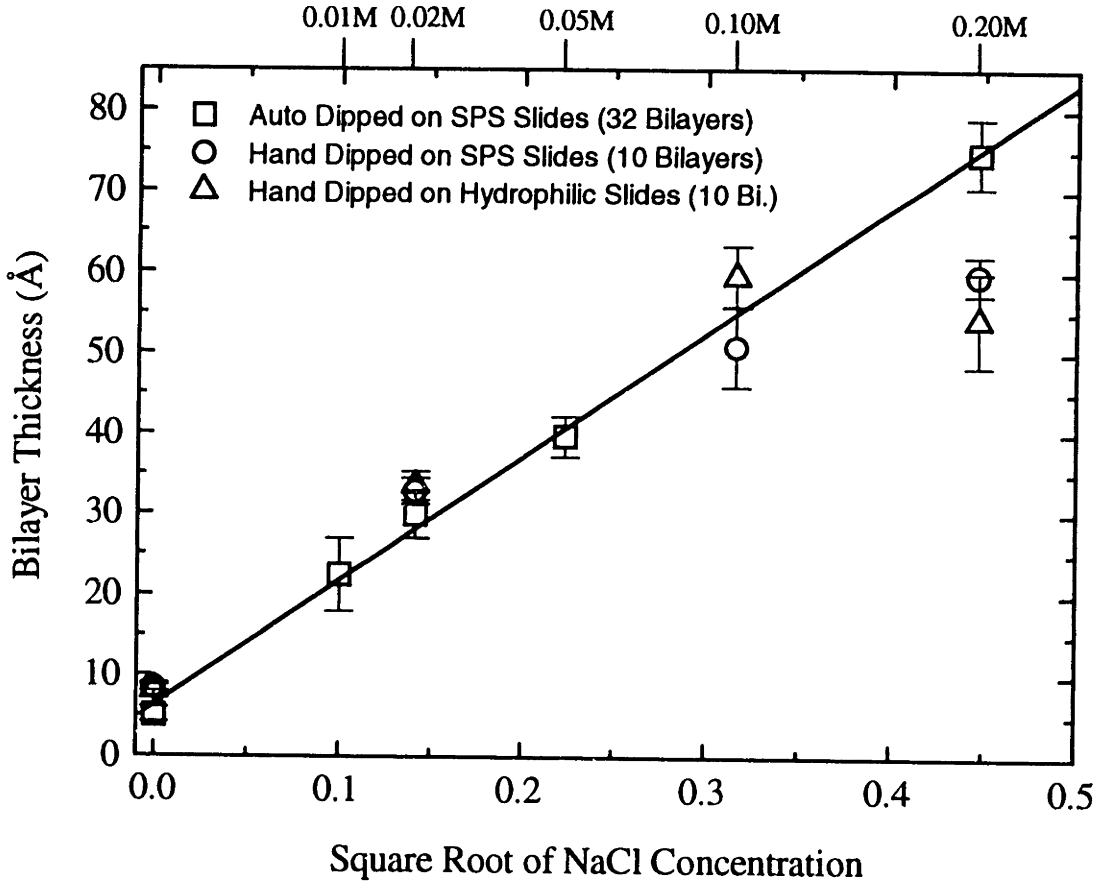

Figure 3.3.4. PAH/PAmA bilayer thickness vs. square root of NaCl concentration added to the poly(amic acid) (PAmA) solution for films adsorbed from a PAH solution at pH 4.0 and a PAmA solution of pH 3.8. Films were prepared via hand-dipping and auto-dipping on hydrophilic and silanized glass.

Because the bilayer thickness increased more substantially to 60-65 Å/bilayer, this roughness is now on the order of two bilayers rather than ten. When the PAmA solution is moved away from the solubility limit by increasing the amount of DMAc to 12% and 20% for solutions which contain 0.1 M NaCl , a drastic reduction in r.m.s. roughness to as low as 42 and 37 Å was achieved with roughly the same average bilayer thickness of 48 and 43 Å/bilayer, respectively. Though this roughness is still higher than those reported for other assembled films measured by SAXR [72,74], the roughness is now less than one bilayer which shows that it is possible to obtain smoother films by simply selecting the correct solution conditions.

The conversion of the PAmA within the assembled films to the polyimide PMDA-ODA was achieved through two different types of imidizing steps - thermal imidization and chemical imidization. Thermal imidization was performed in a vacuum oven at elevated temperatures, while chemical imidization was accomplished by submerging the PAmA/PAH films in a dehydrating solution of acetic anhydride and pyridine in benzene. Though thermal processing schemes vary, a treatment of ≤300 °C for at least 0.5 hours for thin films of pure PAmA is generally accepted as a means of producing a fully imidized film [139,140,141]. However, due to concerns about the thermal stability of the PAH, the thermal conversion used for the assembled films of PAmA involved heating the samples at lower temperatures (185°C) for longer times (18 hrs.). Chemical imidization was accomplished by submerging the PAmA multilayered films in a 1:1 M solution of acetic anhydride : pyridine in benzene at room temperature for the same length of time (18 hours). Both conversion procedures were examined by infrared spectroscopy and showed the emergence of the imide peaks at 1780, 1732, and 1380 cm^{-1} and the decrease in the amide and carboxylic acid peaks at 1610 and 1400 cm^{-1} (see Figures 3.3.5 and 3.3.6).

The percent imidization for both conversion procedures was calculated through a peak area comparison with spin coated samples of comparable thickness which were converted at 300°C for more than 0.5 hours. In order to account for any thickness difference, all the areas of the peaks associated with the imide groups (725, 1380, 1732, & 1780 cm^{-1}) were normalized with respect to the area under the phenyl peaks (1015 &

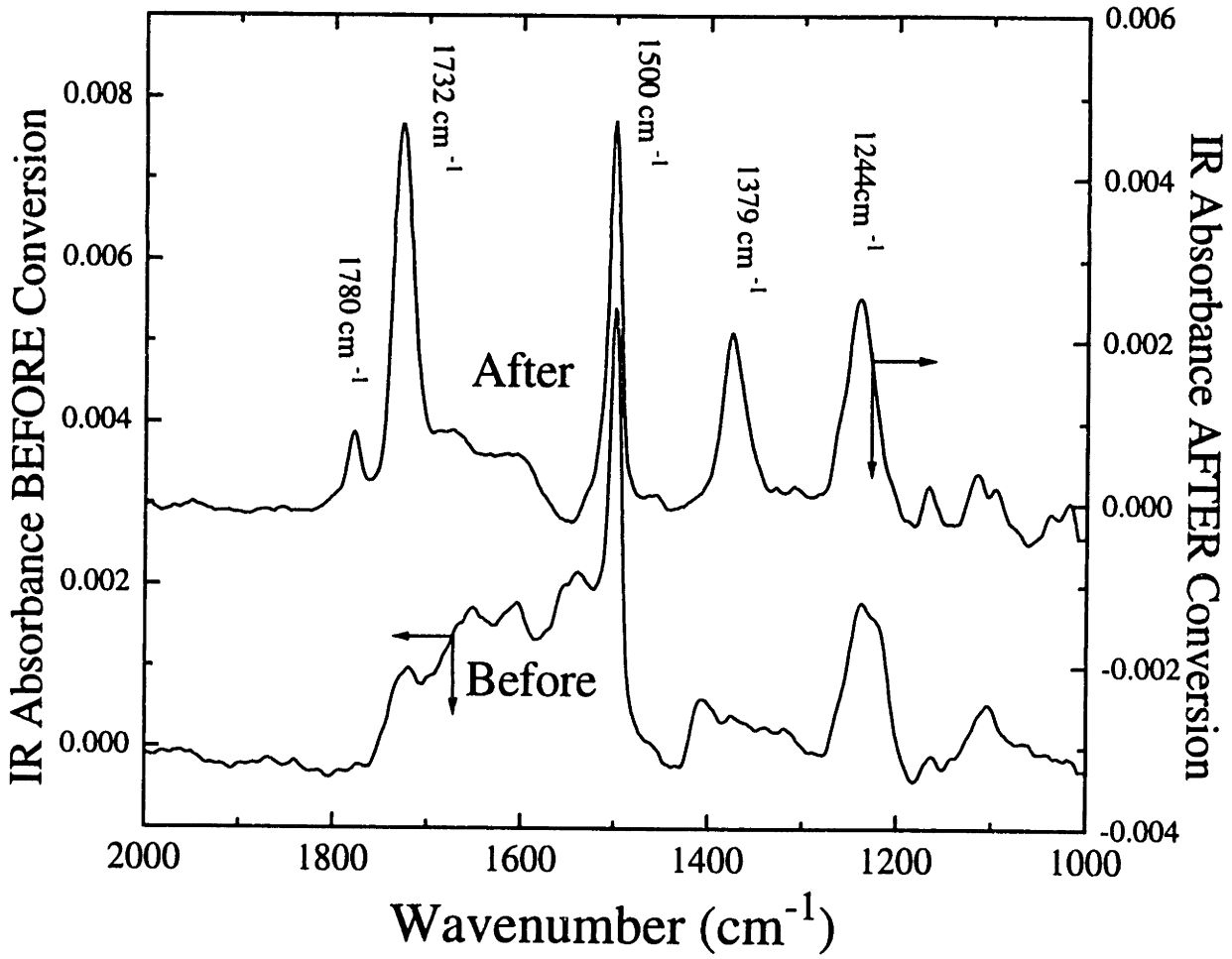

Figure 3.3.5. Infrared spectra of a 10 dip cycle (20 bi.) sequentially adsorbed film of PAmA/PAH made with no ionic strength adjustment of the PAmA solution. Measured before and after thermal conversion into the polyimide PMDA-ODA.

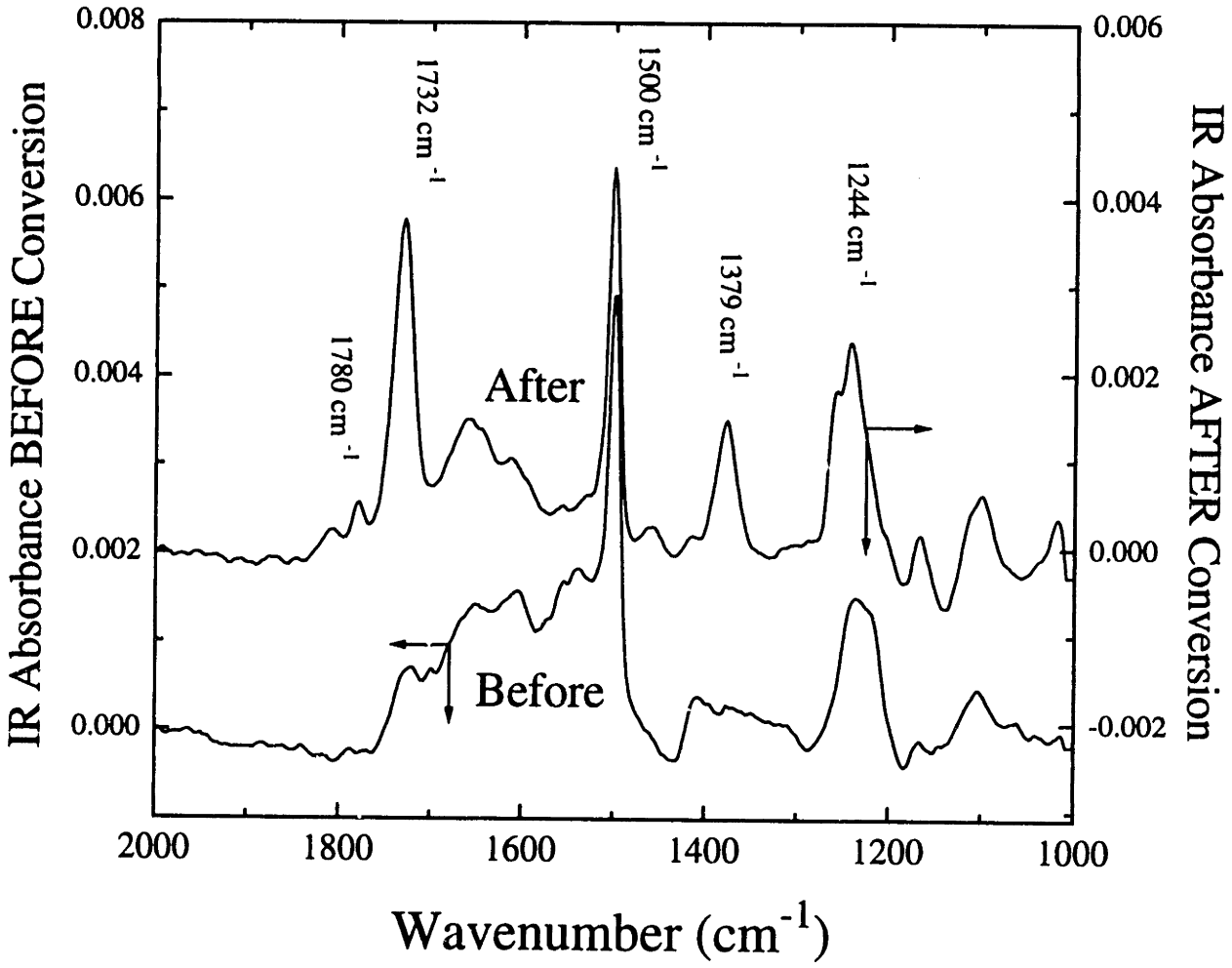

Figure 3.3.6. Infrared spectra of a 10 dip cycle (20 bi.) sequentially adsorbed film of PAmA/PAH made with no ionic strength adjustment of the PAmA solution. Measured before and after chemical conversion into the polyimide PMDA-ODA.

1500 cm^{-1}). By comparing the ratios of the imide peak area to the aromatic peak area for the "fully imidized" reference sample to those of the assembled films, a percent imidization was estimated. The average percent imidization calculated from all of the imide peaks when normalized to both aromatic peaks was 92% for the thermally imidized sample and 68% for the chemically imidized sample. It has been suggested that the C-N stretch at 1380 cm^{-1} is the imide peak which is the least affected by complicating factors such as anhydride absorption and anisotropy [142]. The average percent imidization calculated from just this peak, when normalized with respect to the 1500 cm^{-1} and 1015 cm^{-1} aromatic peaks, was 100% for the thermally imidized sample and 61% for the chemically imidized sample, which is in good agreement with the values calculated from all of the imide peaks. The lower percent conversion of the chemically imidized film is likely due to the slower kinetics of the chemical reaction and to side reactions with residual and atmospheric water. The conversion rate could likely be increased by raising the temperature of the imidizing solution [142]. Thus, it has been shown that PAmA can be assembled with PAH in a linear fashion, that the thickness of the resultant film can be controlled through the addition of salt to the polyelectrolyte solution, and that the PAmA contained in each film can be successfully converted to PMDA-ODA using either thermal or chemical means.

3.3.B. Sequentially Adsorbed Films of PAmA and PAni

The second polymer examined for sequential adsorption with PAmA was the conjugated electrically conducting polymer polyaniline (PAni). In contrast to the PAmA/PAH system, this system could be monitored during build-up by visible spectroscopy due to the visible absorbance of the PAni. Because the emeraldine base form of PAni relies on the protonation of nitrogen groups to achieve both polycation-type behavior and electrical conductivity [136], particular attention was paid to the pH of the dipping and rinsing solutions. Ideally, the sequential adsorption of PAni would be performed by setting the pH of all the solutions and rinse water to an acidic pH of 2.5 to ensure that the PAni maintains the same level of positive charge density and protonic acid

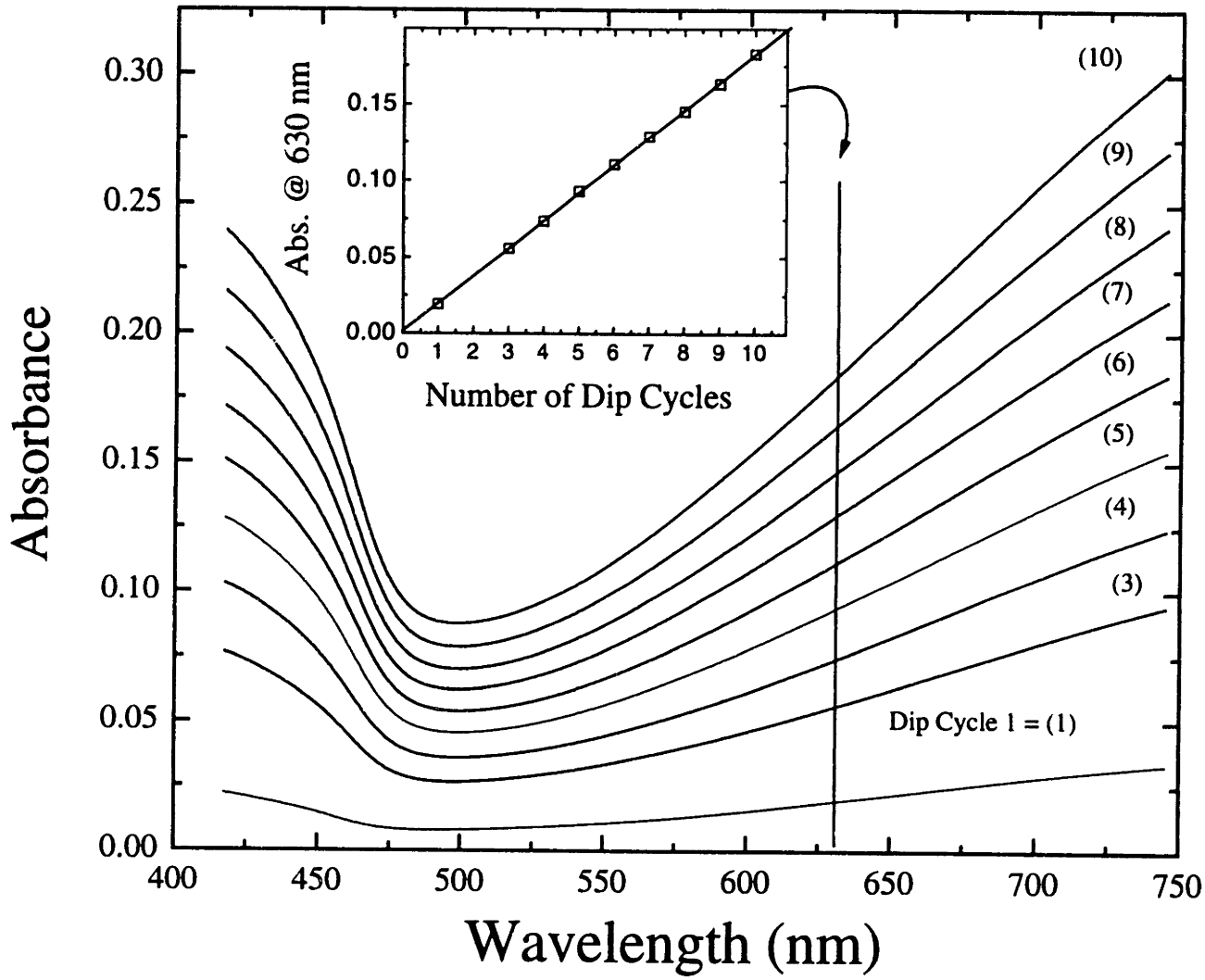

Figure 3.3.7. Absorbance spectra of a sequentially adsorbed film of PAmA/PAni recorded during build-up of a 10 dip cycle film. Plot shows the summation of the absorbances of the front and back films (i.e. "10 dip cycles" = 10 bi. of front film + 10 bi. of back film= 20 bi. total). The inset shows absorbance as a function of the number of dip cycles during build-up of the film.

"doping". However, in this particular case, the pH of the PAmA solution could not be lowered below 3.0 without precipitation and could only be kept stable near a pH of 3.5. Despite this increased pH, films were successfully assembled with a PAmA solution pH of 3.5 and a PAni solution pH of 2.5. Additionally, it made little difference to the measured visible absorbance per bilayer and to the bilayer thickness of 48 Å/bilayer (as measured by profilometry) of the resultant films whether the pH of the rinse water was left unadjusted at ~5.5 or if it was adjusted to 2.5 with methane sulfonic acid. Figure 3.3.7 displays the visible absorbance spectra as a function of the number of dip cycles for a 10 dip cycle (20 bi.) PAni/PAmA film which is partially doped. The absorbance in this figure includes contributions from the front and the back sides of the assembled PAni film on glass. The inset of Figure 3.3.7 displays the absorbance at 630 nm recorded as a function of the number of dip cycles for films with no ionic strength adjustment.

Likewise, films built with an ionic adjustment to the PAmA solution of 0.2 M NaCl were found to be insensitive to the pH of the rinsing solution. They also gave approximately the same amount of PAni absorbance per bilayer as those without ionic strength adjustment. However, the film thickness of the ionic strength adjusted film was drastically increased to 100 Å/bilayer. The fact that such a large thickness was obtained and that assembly still occurs for PAni with a much lower charge density, may indicate that other types of interactions, including hydrogen bonding, may be playing a role in PAni adsorption as has been previously observed [143].

By completely dedoping a film with pH 12 ammonium hydroxide and measuring the absorbance maximum at 630 nm, the amount of PAni in the assembled films could be calculated from the measured film thickness and a previously determined extinction coefficient of 7.2×10^4 absorbance units/cm [112]. This calculation revealed that the bilayer structure contained roughly 20 - 24% PAni for those films which had been assembled from unadjusted PAmA solutions and 12 - 13% for those with ionic strength adjustment of 0.2 M NaCl. This illustrates that, as expected, the bilayer thickness increase observed with an increase in ionic strength of the PAmA solution is due to more adsorption of the PAmA and not more adsorption of the PAni. Assuming a continuous trend between PAmA solution ionic strength and bilayer thickness similar to that observed

for the PAH/PAmA films, this observation makes it possible to again tune the volume fraction of PMDA-ODA by simply adjusting the ionic strength of the PAmA solution.

Several of the 10 bilayer PAni/PAmA films were doped prior to imidization by placing them in a solution of hydrochloric acid at pH 0 for several seconds. Time resolved UV-Vis spectroscopy revealed that the doping occurred within 20 milliseconds for such thin films. The films were blown dry with compressed air and then measured for their conductivity. The average conductivity for the doped films prior to imidization was measured to be 0.5 S/cm for films from the unadjusted solutions and $< 10^{-4}$ S/cm (the limit of our measurement capability) for ionic strength adjusted films. The optical spectra of both films showed them to be doped to approximately the same extent.

The drastic decrease in conductivity in going from PAmA/PAni films fabricated without added salt in the PAmA solution to those films made with 0.2M NaCl added to the PAmA solution can likely be attributed to attaining a PAni volume fraction which is below the percolation threshold for conduction. The observation of high conductivity at a PAni volume fraction of 20-24% and the low conductivity at a volume fraction of 12-13% is in agreement with the percolation threshold of 16 vol. % calculated for a well mixed system [144]. This would imply that film structure created in the PAmA/PAni films is more like a homogenous polymer blend than a multilayered heterostructure with well connected thin layers of conducting polymer. This is supported by the suggestion that nano-sized aggregates are formed in both the PAni and the PAmA solutions due to their proximity to their respective solubility points in the DMAc/water mixed solvent system [144]. The adsorption of aggregates would also help to explain both why the roughness is so much higher (50-100Å r.m.s.) and the bilayer thickness is so much larger than sequentially adsorbed films made from completely water soluble polyelectrolytes [78].

After the thermal imidization of the doped, unadjusted PAmA/PAni films was performed for 16 hr. at 185° C, the films could still be re-doped to approximately the same degree as before imidization, indicating that little degradation of the PAni occurred. Measuring the conductivity in the same manner as the unconverted films, the values were observed to be much lower and very close to the measurement capability of the instrument (10^{-4} S/cm). The fact that a similar response was observed for the chemically imidized

films suggest that the decrease in conductivity is due to a "pinching off" of the conduction paths by the subtle changes in structure which accompany the conversion of PAmA to PMDA-ODA. Overall, it has been shown that PAmA can be successfully sequentially adsorbed with PAni under a variety of different processing conditions, that the increase in bilayer thickness with an increase in the ionic strength of the PAmA solution comes from an increase in the amount of PAmA adsorbed, that the difference in conductivity between films made with and without ionic strength adjustment to the PAmA solution suggest a well mixed system, and that the conductivity of the films made with no ionic strength adjustment to PAmA solution drastically decrease with either thermal or chemical imidization.

3.3.C. Sequentially Adsorbed Films of PAmA and pPPV

The third polymer examined for sequential adsorption with PAmA was a tetrahydrothiophenium precursor to PPV (pPPV). The build-up of PAmA with pPPV was monitored both on ZnSe by IR and on silanized silicon wafers by ellipsometry. Infrared spectra recorded for films with no ionic strength adjustment made to the PAmA solution as a function of the number of bilayers adsorbed, showed a linear build-up and a peak absorbance at 1500 cm^{-1} which was roughly twice that observed for films of PAH/PAmA. Measurements made by ellipsometry at three different wavelengths also showed a linear build-up and gave an average bilayer thickness of 32Å/bilayer. However, profilometry measurements on the same films gave a bilayer thickness of 24Å/bilayer. This difference may be due to the difference in measurement technique (optical versus mechanical measurement).

When PAmA/PPV films on ZnSe are heated at 185° C for 16 hours, the peaks associated with the thermal conversion of the PAmA into PMDA-ODA (1780, 1732, and 1379 cm^{-1}) emerged, while those associated with the PPV conversion (3020, 963, 837 cm^{-1}) were not observed. Though the conversion of the PPV precursor to PPV could not be substantiated by infrared spectroscopy, results obtained from similar films assembled on

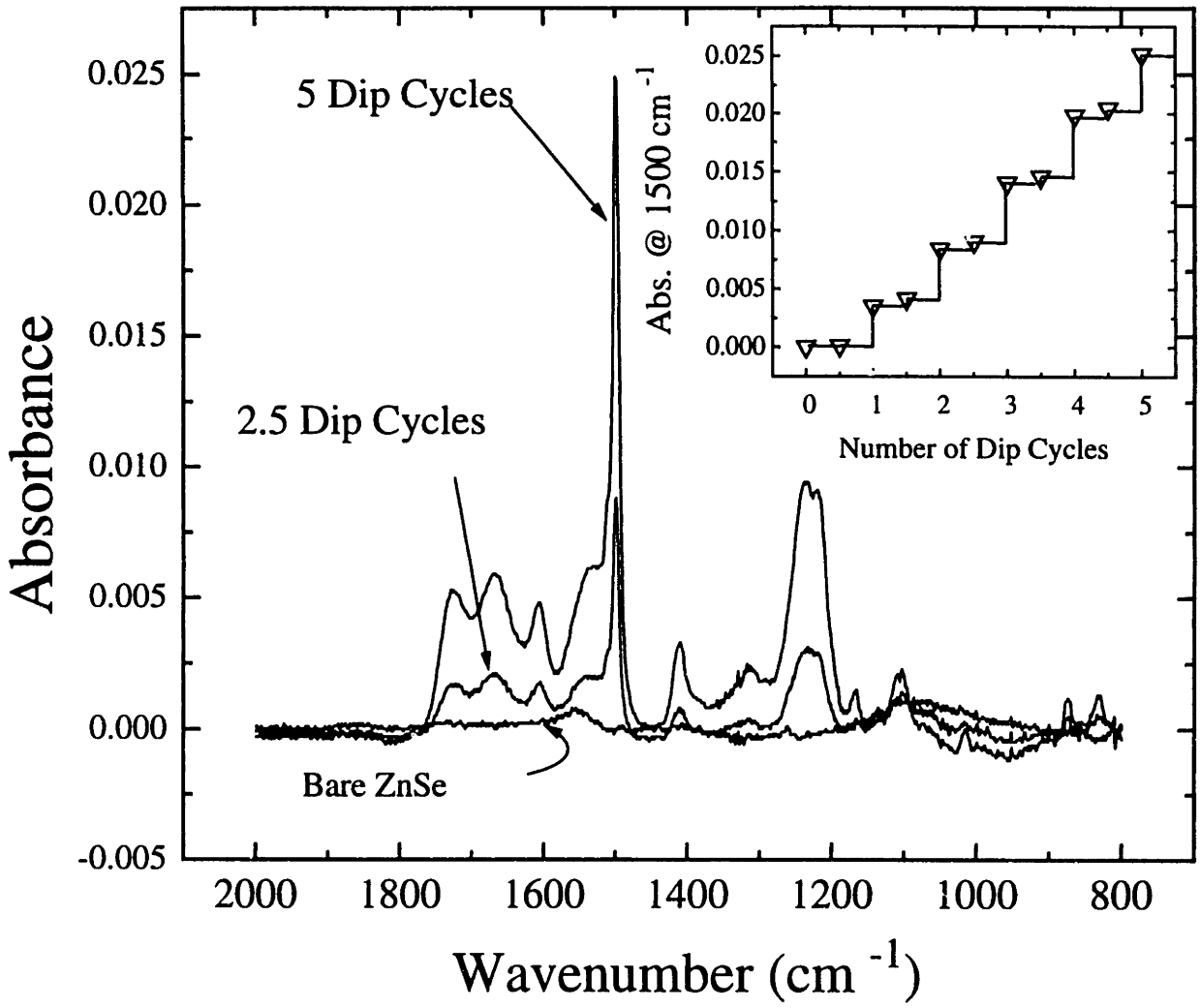

Figure 3.3.8. Build-up of a 5 dip cycle (5 bi. front film + 5 bi. back film = 10 bi. total) film of an ionic strength adjusted film of PAmA/pPPV as monitored by infrared spectroscopy. The inset shows the absorbance at 1500 cm^{-1} as a function of the number of dip cycles.

glass confirmed the presence of PPV through the emergence of a strong visible absorbance near 420 nm. The absence of the PPV IR peaks is likely due to a lower volume percent of PPV and to the fact that the oscillator strength of the PPV near 1500 cm^{-1} is roughly four times smaller that of the PMDA-ODA as found through a comparison of the peak height to thickness ratio for cast films of each. Based on the estimate of 24Å/bilayer, on the measured oscillator strength difference, and on the ratio of peak absorbance at 1500 cm^{-1} to film thickness for cast films of each; an estimate of 60 to 70 vol. % PMDA-ODA was made for the assembled films without ionic strength adjustment. Films on ZnSe which were chemically imidized though submersion in the imidizing solution for 18 hours also showed IR peaks which correlate with the formation of the polyimide but gave no evidence of PPV formation. Using the average of all of the imide to aromatic peak area ratios, the percent imidization of the thermally converted PAmA/PPV films were determined to be 92% while the chemical converted films were determined to be 75% imidized. These values were similar to those obtained for the PAmA/PAH films calculated in the same manner.

When the ionic strength of the PAmA solution was increased to 0.2 M NaCl, linear build-up was obtained with an IR absorbance per bilayer four times larger than that of a film without ionic strength adjustment. In this instance, an IR spectrum was taken after every layer and the film was built to a final thickness of 5 dip cycles (Figure 3.3.8). The bilayer thickness was measured by profilometry to be 76 Å/bilayer. Using the ratio of peak absorbance at 1500 cm^{-1} to film thickness derived from spin-coated samples, this assembled film is estimated to be 87% PMDA-ODA, which again indicates that the bilayer thickness increase is due to the increase in the volume fraction of PMDA-ODA with only 8-9Å of the assembled bilayer thickness due to the PPV. Films assembled under identical conditions on substrates of acid cleaned (hydrophilic) glass, silane treated glass, and silane treated silicon also gave a linear build-up with average bilayer thickness values as measured by profilometry of 63Å, 70 Å, and 74Å, respectively. It is interesting to note that from a comparison of these differences in bilayer thickness and sessile water drop contact angle measurements made on each bare substrate, it appears that more hydrophobic substrates lead to a slightly larger thickness.

Each of the films on the different types of substrates (silane treated glass, silane treated silicon wafer, hydrophilic glass, and ZnSe) were placed in the chemically imidizing solution and monitored as a function of time. The films on ZnSe were monitored by IR spectroscopy, the films on silicon were monitored by ellipsometry, and the films on glass were monitored by UV-Vis spectroscopy. All the films were blown dry prior to measurement to remove excess amounts of the imidizing solution. The films on ZnSe were shown to be fully imidized after approximately 70 hours in the imidizing solution which explains the low percent imidization achieved for the chemical imidized PAmA/PAH and PAmA/PAni films that were placed in the imidizing solution for only 18 hrs. The films on glass were also monitored for 70 hours and were shown to develop an absorbance peak near 400 nm. In order to determine if the peak near 400 nm was being caused by the conversion of the precursor PPV by the imidizing bath, cast films of PAmA and PPV precursor on glass were monitored by UV-visible spectroscopy as a function of time in the chemically imidizing solution. By observing the formation of the absorbance peak near 400 nm for only the PAmA cast films, it was concluded that the peak was not associated with the partial conversion of pPPV in the imidizing bath. Because the peak was removed when the PAmA cast films were subsequently heated in the vacuum oven, it is believed that the peak observed near 400 nm during the chemical imidization is likely caused by an intermediate or side-reacted species of the PAmA formed in the presence of imidizing solution components. The fact that the sequentially adsorbed films and cast films of pPPV which had been subjected to the chemical imidizing solution could still be thermally converted to produce a characteristic absorbance peak near 420 nm indicates that the PPV can be converted independent of the PAmA chemical imidization.

Thus, it has been shown that sequentially adsorbed ultrathin films of PAmA and pPPV can successfully be fabricated, that the relative composition of the bilayer can be controlled through adjustment of the polyelectrolyte solution parameters, that it is possible to make ultrathin films of two intractable polymers such as PPV and PMDA-ODA by assembling them as polyelectrolyte precursors and then converting them, and that it is possible to convert the PMDA-ODA separately from the PPV. This could open a new

processing route to obtaining designed supramolecular structures composed of containing non-charged molecules for use in a variety of applications.

3.3.D. Heterostructures for Acid Barrier Testing

As an example of the type of heterostructures which can be made from charged and non-charged molecules via layer-by-layer assembly, acid barrier structures involving the sequential adsorption of 4.5 bilayers of PAni (PAni on top) with poly(vinylpyrrolidone) (PVP) followed by PMDA-ODA assembled layers of varying thickness were constructed to assess the ability of the PMDA-ODA containing bilayers to act as a barrier layer to acid migration. The visible spectrum of PAni is known to be very sensitive to pH, due to the sensitivity of the free charge carrier absorption band near 880 nm to the level of protonic doping of the emeraldine base [134]. Thus, the films of PAni/PVP were used as a pH indicators. On top of these pH indicators, 1,2,5, and 10 bilayer films of either 0.2M NaCl ionic strength adjusted PAmA/PAH or 0.2M NaCl ionic strength adjusted PAmA/pPPV were assembled. By measuring the time needed for a 20 μl drop of pH 0.8 methane sulfonic acid to turn the heterostructure film from blue to green (de-doped to doped), the effectiveness of the top barrier film could be gauged.

Prior to conversion of the PAmA to PMDA-ODA, the change in color in all films was nearly instantaneous. But, after thermal conversion, the time needed for the color change scaled with the number of barrier bilayers,with the barrier bilayers of PPV/PMDA-ODA being two to three times better at delaying the color change. However, none of the barrier layers were successful at completely stopping the color change and even the best delays were only on the order of several minutes. Nevertheless, this barrier layer study illustrates that a heterostructures with nanometer thick bilayers of simple polyelectrolytes, precursor polymers, and conducting polymers can easily be fabricated to exploit one, or all, of the component properties.

3.5 Concluding Remarks

It has shown that despite the differences in the nature of the polycations, this technique delivers a linear build-up during film deposition with a thickness per bilayer that can readily be adjusted by manipulating the ionic strength of the poly(amic acid) solution. Infrared and visible spectroscopy confirm that in all three systems it is possible to convert the poly(amic acid) into the polyimide through either thermal or chemical means. For the sequential adsorption of the poly(amic acid) with the tetrahydrothiophenium precursor to poly(p-phenylene vinylene), it was demonstrated that it is possible to assemble two precursor polyelectrolytes and to either convert both precursors thermally into their respective intractable forms or to chemically convert just the poly(amic acid) into the polyimide. It is also proven that more complex heterostructure systems composed of layers of poly(amic acid), poly(allyl amine), precursor poly(p-phenylene vinylene), polyaniline, and poly(vinylpyrrolidone) can readily be fabricated. Thus, layer-by-layer assembly provides a simple method for the fabrication of ultra-thin films with complex supramolecular architectures.

Chapter 4. - Förster Energy Transfer within Sequentially Adsorbed Heterostructures: A Means to Estimate Layer Penetration

4.1 Introductory Remarks on Layer Interpenetration

For all of the diverse materials mentioned in the previous chapters which have been sequentially adsorbed, the level of interpenetration of the adsorbed layers is a common structural parameter of concern. In the case of interpenetration of adsorbed polyelectrolytes layers, an early work which used Small Angle Neutron Reflectivity (SANR) with deuterated and non-deuterated versions of sulfonated polystyrene (d-SPS, SPS) assembled with poly(allyl amine hydrochloride) (PAH) under high ionic strength solution conditions (2M NaCl) has estimated the level of interpenetration for a 55Å bilayer composed of ~20Å of PAH and ~35Å of SPS or d-SPS to be about 12Å - less than the thickness of one bilayer [74]. A more recent study based on XPS and contact angle data of assembled films of SPS and PAH on surface treated poly(ethylene terephthalate) (PET) has likewise concluded that the layers are well "stratified" even for very thin bilayers [116]. In contrast, other recent studies on sequentially adsorbed films SPS/PAH have found very different results. One recent work which uses a Surface Force Apparatus (SFA) on assembled films of SPS and PAH has concluded that a SPS segment can penetrate through three adjacent layers which implies that the SPS "layer" can actually be spread out over three bilayers [71]. Similarly, a recent work which estimates the interpenetration of layers by measuring the electron transfer between a polyelectrolyte containing a electrochemical viologen and a treated gold substrate separated by varying numbers of spacer bilayers of SPS/PAH concludes that the redox active viologen was distributed over a distance of at least 2.5 bilayers from the layer's nominal location [145]. Yet, the necessity of being close to the substrate coupled with the nonlinear deposition of the first several bilayers observed in this study, question whether the same conclusion could be drawn for bilayers away from the influence of the substrate. The same concern as to whether, or not, the measurements taken by surface sensitive techniques such a XPS,

sessile water drop contact angle measurement, and SFA are representative of the penetration within the bulk of the film can be raised. This is especially true for polyelectrolyte layers which have very different structures when dried than when hydrated in solution. For example, it has been shown that an adsorbed SPS layer with a dried thickness of about 7Å can extend 25-40Å out from the surface when hydrated [71]. Within this paper we discuss the use of Förster-type energy transfer between sequentially adsorbed layers of poly(p-phenylene vinylene) (PPV) and a derivatized poly(p-phenylene) (dPPP) to spectroscopically estimate the level of interpenetration between layers in a multilayered heterostructure.

4.2 Förster Energy Transfer Theory

Both PPV and dPPP are highly fluorescing, conjugated polymers which can be processed in the aqueous medium which is typically used for sequential adsorption. For PPV, a film can be assembled using the water soluble tetrahydrothiophene salt precursor and then thermally treated to convert the precursor to the non-water soluble PPV within the assembled film. Similarly, organic light emitting devices (LEDs) which have a film of PPV as the emitting layer are often made by spin coating the precursor form of PPV (pPPV) onto a conducting substrate and then thermally converting to the final conjugated polymer [146]. However, as has been demonstrated by our group previously, sequential adsorption can also form very thin and uniform LEDs whose planar architecture film can readily be changed in order to both optimize and understand the operation of these thin film devices [108,147]. Assembled films of dPPP have also been incorporated into organic LEDs as a blue emitting layer with results summarized in Chapter 5 and elsewhere [148]. Within the context of this paper, PPV and dPPP are used as luminescent materials which can transfer energy via the Förster dipole-dipole energy transfer mechanism.

Förster energy transfer, also sometimes referred to as the "spectroscopic ruler", was first derived by Förster [149] and involves a spatially mediated, dipole-dipole interaction which can transfer excitation energy from a donor to an acceptor over separation distances of anywhere from 10 to 100 Å [150]. Because the probability of transfer between donor and acceptor is dictated by the distance between the two, this

transfer has been widely used to determine molecular distances, and thus structure, in the three dimensional molecular arrays of protein folding experiments [151] and polymer-polymer diffusion studies[152] and in two dimensional, planar molecular arrays of Langmuir-Blodgett films [153,154]. Recently, Förster energy transfer studies have also been extended to the case of a energy transfer from a 2-D planar array of donor molecules to a 3-D array of acceptor molecules [155].

Energy transfer between donor and acceptor molecules can be measured in one of two ways. The quenching of the donor photoluminescence in the presence of the acceptor molecule can be compared to the fluorescence of the donor molecule with no acceptor molecule present, or the increase in the acceptor molecule photoluminescence can be compared to the photoluminescence obtained in the absence of the donor molecule. For this paper, we choose the former method because there is some overlap in the absorbance spectra of the dPPP and PPV which would make it difficult to distinguish between an increase in PPV photoluminescence from energy transfer and from increased direct excitation of the molecules. The dependence of the donor and acceptor separation distance on the donor photoluminescence intensity can then be written as:

$$\left(\frac{I_d}{I_\infty}\right) = \frac{1}{1+\left(\frac{d_o}{d}\right)^X} \qquad (4.2.1)$$

where I_d is the photoluminescence intensity for donor molecules spaced an average distance of d away from the acceptor molecules, I_∞ is the photoluminescence intensity of the donor molecules in the absence of acceptor molecules, and d_o is the critical spacing between layers corresponding to a 50% probability of energy transfer. Both d_o and X are a function of the geometry assumed. For example, X is equal to 6 in the case of a donor molecule transferring energy to an acceptor molecule in 3-D space [149, 150], X is equal to 4 in the case of a plane of donor molecules transferring energy to a plane of acceptor molecules [153,154], X is equal to 3 in the case of a plane of donor molecules transferring to a 3-D array of acceptor molecules [155], and X is equal to 2 in the case of transfer

between J-type aggregates in a planar array [156]. Likewise, d_o, which can be calculated theoretically, also varies with the assumed geometry. Layer-by-layer assembled films are assumed to be analogous to Langmuir-Blodgett films whose d_o for plane to plane transfer is given as:

$$d_o^4 = \frac{\alpha^4 \cdot \Phi_D}{n^4} * \int_0^\infty A_\lambda I_\lambda \lambda^4 d\lambda \qquad (4.2.2)$$

where α is an orientation factor taken to be 0.12 for layers of randomly oriented dipoles, n is the index of refraction of the materials between the donor and acceptor, Φ_D is the photoluminescence quantum yield of the donor, and the integral represents the spectral overlap of the absorbance of an acceptor layer as a function of wavelength (A_λ) with the normalized donor photoluminescence intensity (I_λ) as a function of wavelength [157]. The donor photoluminescence intensity is normalized such that :

$$\int_0^\infty I_\lambda d\lambda = 1 \qquad (4.2.3)$$

As can be observe from the integral portion of Equation 2, one of the conditions for efficient transfer of energy via the Förster mechanism is a significant spectral overlap of the photoluminescence of the donor molecule and the absorbance of the acceptor molecule. It should be noted that this is the same condition which would be needed for the acceptor molecules to simple absorb photons emitted from the donor molecule. However, the contribution to the donor photoluminescence quenching from re-adsorption can easily be quantified by knowing the absorbance of the acceptor molecules. Because sequential adsorption produces very thin acceptor layers with low absorbance, re-absorbance of the donor photoluminescence by the acceptor is not considered to be significant in comparison to quenching by the Förster mechanism.

By assuming or measuring the parameters on the right hand side of Equation 2, a theoretical value for d_o can be obtained. By then comparing this theoretical value with a

value obtained experimentally, researchers have obtained information about the amount of the "perfection" of a LB layered structure [158], the ability of small molecules to penetrate through the layered system[159], and the structural differences of wet versus dried LB film assemblies [160]. Because LB films are assumed to be similar to sequentially adsorbed films, these same type of studies can be carried out. In fact, this technique has already been used to characterize the diffusion of small molecules through assembled films [161]. Additionally, by using time-resolved fluorescence measurements, information could be gathered not only on the average separation distance of donor and acceptor molecules, but also on the distributions of distances between the donor and acceptors. This has been done on end-tagged polymers [162] and other layered structures [163].

In this study, the steady-state Förster energy transfer of excitation energy from adsorbed layers of dPPP, a derivatized conjugated polymer of poly(p-phenylene), to layers of poly(phenylenevinylene) (PPV) is discussed. By building heterostructures in which the layers of dPPP and PPV are separated by increasing numbers of non-interacting bilayers, measuring the reemergence of the quenched dPPP photoluminescence with increasing separation from the PPV layer, and then comparing the experimental results to those predicted by theory, one can gain structural information concerning the relative level of interpenetration of the assembled layers. The primary polycation/polyanion non-interacting spacer pair considered is poly(methacrylic acid) (PMA) and poly(allylamine hydrochloride) (PAH), but additional results using spacer bilayers of PAH with sulfonated polystyrene (SPS) and with poly(acrylic acid) (PAA) will be briefly discussed.

The fabrication of assembled films of the non-conjugated polyion PAH with a variety of polyanionic species (usually SPS) has been investigated thoroughly within the literature,[1,69,72-74,98, 100-101,116,164,165,166,167] but the assembly of films containing PMA and PAA have been reported to a lesser extent [166,110]. Our group has thoroughly investigated the assembly of PAH with PMA and PAA under a variety of different solution conditions[168]. Because all of these non-conjugated spacer polymers do not absorb in the spectral regions of interest, they can be used as inert spacer layers between photophysical interacting layers of dPPP and pPPV in this investigation. The chemical structures of these materials are displayed in Figure 4.2.1

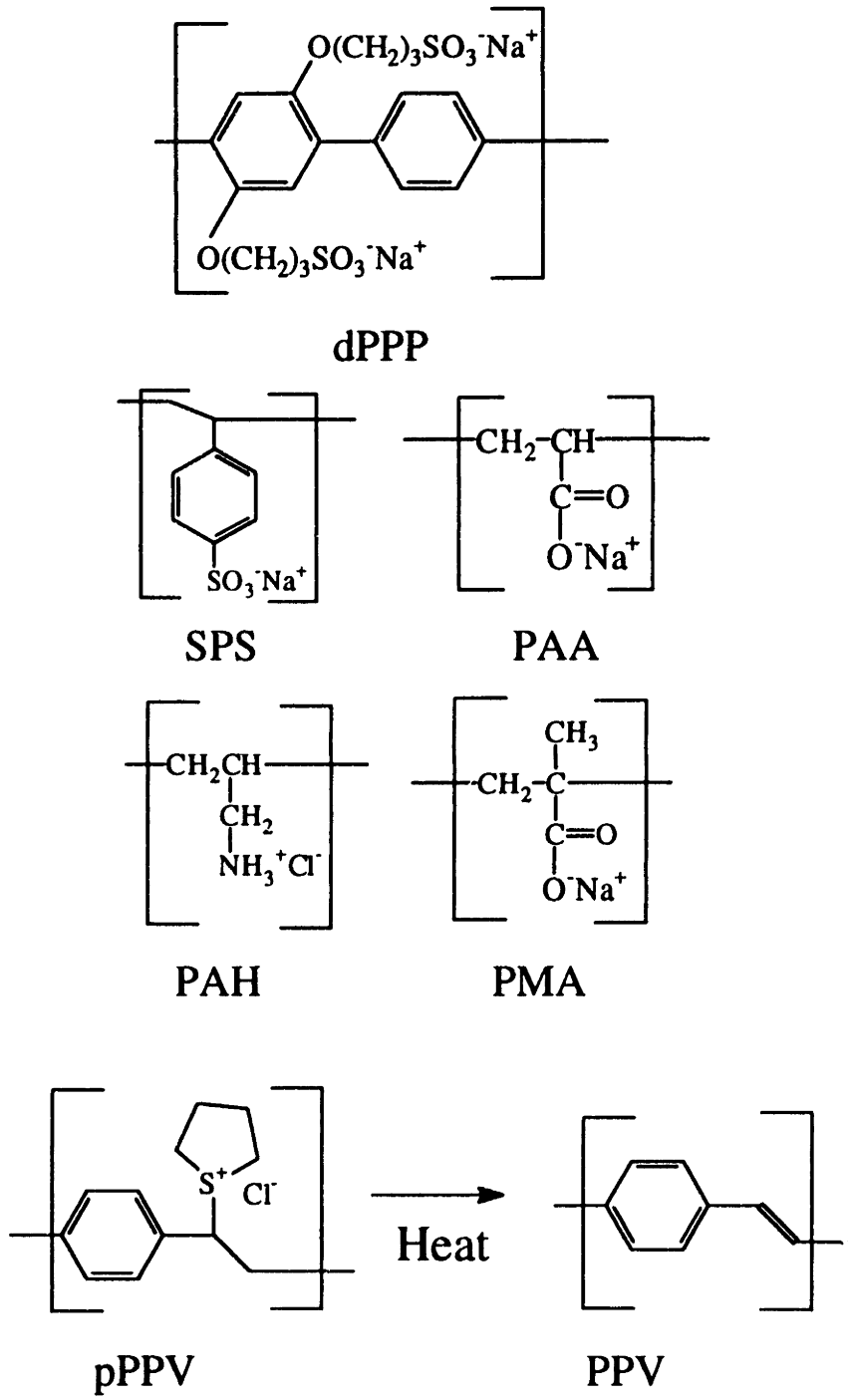

Figure 4.2.1. Chemical structures of the polymeric materials used.

4.3 Experimental

The sodium salts of poly(methacrylic acid) and poly(acrylic acid) were received from Aldrich as a 30% and 25% aqueous solution with molecular weights of 15K and 90K, respectively. The poly(allylamine hydrochloride) was received from Aldrich as a powder with a molecular weight of 50-65K. The sodium salt of the poly(styrene sulfonate) was received from Polysciences as a powder with a molecular weight of 500K. For heterostructures with PMA/PAH spacer layers, the tetrahydrothiophenium precursor to the poly(p-phenylenevinylene) was synthesized by the THT method [169] and provided by Dr. B. R. Hsieh of the Xerox corporation as a viscous aqueous solution with a concentration of approximately 0.001 M (moles of monomer). For heterostructures with spacer bilayers of SPS/PAH or PAA/PAH, the tetrahydrothiophenium precursor to the poly(p-phenylenevinylene) was purchased from Lark Enterprises (Webster, MA) as a 0.01M solution. The synthesis of the linear, water soluble, derivatized poly(p-phenylene) (dPPP), poly[2,5-bis(3-sulfonatopropoxy)-1,4 phenylene-alt-1,4-phenylene], has been previously described [170].

The solution conditions for the three sequentially adsorbed heterostructures examined are summarized in Table 1. The sodium salt of dPPP was dissolved from a powder, diluted to a concentration of 10^{-3} M in Milli-Q water, pH adjusted to 3.5, and suction filtered through a 0.8 μm filter immediately prior to use. The sodium salt of poly(methacrylic acid) was diluted in Milli-Q water solutions to a concentration of 0.005 M, pH adjusted to 3.5, and suction filtered through a 0.8 μm filter immediately prior to use. The sodium salts of poly(styrene sulfonate) and poly(acrylic acid) were diluted to concentrations of 0.01M, pH adjusted to 4.5 , and suction filtered through a 1.0 μm filter immediately prior to use. For the PMA/PAH and the SPS/PAH spacer bilayers, a 0.005 M PAH solution at pH 3.5 was used. For the PAA/PAH spacer bilayers, a 0.01M, pH 4.5 PAH solution was used. All PAH solutions were also suction filtered through a 1.0 μm filter immediately prior to use. The precursor PPV solution received from B. Hsieh was diluted by a factor of 50 with Milli-Q water (~0.0002M with an unadjusted pH of ~5), but was not filtered due to the high viscosity. A similar concentration was used for the PPV

precursor received from Lark Enterprises for films with SPS/PAH spacer layers (~0.0002M with pH ~3.5). The heterostructures made with spacer bilayers of PAA/PAH used a dilution of the PPV precursor received from Lark Enterprises of 1:100 at pH 4.5. All Lark precursor PPV solutions were filtered through a 20μm glass filter immediately prior to use. Though the viscosities of the two type of precursor PPV (pPPV) varied greatly, their photophysical properties of interest were the same. Furthermore, the effect that any of the changes in solution conditions had on the amount of materials adsorbed was quantified during the characterization of the films.

Table 4.3.1 - Solution conditions used for the three heterostructures examined

Spacer Bilayer	dPPP Solution Conditions	pPPV Solution Conditions	Polyanion Solution Conditions	PAH Solution Conditions
PMA/PAH	0.001 M pH 3.5	0.0002 M pH 4.5[a]	PMA - 0.005 M pH 3.5	0.005M pH 3.5
SPS/PAH	0.001M pH 3.5	0.0002 M pH 3.5[b]	SPS - 0.01 M pH 2.5	0.005M pH 3.5
PAA/PAH	0.001M pH 3.5	0.001 M pH 4.5[b]	PAA - 0.01M pH 4.5	0.01M pH 4.5

a - pPPV received from B. Hsieh (Xerox), b- pPPV received from Lark Enterprises

Substrates used for assembly included hydrophilic glass slides, silanized glass slides, and hydrophilic single crystal silicon wafers. The hydrophilic glass slides were prepared as previously noted [166]. The silicon substrates for the PMA/PAH spacer heterostructure were cleaned similar to the hydrophilic glass with the exception that they were only exposed to the piranha solution for 30 minutes due to this solution's tendency to etch the surface of the silicon at longer times. To avoid this etching, the silicon wafers used for the subsequent PAA/PAH and SPS/PAH spacer heterostructures were cleaned by submerging them into a sulfuric acid solution saturated with chromium trioxide ("Chromerge" solution) for at least 4 hours. Similar behavior was obtained on both types of cleaned substrates. Prior to dipping, a preparatory bilayer of PMA/PAH was adsorbed to the silicon surface to promote build-up.

The silanized substrates were prepared by submerging freshly clean glass slides into solutions of methanol, 1:1 methanol : toluene, and toluene for several minutes each and, then into a covered 1 vol.% solution of n-(2-aminoethyl)-3-aminopropylmethyl trimethoxysilane in toluene for approximately 14 hours. The substrates were then taken through the toluene/methanol solutions in reverse order (toluene, toluene : methanol, methanol) for several minutes each. Following the organic solutions, the substrates were thoroughly rinsed with Milli-Q water and submerged into a 10^{-2} monomolar solution of sulfonated polystyrene with 0.1 M NaCl. The substrates were then air dried and stored until used.

The procedure used for sequential adsorption was the same as that given in Chapter 2 on page 42. All rinse water was used without pH adjustment with the exception of the PMA/PAH spacer heterostructure with one bilayer of separation which required pH 3.5 rinse water in order to obtain a high quality film. Once assembled onto the substrates, the polymeric films were characterized using profilometry, ellipsometry, contact angle measurements, and UV-Visible spectroscopy. A Sloan Dektak 8000 profilometer with a 2.5 μm stylus with a weight of 10 mg and a medium scan rate was used to determine the step heights of scratched films on hydrophilic glass and silicon substrates. A Gaertner multiple wavelength ellipsometer was used to determine the index of refraction and film thickness of the films assembled on silicon. An index of refraction of 1.550 was assumed for films below 200Å due to the fact that the ellipsometer had trouble converging to consistent values for both the film thickness and index of refraction for such thin films.

A Spex Fluorolog with a CCD detector was used to determine the photoluminescence intensity spectrum of both films on glass and of dPPP solutions in cuvettes. The films on glass were mounted perpendicular to the incident radiation and measured in "front face" mode at an angle of 22.5° from the incident radiation. The dPPP solution was placed in a 1 cm path length cuvette which was polished on all four sides, mounted so that the incident radiation was perpendicular to one of the sides of the cuvette, and then measured in both "front face" mode and at a right angle to the incident radiation. The quantum yield of dPPP was estimated based on a comparison of the

normalized solution photoluminescence of dPPP against dilute solutions of Stilbene 420 (a.k.a. Stilbene 3) and Coumarin 440 (a.k.a. Coumarin 120) which have reported theoretical quantum yields in methanol of 71% and 72%, respectively [171]. Both of these laser dyes absorb and fluorescence in the same spectral regions as dPPP. By measuring the dPPP solution photoluminescence for a range of concentrations, it was observed that the more concentrated solutions had lower normalized photoluminescence intensities. For a concentration range of 4×10^{-6} M to 1×10^{-3} M, which corresponded to a sample absorbance of 0.046 to 1.024, the estimated quantum yield exponentially decayed from 15% to 0.34 %. When the normalized photoluminescence of the dPPP in solution was compared against the dPPP in several sequentially adsorbed films which were believed not to be quenched or shifted by the presence of the PPV, nearly the same values and the same decrease with increasing sample absorbance was observed. The exponential decrease in photoluminescence intensity and the fact that nearly the same decrease was observed for solutions as for films suggests a decreased photoluminescence from re-adsorption. Therefore, it was assumed that the quantum yields determined from the dPPP solutions are viable estimates of the quantum yield of the dPPP molecules in the film for a given sample absorbance. Because most of the dPPP containing films had an absorbance of below 0.2, the range of estimated quantum yields for the dPPP films could be narrowed to 5-15%.

4.4 Experimental Results of PMA/PAH Separation Study

To put the results obtained from the heterostructure films into context, a discussion of the build-up and the photophysical properties of the sequentially adsorbed films of dPPP and pPPV will precede the experimental results obtained for the heterostructure films with spacer bilayers of PMA/PAH. This experimental results will then be analyzed in terms of a proposed model of energy transfer between diffuse layers. A brief summary of the results obtained for heterostructure films with spacer bilayers of SPS/PAH and PAA/PAH will then follow.

4.4.A. Assembly and Characterization of pPPV/dPPP Sequential Adsorbed Films

Using the typical dipping parameters mentioned in the experimental section of this paper, assembled films of pPPV with dPPP (no spacer layers) were fabricated from

solutions with no ionic strength adjustment on a variety of substrates including hydrophilic glass, silanized glass, and silicon wafers. Regardless of the substrate used, the build-up of each film was shown to proceed linearly up to over 40 bilayers as measured either by ellipsometry and/or as determined by UV-Vis adsorption at the dPPP absorbance maximum near 360 nm. Figure 4.4.1 illustrates the linear build-up of a dPPP/pPPV film on hydrophilic glass by UV-Visible absorbance. This linearity in build-up implies that the same amount of material is being deposited in each bilayer deposition cycle for all the various substrates. Despite the commonality of linear deposition, there were some slight differences in the amount deposited per dipping cycle. The films on silanized substrates appeared to give slightly more material adsorbed per bilayer, followed by the films on the hydrophilic substrates and films on the silicon substrates. However, the bilayer thickness values of the dPPP/PPV films on the different substrates were very low (3-5Å/bilayer).

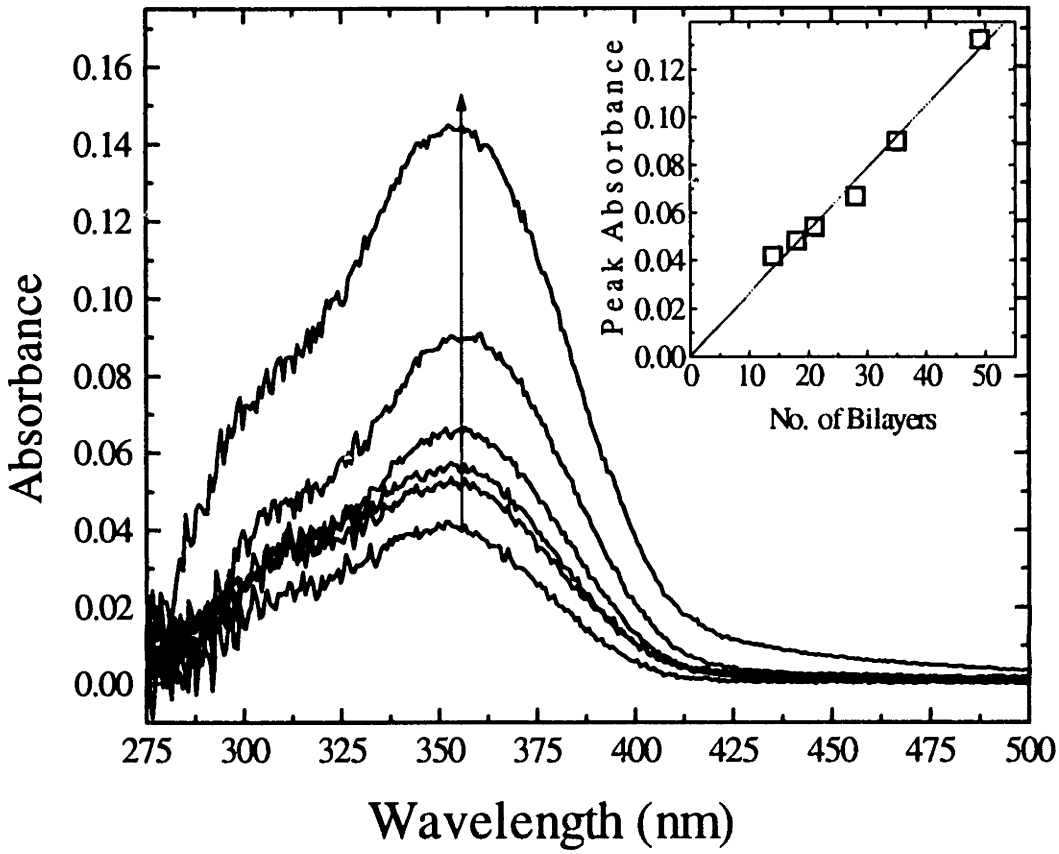

Figure 4.4.1. Linear build-up of dPPP/pPPV film on hydrophilic glass as measured by UV-Visible absorbance. Inset: dPPP peak absorbance as a function of the number of bilayers.

While such thin bilayers have been reported for bilayers of a PPV and polyvinyl sulfate (PVS) [172] and for bilayers of PAH and PVS between Langmuir-Blodgett layers [80], it is likely that the thin bilayers and the slight sensitivity of the bilayer thickness to the nature of the surface may be indicative of either incomplete surface coverage or a "filling in" of sites left empty by previous adsorption steps . In an effort to promote more complete monolayer deposition, preparatory bilayers of PMA/PAH were adsorbed to the substrates prior to adsorption of the pPPV or dPPP. Based on absorbance values for dPPP and PPV, films which were built on hydrophilic glass with prep layers of PAH/PMA gave approximately double the amount of both dPPP and pPPV deposited per bilayer. The build-up dPPP/pPPV was also found to be independent of whether one or six bilayers of PAH/PMA were used on the hydrophilic surface. Those films built on silicon substrates coated with one bilayer of PAH/PMA, gave a bilayer thickness of 5-8 Å which was double the value obtained with no "prep" bilayer (3 Å/bilayer). It is believed that the increase in the amount of dPPP and pPPV adsorbed with the use of preparatory bilayers is linked to the creation of a loopy surface which has a lower entropic penalty for adsorption (as mentioned in Chapter 1) and more overall charge than the planar substrate.

While using "prep" layers on a substrate appears to give bilayer thickness values which are more consistent with full surface coverage, one can also increase the amount of material deposited per bilayer by adjusting the ionic strength of the polyelectrolyte solutions. By adding a salt such as NaCl to a polyelectrolyte solution, the charges along the polymer backbone can be shielded from one another to the extent that the adsorbing polymer molecule can assume a more loopy conformation which results in more material being deposited and an overall thicker bilayer. Several, 10 to 20 bilayer assembled films of dPPP/PPV were fabricated under three different dPPP solution salt conditions of no salt, 0.1 M NaCl, and 0.4 M NaCl on both hydrophilic glass slides and hydrophilic glass slides coated with 5 bilayers of PAH/PMA. Solutions with 0.5 M NaCl were observed to precipitate when left standing at room temperature overnight and were therefore considered to be the solubility limit for this solution. For all films a linear build-up of dPPP was observed by UV-Visible absorbance. As can be observed from Figure 4.4.2, the increase in dPPP peak absorbance per bilayer scaled with the square root of the salt

concentration for films both with and without preparatory layers as predicted by single layer adsorption theory [17]. This same trend has been previously observed for other sequentially adsorbed systems [164]. The observation from UV-visible spectroscopy after conversion that the absorbance of the dPPP and the PPV maintains approximately the same ratio for all of the films examined is consistent with the contact-ion pair mechanism of sequential adsorption discussed in Chapter 2 in which an increase in the thickness of one layer causes a corresponding change in the thickness of the other layer as the system attempts to maintain charge stoichiometry [71]. It is also interesting to note that even though the added salt increased the amount of material deposited, which made it more likely that full surface coverage was being achieved, there was still some additional amount of material adsorbed when PAH/PMA preparatory layers were used on the substrates.

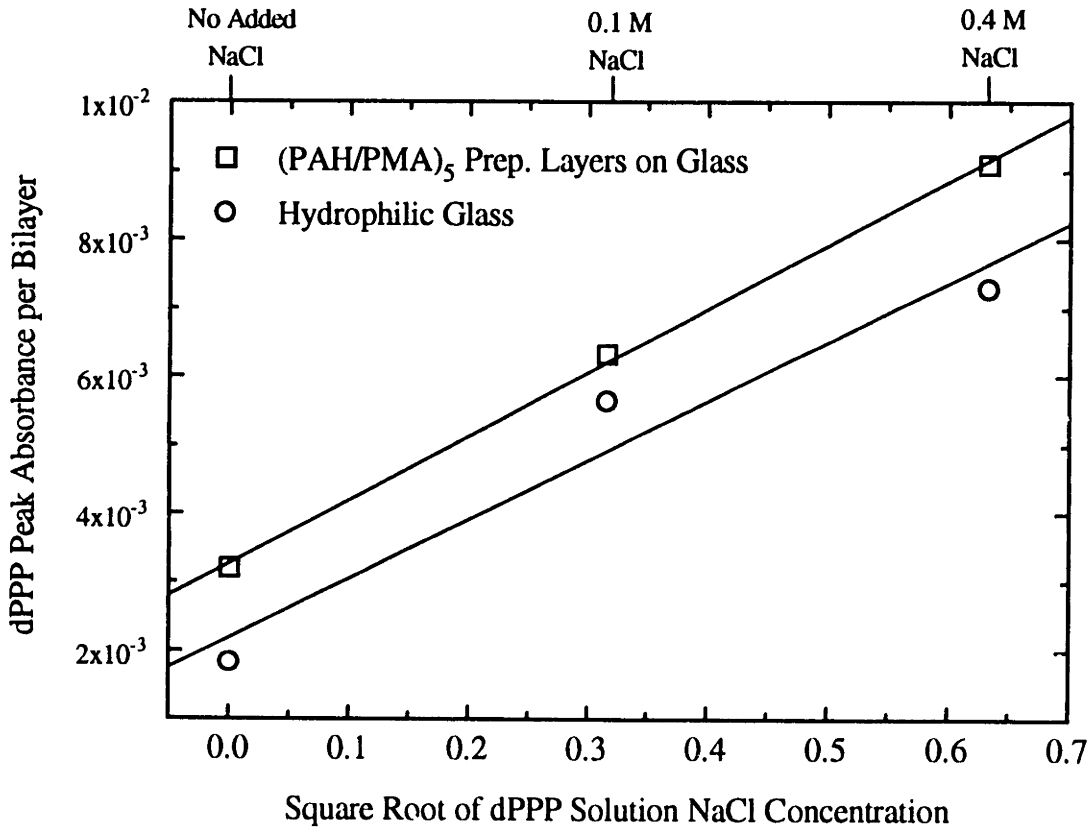

Figure 4.4.2 The peak absorbance of dPPP per bilayer as a function of the amount of NaCl added to the dPPP solution for films adsorbed onto bare hydrophilic glass and glass with 5 bilayers of PMA/PAH.

Figure 4.4.3 shows that the photoluminescence peak of the dPPP from the dPPP/pPPV films (before conversion) was observed to be broadened and red-shifted relative to those peaks observed from dPPP solutions and assembled films of dPPP and PAH. In order to help determine the origin of this red-shift, films were cast from solutions containing both dPPP and pPPV in various molar ratios, allowed to dry in air at room temperature, and measured before conversion. Because the red-shifting scaled with the amount of pPPV present and there was both a small amount of absorbance near 350 nm and a photoluminescence peak near 500 nm for a 100% pPPV cast film, it was concluded that the red-shifting was likely caused by the partial conversion of pPPV to PPV during assembly and film storage at room temperature. No difference in the absorbance spectra of the dPPP/pPPV films was observed because the absorbance of the partially converted pPPV was small and overlapped the absorbance of the dPPP. This conclusion of partial conversion of pPPV was further supported by the fact that the amount of red-shifting scaled with the length of time the film was stored at room temperature before measurement. This demonstrates the strong influence that PPV has on the photoluminescence of the assembled film.

To fully convert the pPPV, a thermal conversion of 210° C for 11 hours under dynamic vacuum was performed. As can be observed in Figure 4.4.4, the thermal conversion of pPPV to the conjugated PPV was marked by the formation of an absorbance peak at higher wavelength from the dPPP absorbance peak. Because this peak overlapped the absorbance peak of the dPPP, a simple deconvolution involving the subtraction of the dPPP absorbance before conversion from the absorbance spectrum after conversion was made in an attempt to determine the absorbance of the PPV. By measuring the absorbance spectra of several 100% dPPP cast films before and after the same thermal treatment, it was known that the absorbance spectrum of the dPPP did not significantly change under such thermal conditions. The deconvolution revealed a PPV absorbance centered around 420-430 nm for all the films examined. This is similar to what has been observed previously in our group for assembled films of PPV with other sulfonic acid containing polymers such as sulfonated polystyrene (SPS) [108].

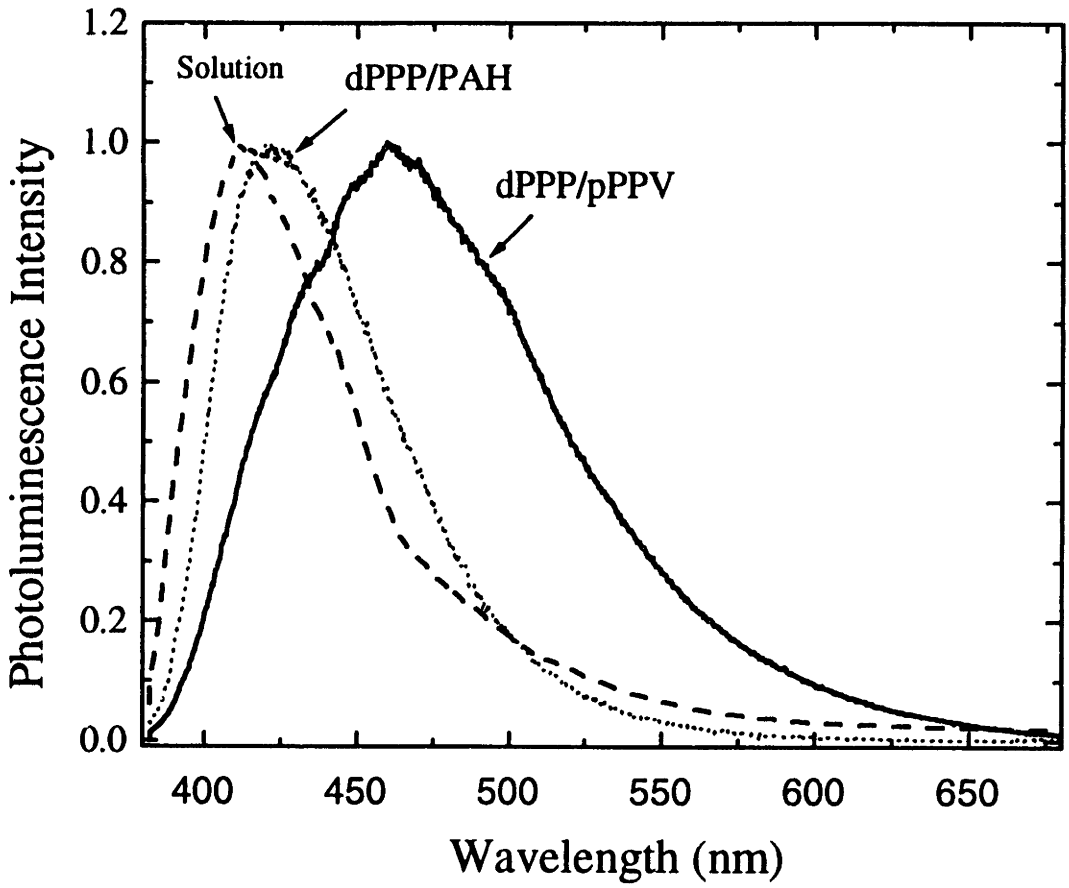

Figure 4.4.3 Normalized photoluminescence spectra showing the red-shifting of the dPPP/pPPV films relative to films of dPPP/PAH and the dPPP in solution.

It can be observed from the deconvoluted PPV peak in Figure 4.4.4 that there was still a small, but significant, amount of PPV absorbance at 350 nm and lower. This is significant because it means that when the photoluminescence of converted films is measured with an excitation wavelength at 350 nm, or lower, both the dPPP and the PPV molecules will be directly excited into luminescence. However, when such a measurement was made for these films, the result that was actually obtained was that the dPPP photoluminescence peak which was typically observed at 420 nm was entirely quenched and only those peaks associated with the PPV were observable as denoted in Figure 4.4.5. Given that the dPPP photoluminescence peak and the PPV absorbance peak occurred in the same spectral region, simple re-adsorption of the blue light by the PPV

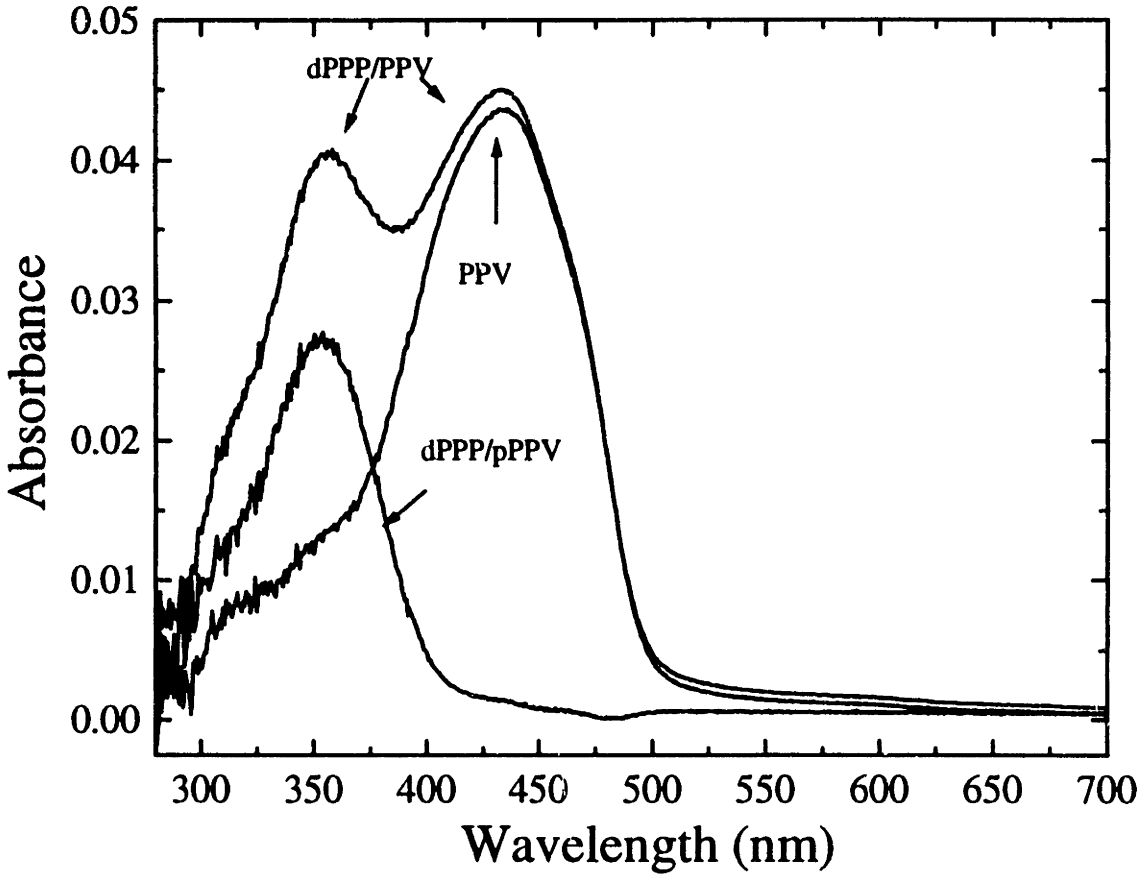

Figure 4.4.4 Deconvolution of the absorbance spectrum of a dPPP/PPV film (after conversion) with the film absorbance before conversion (dPPP/pPPV) to obtain the absorbance spectra of the converted PPV.

would most certainly be occurring. However, because the PPV layers are thin and their overall absorbance is low, re-adsorption of the radiation can be calculated to account for only 10% of the loss in dPPP photoluminescence. Given the electron-donating nature of PPV, photo-induced electron transfer from dPPP to PPV also seemed unlikely to account for such quenching. Exciton migration and transfer from the dPPP to the PPV offers one possibility for such thin and likely heavily interpenetrated films, but given the excellent spectral overlap of the dPPP photoluminescence peak with the PPV absorbance peak, quenching via a Förster energy transfer mechanism seems more probable. By using layer-by-layer assembly to make a supramolecular structure with dPPP separated from PPV by a certain number of non-conjugated spacer layers, measuring the dPPP photoluminescence quenching, and making the corresponding theoretical calculations; one can not only show that the quenching follows the spatial dependence of a Förster energy transfer mechanism,

but can also gain important structural information regarding the level of interpenetration of the spacer layers.

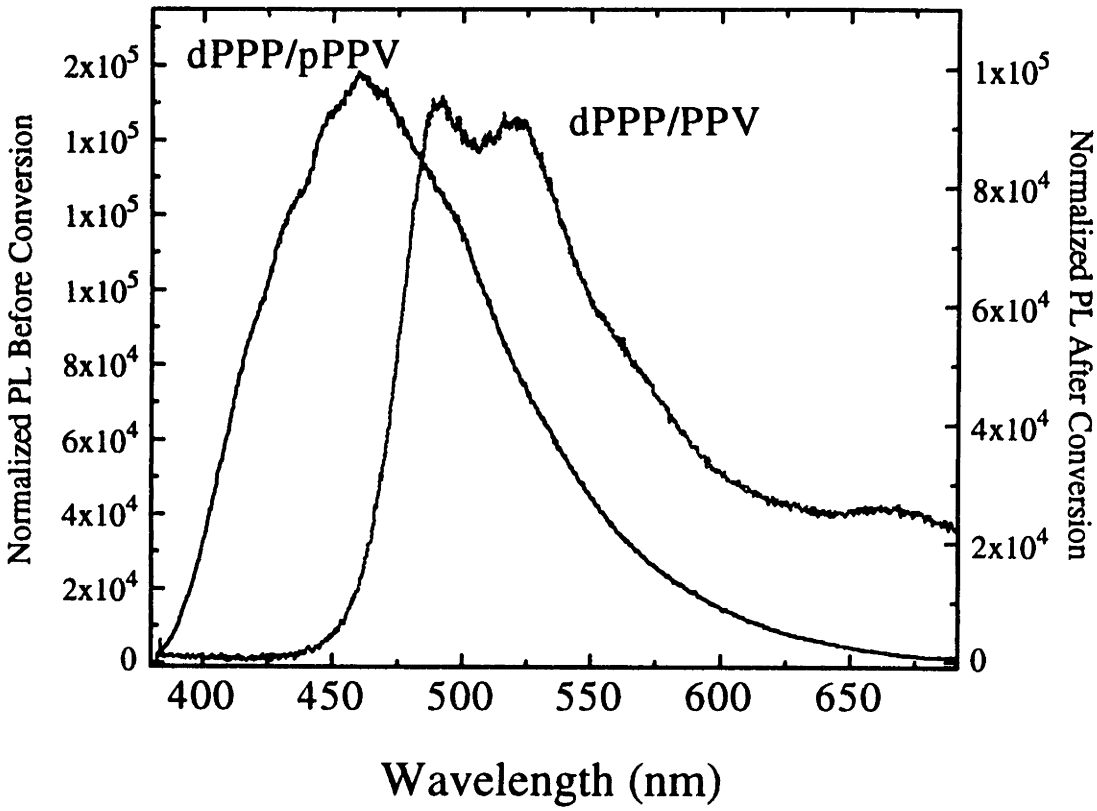

Figure 4.4.5 Photoluminescence spectra of dPPP/pPPV (before conversion) and dPPP/PPV (after conversion) excited at 350nm.

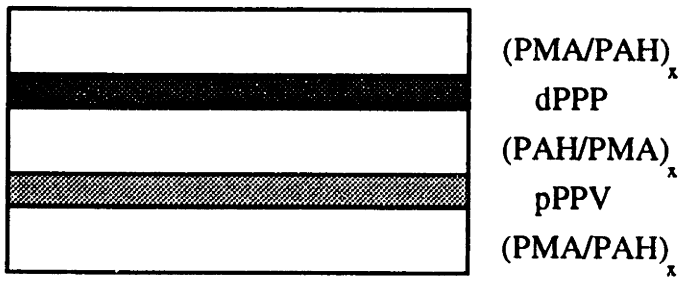

x = 1,2,3,4,5,6

Figure 4.4.6 Schematic of idealized PMA/PAH heterostructure with a layer of dPPP separated from a layer of pPPV by varying number of PMA/PAH bilayers. Total film structure = $[pPPV/(PMA/PAH)_x/dPPP/(PAH/PMA)_x]_5$.

4.4.B. PMA/PAH Heterostructure Assembly and Characterization

Sequentially adsorbed films of PAH/PMA have been fabricate under a variety of different solution condition to give uniform and optically clear films with controllable bilayer thickness. Films made with the same solution parameters as will be used for the heterostructure described below have specifically given an average bilayer thickness of 20 ± 3 Å as determined by profilometry, ellipsometry, and Small Angle X-ray Reflectivity (SAXR) on substrates of hydrophilic glass, aminosilane functicnalized glass, and silicon wafers. The average root mean square surface roughness of the film-air interface was also determined to be 18 Å at 20 bilayers and 27 Å at 40 bilayers by SAXR on silicon as discussed in Chapter 2.

Similar to the idealized structure shown in Figure 4.4.6, complex heterostructures involving dPPP layers separated from pPPV by 1 to 6 bilayers of PMA and PAH were fabricated and were characterized by UV-visible spectroscopy, photoluminescence spectroscopy, profilometry, and ellipsometry. As is demonstrated in Figure 4.4.7 for the case of a one bilayer of separation between the pPPV and dPPP layers, the assembly of these complex heterostructures system proceeds linearly as determined by the absorbance of the dPPP and the deconvoluted absorbance of the PPV. One can also monitor the single layer build-up of the heterostructure using ellipsometry, as is shown in Figure 4.4.8 for the same case. It is remarkable to note that the single layer thickness obtained in Figure 4.4.8 is actually a compilation of data taken for different samples with different numbers of total bilayers which remained wet during assembly and for single films which were dried and measured during the assembly process. It is also interesting to note that the average bilayer thickness of 22 Å which was measured for both of the spacer layers within the [PPV/$(PMA/PAH)_{x=1}$ /dPPP/$(PAH/PMA)_{x=1}$] heterostructure repeat unit is very close to that obtained for assembled films of pure PMA/PAH of 20 Å. The average single layer thickness contribution from dPPP and pPPV was measured to be 16 Å and 8 Å, respectively.

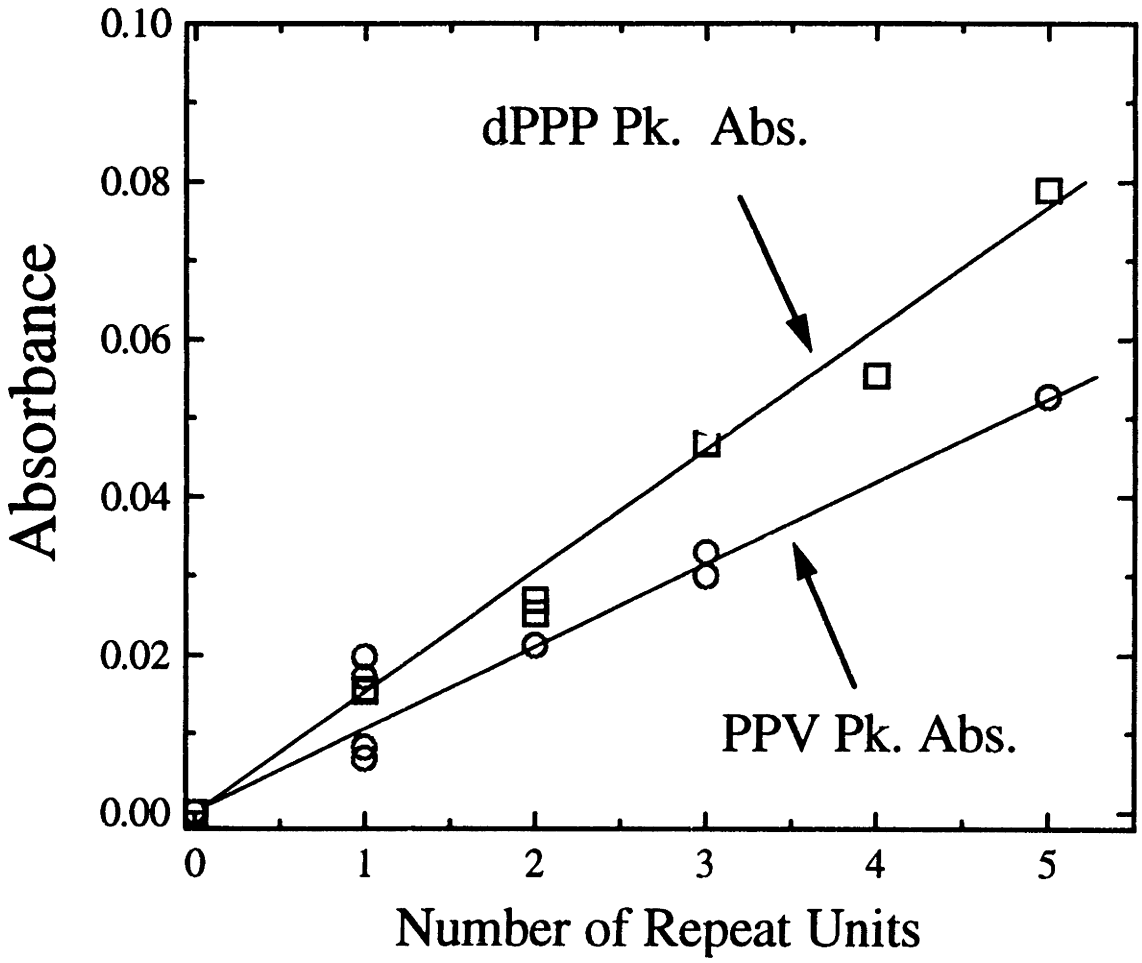

Figure 4.4.7. Linear build-up of heterostructure assembly with 1 bilayer of separation between layers of dPPP and pPPV as measured by dPPP peak absorbance during build-up and deconvoluted PPV absorbance after conversion for several films on glass.

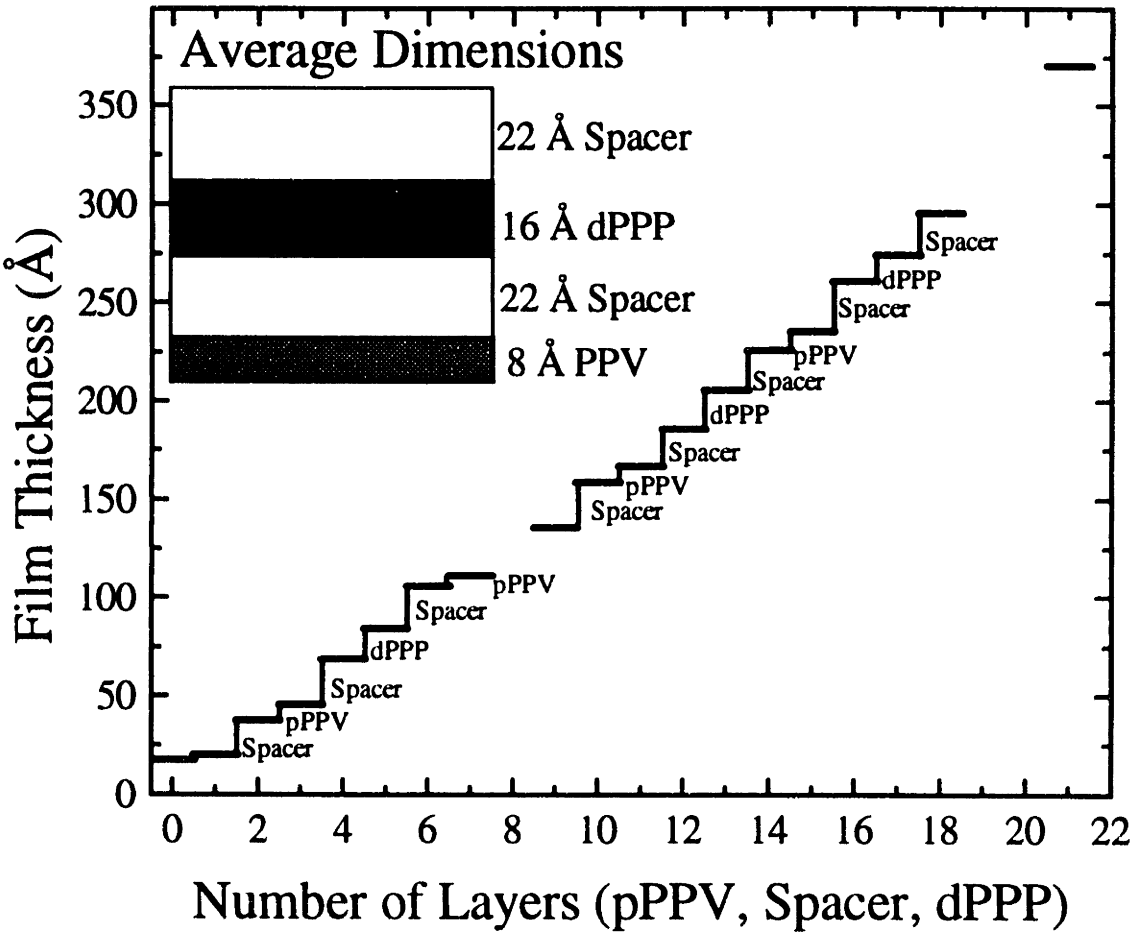

Figure 4.4.8 Thickness build-up of a heterostructure assembly with 1 bilayer of separation between layers of dPPP and pPPV as measured by ellipsometry on silicon with a 18Å native oxide.

As can be observed in Figure 4.4.9, the thickness of the heterostructure repeat unit, as measured by profilometry, with increasing numbers of separation bilayers scales linearly with the number of separation bilayers (x=1,2,3,4,5,6). Comparing values before and after conversion reveals that there is a contraction in the film thickness which scales with the number of spacer layers and can account for a decrease in film thickness of up to 18%. From the slope of the "after conversion" line, an average spacer bilayer thickness of 19 Å (21Å from the "before conversion" line) can be determined under the assumption that the amount of donor and PPV remains constant as the number of separation bilayers is increased. However, as can be observed in Figure 4.4.10, there are some fluctuations in the amount of dPPP and PPV incorporated into the heterostructure with increasing number of spacer bilayers. For example, one can observe a drastic increase in the amount of dPPP and PPV incorporated in the structure in going from no separation layers to 1 bilayer of separation. This is caused from the change in the nature of surface onto which the PPV and the dPPP molecules are adsorbed. For example, much more material should be adsorbed to the loopy surface which is expected for PMA/PAH than should be adsorbed for the relatively flat surface which is expected from the assembly of two highly charged molecules such as dPPP and pPPV. This is also consistent with the observation of increased adsorption of both dPPP and PPV with the use of "prep" layers of PMA/PAH. As the number of separation bilayers is increased to 6, one can observe a gradual decrease in the amount of PPV and a significant increase in the amount of dPPP. This decrease in the absorbance of the PPV may be linked to a decrease in the conversion efficiency in thicker films (over 65 bilayers assembled in the case of 5 heterostructure repeat units with 6 bilayers of separation). The increase in dPPP may be related to the increase in surface roughness or loopiness as the number of spacer bilayers is increased. It should be noted that though all the other films examined throughout this study were relatively uniform and clear, the films with one bilayer of separation required rinse baths which were pH adjusted to 3.5 in order to achieve similar uniformity.

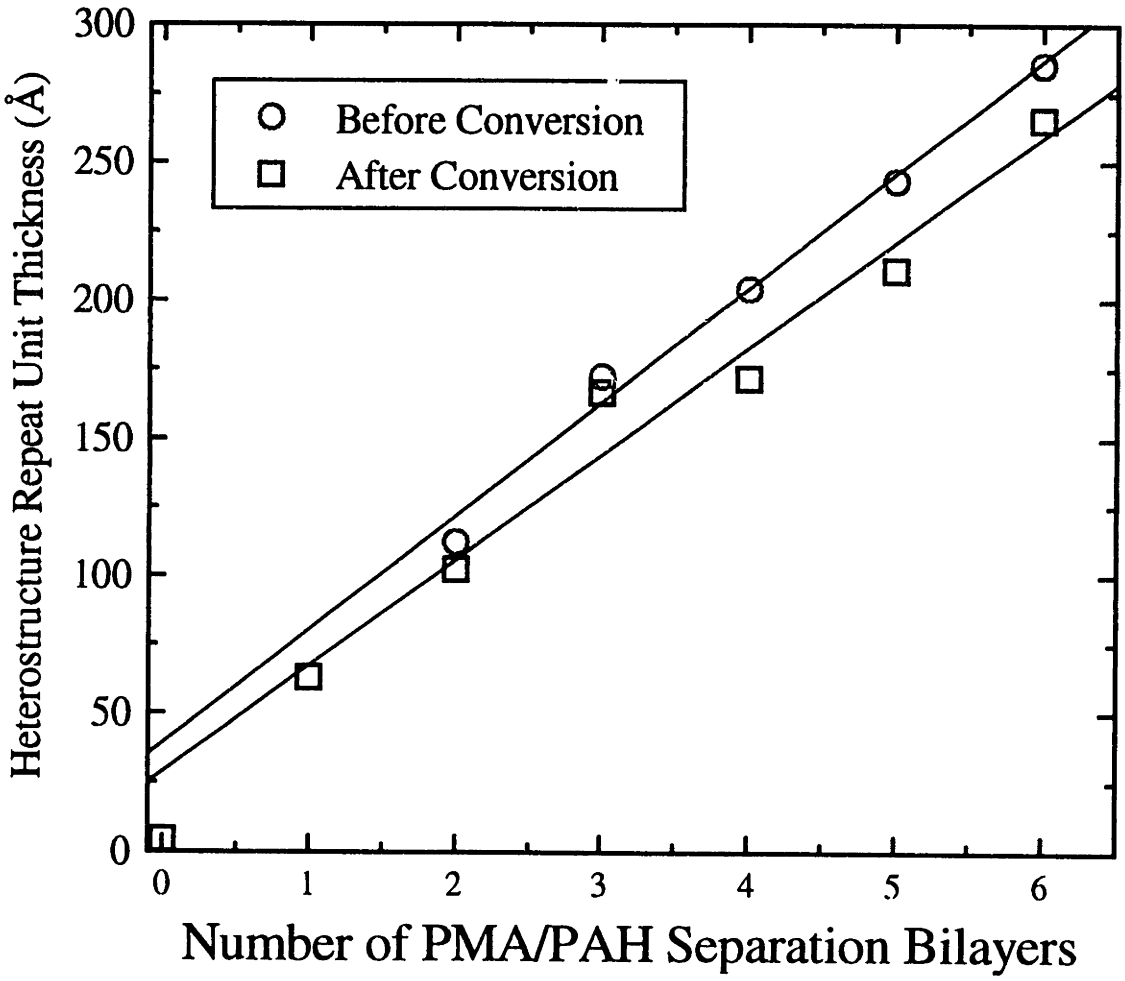

Figure 4.4.9 Heterostructure repeat unit thickness as a function of the number of PMA/PAH bilayers separating the dPPP from the pPPV as measured by profilometry before and after thermal conversion.

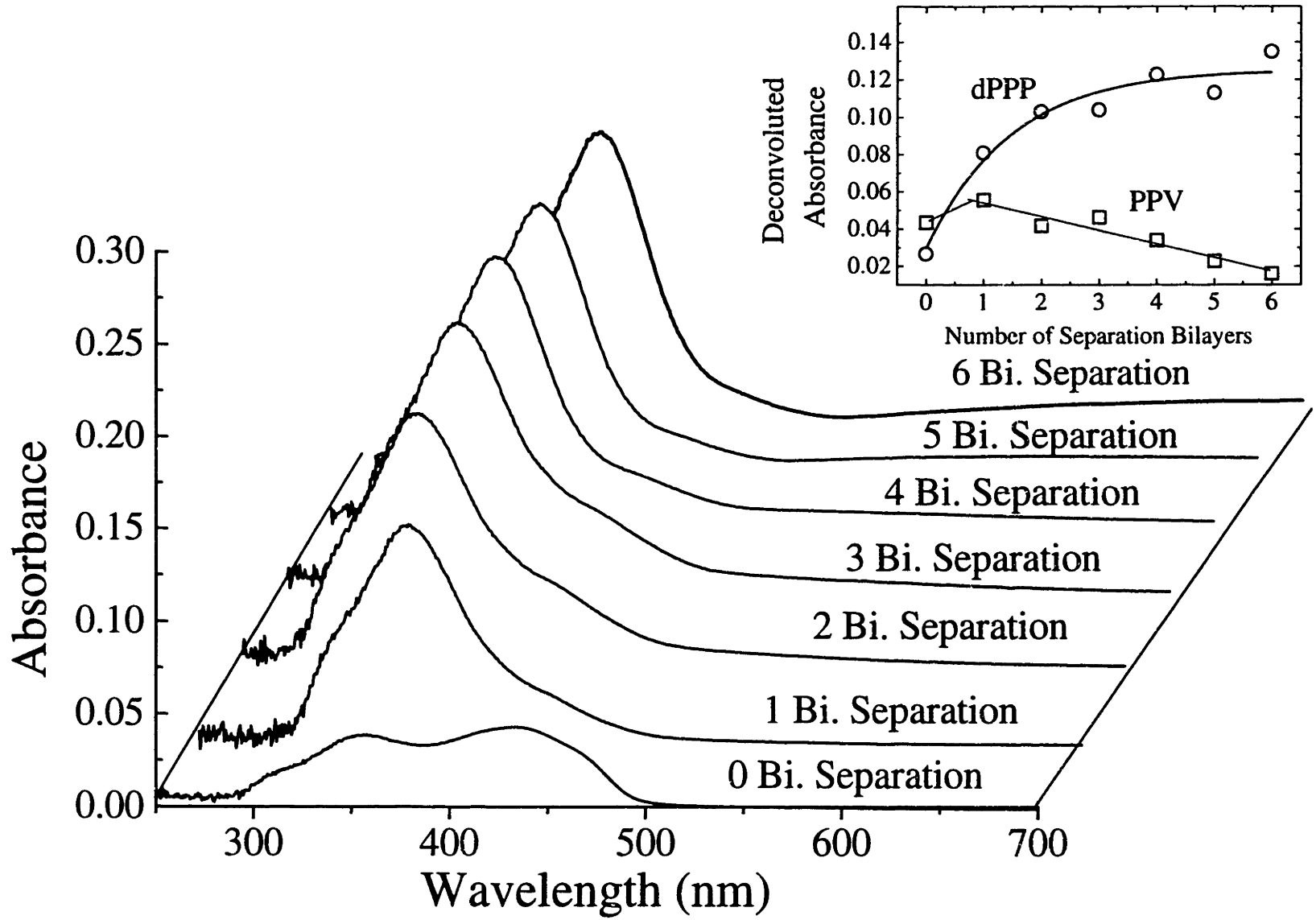

Figure 4.4.10. Film absorbance of 10 repeat units of dPPP/PPV heterostructure films with an increasing number of separation bilayers on glass after conversion. Inset: dPPP and PPV peak absorbance as a function of the number of bilayers of separation.

Another interesting effect which was observed with the addition of spacer bilayers is that the maximum wavelength of the PPV absorbance is blue shifted. In the non-separated PPV/dPPP films the deconvoluted PPV absorbance is centered around 425 - 430 nm which is close to the maximum observed for assembled films of PPV and sulfonated (polystyrene) (SPS) of 420 nm [108]. When the PPV is then separated from the donor polymer by one spacer bilayer, one can observe a shift to around 390 nm. With further separation, the PPV maximum remains constant near 390 nm, which is close to the PPV maximum typically observed for assembled films of PMA and PPV of 380 nm [108]. This change in PPV absorbance with local environment can be attributed to an increase in conjugation length due either to an increase in conversion efficiency in the presence of the sulfonic acid or to the ability of the PPV molecule to obtain a more planar conformation in the presence of SPS. This trend has been further substantiated by others within our group who have assembled pPPV with poly(acrylic acid) (PAA) and carboxylic acid derivatized polystyrene (CPS) (derivatized so as to have a carboxylic acid group in the para position as opposed to the sulfonic acid [173].

By combining all of the data taken on the heterostructure films by profilometry, ellipsometry, and UV-visible spectroscopy, estimations of the film structure for each heterostructure were made which took into account any fluctuation from the idealized heterostructure repeat unit shown in Figure 4.4.6. The resultant estimations were remarkable consistent as can be observed from a comparison of the estimated layer thickness values for a heterostructure with a separation of one PMA/PAH bilayer as measured by profilometry and UV-visible spectroscopy on glass (PPV = 7.7Å, PMA/PAH = 22.6Å, dPPP = 15.2Å) with that measured by ellipsometry on silicon (PPV = 8Å, PMA/PAH = 22Å, dPPP = 16Å). As the dPPP and PPV layers are further separated, the spacer layer thickness are calculated to remain relatively the same at 20.3 ± 2.2 Å while the PPV thickness contribution decreases to a low of 2-3 Å for the heterostructure separated by 6 bilayers and the dPPP thickness contribution increases to a high of 25 Å for the same film (all estimated after conversion).

When the pPPV in the heterostructures was converted to PPV with a thermal treatment of 210 ° C for 11 hours and the film photoluminescence was measured, one could observe the reemergence of the photoluminescence of the dPPP with increasing spacer bilayers. In order to quantify the amount of reemergence, the photoluminescence spectrum of the dPPP was separated from that of the PPV by a deconvolution which involved subtracting the product of the adjusted donor photoluminescence spectrum before conversion (adjusted such that the maximum is set equal to one) and a constant, from a similarly adjusted photoluminescence spectrum of the film after conversion. The value of the constant was found iteratively by deducing the value which gave flat baselines for the remaining PPV photoluminescence spectrum. This method effectively calculated the proportion of the converted film photoluminescence spectrum which could be attributed to the photoluminescence of the dPPP and the proportion attributed to the PPV. An example of this deconvolution can be viewed in Figure 4.4.11 for the case of a dPPP/PPV heterostructure with 3 bilayers of separation. After determining the relative proportions of the photoluminescence peaks of the dPPP to that of the PPV in the converted film, the experimental photoluminescence intensity (in counts per second) of both the donor and the PPV could be obtained by simply multiplying by the maximum of the initial experimental photoluminescence spectrum of the converted film. With the deconvoluted photoluminescence spectra of the donor and the PPV now in units of counts per second, each individual component can be normalized to the absorbance of the individual components.

Normalizing the photoluminescence spectra of the dPPP before conversion by the film absorbance, provided an average photoluminescence efficiency in the absence of the acceptor molecule, I_{∞}. Because the photoluminescence peak shape of the dPPP was consistent and not broadened in all of the separated films examined, photoluminescence intensity comparisons were made with peak maximums rather than the area under the peak. The average photoluminescence peak maximum per absorbance unit and exposure time for dPPP was determined to be 1.9×10^6 cts/(abs. unit * s) with a high standard deviation of 1.6×10^6 cts/(abs. unit * s) which is probably linked to the self-

quenching observed in the solution state. However, the normalized dPPP photoluminescence intensity changes through several orders of magnitude with quenching which makes such trends easily discernible over this inherent noise. For clearer viewing, photoluminescence intensities were plotted on a log scale which translates into normalized photoluminescence intensity with no energy transfer of 6.1 ± 0.4 Log[cts/(abs. unit * s)].

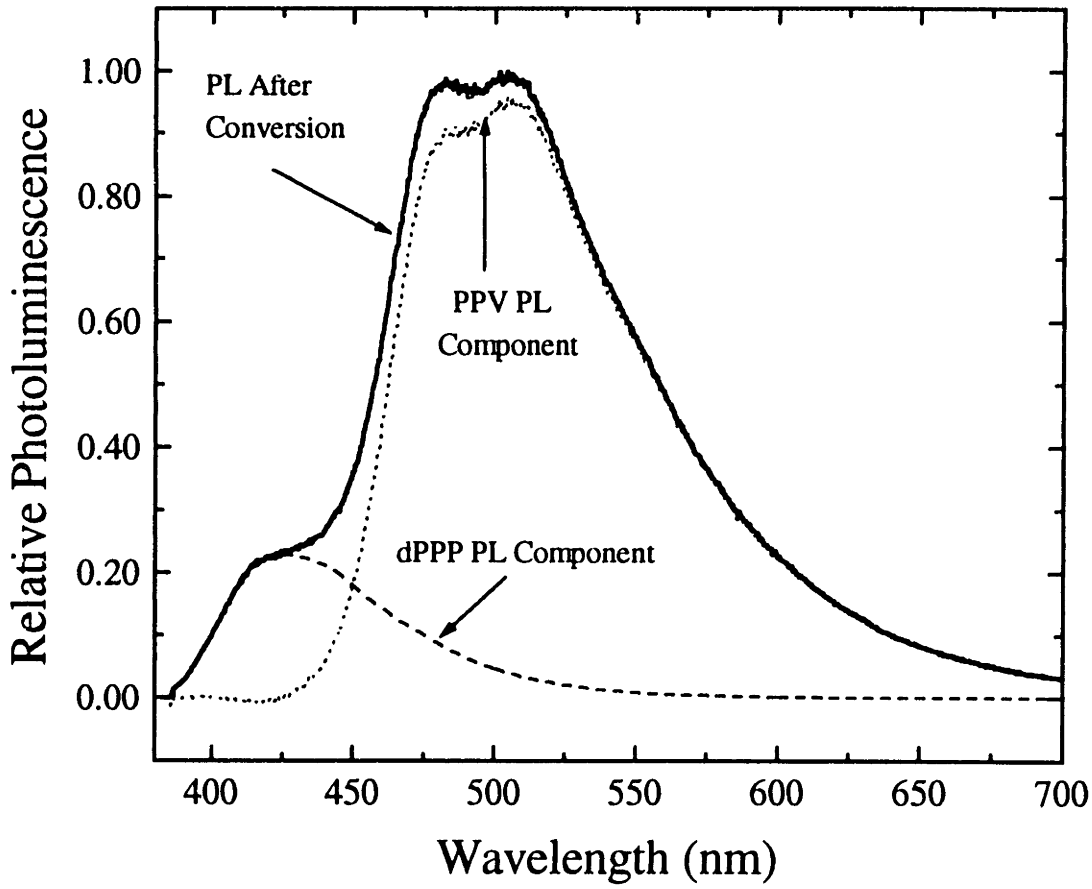

Figure 4.4.11 Photoluminescence peak deconvolution of the dPPP and PPV emitting components for a heterostructure film with 3 bilayers of PMA/PAH separating the dPPP layer from the PPV layer.

Using these methods to obtain the normalized photoluminescence efficiency of both PPV and dPPP after conversion, the energy transfer from dPPP to PPV can be followed through the reemergence of the dPPP photoluminescence. As can be viewed in Figure 4.4.12, the majority of the normalized dPPP photoluminescence reemerges after only one bilayer of separation. However, the quenched normalized photoluminescence of the dPPP is still below one standard deviation of the average normalized photoluminescence prior to conversion and requires a third bilayer of separation before being completely returned to the pre-conversion efficiency. Further analysis of the data can be made in the context of Förster energy transfer theory to estimate the level of penetration within the layers of the heterostructure.

4.4.C. Discussion of PMA/PAH Heterostructure Results

Using Equation 1 with X = 4 which describes a two dimensional layered structure with a donor-acceptor layer separation of d, a theoretical relationship between the amount of dPPP photoluminescence quenching and the layer separation can be calculated for a known d_o. As denoted in Equation 2, d_0, in turn, can be calculated by making reasonable assumptions regarding the orientation of the dipoles and by using experimentally determined values for the remaining variables which include the dPPP quantum yield, the index of refraction, the PPV layer absorbance, and the spectral overlap integral of the PPV absorbance and the dPPP photoluminescence. The dPPP quantum yield was estimated to be 5-15% as previously discussed. The index of refraction of PAH/PMA assembled films was measured by ellipsometry to be approximately 1.55 at 633 nm. The spectrum of the PPV absorbance was obtained by the previously mentioned deconvolution of the converted film absorbance spectrum. And, the overlap integral was calculated numerically using the deconvoluted PPV absorbance spectrum and the non-shifted dPPP photoluminescence spectrum. Using these pieces of experimental data, a theoretical range for d_o of 40 to 53 Å was calculated for the given films.

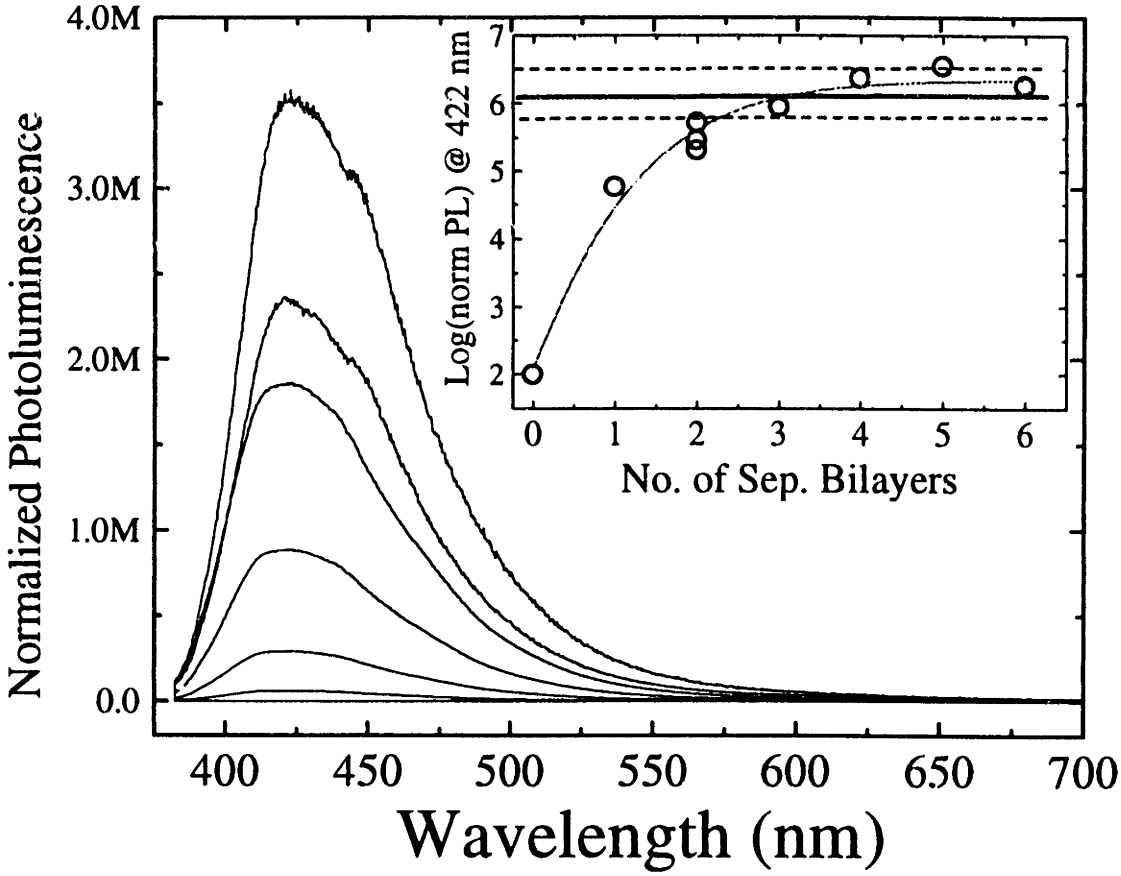

Figure 4.4.12 Re-emergence of deconvoluted dPPP photoluminescence as a function of the number of bilayers of separation from PPV. Inset: Peak photoluminescence as a function of the number of bilayers of separation relative to the average, non-quenched dPPP photoluminescence (solid line) and one standard deviation variance (dashed line).

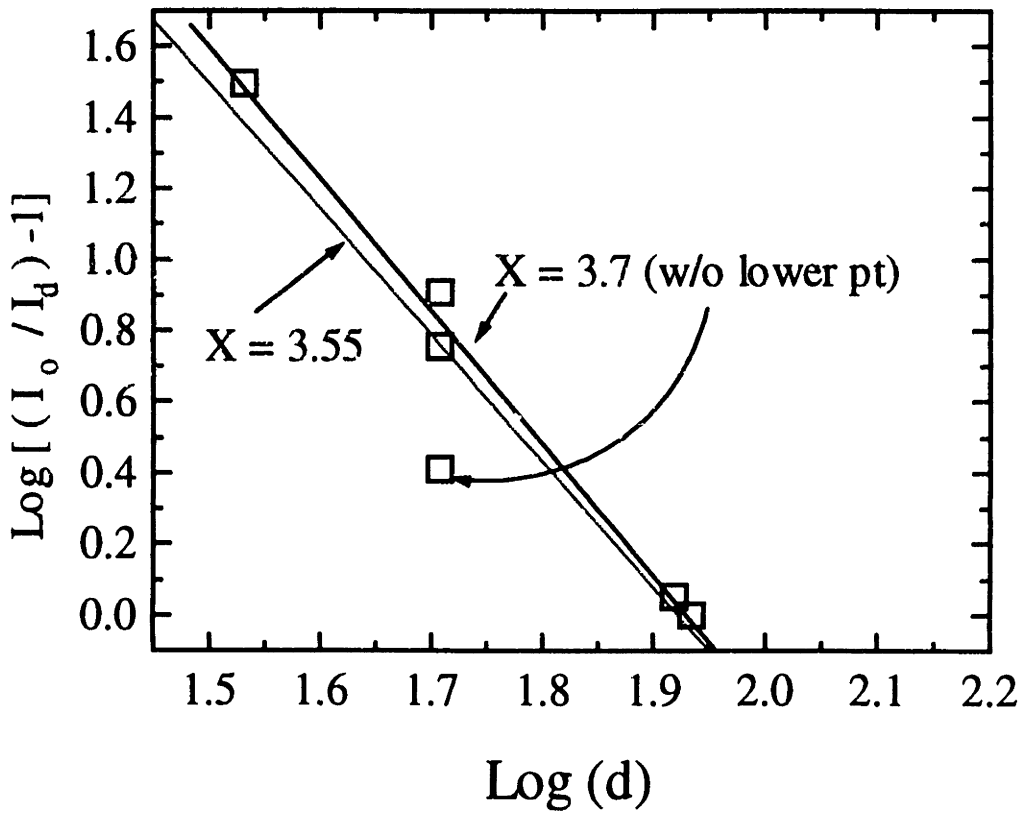

Figure 4.4.13 Determination of experimental quenching exponent X

By combining the structural information gain by ellipsometry, profilometry, and UV-Visible spectroscopy with the normalized photoluminescence data, the assumption in Equation 1 that the exponent X is equal to 4 was tested by measuring the slope of the line given by a plot of log(d) vs. $\log[(I_\infty/I_d)- 1]$ where d is taken as the distance between the centers of each layer. As can be observed in Figure 4.4.13, such a plot leads to a slope of -3.55 which corresponds to X = 3.55. If the lower point for the film with two bilayers of separation is removed, a much better fit through the remaining data and a value of X = 3.70 is obtained. While these values are close to the theoretical value of 4 for perfect discrete layers, a value of less than 4 suggest that there is some diffuseness in the layer which is analogous to the energy transfer between a plane and an array of molecules for which X = 3.

4.5 Application of a Diffuse Layer Energy Transfer Model

In an attempt to quantify the diffuseness of the sequentially adsorbed layers, the layers were mathematically modeled as having some level of interpenetration into the adjacent layers. Using an error function, the average layer density profile of a relatively discrete layer could be modeled as a "block" function with slightly rounded edges, while a very diffuse layer could be modeled as a very broad Gaussian distribution of segments. Both of these distributions, as well as all the intermediate distributions, were assumed to be symmetric about a distribution center. The separation between distribution centers was based on estimations of the layer separations derived from experimental data. The area under the distribution curve was also adjusted to correspond to the experimentally determined contribution that a layer made to the film thickness under the assumption of constant density. As a simplifying assumption, the same level of interpenetration was assumed for both the dPPP and the PPV layers.

The quenching efficiency of a certain distribution was calculated by first determining the probability of transfer (p_i) for an individual section i of donor molecules to an individual section of acceptor molecules at a fixed separation distance (d_j) using Equation 1 with a theoretical derived value for d_o [$p_{i,j} = f(d_j, d_o)$] given as

$$p_{i,j} = \frac{d_o^4}{d_j^4 + d_o^4} \tag{4.5.1}$$

Of course, because the acceptor molecules have an assumed spatial distribution of their own, one actually calculates a range of values $p_{i,j}$ corresponding to different values for d_j. Because the molecular density distributions are suppose to represent a 1-D cross-sectional average of a 3-D film, a weighting function (w_k) which is proportional to the acceptor molecular density at distance d_j should be multiplied by the probability of transfer for the slice of donor molecules. This weighting function takes into account the fact that a small amount of material in the tail of the acceptor molecule distribution which will appear

to be the closest to the donor slice (and therefore have the highest probability for transfer) in a 1-D representation, but may actually be spaced far apart in 3-D space. Instead, the probability of a donor slice being close to such segment will be proportional to the average amount of acceptor molecules within a particular 1-D slice. If this weighting function were not used, every slice of donor molecules would transfer energy to the same few acceptor molecules because in a 1-D representation they appear to be the segments closest to the donor distribution. It was then assumed that each slice of donor molecules will transfer energy at a distance $\underline{d}$ which corresponds to the maximum in the weighted probability distribution given by the multiplication of p_i by w_k as shown in Figure 4.5.1. The probability of transfer for that slice of donor molecules can then be calculated by substituting this distance into the following equation:

$$P_i = \frac{d_o^4}{(\underline{d})^4 + d_o^4} \tag{4.5.2}$$

where $\underline{d}$ is d_j at the maximum of $p_{i,j}*w_k$. Knowing the probability of transfer for each slice of donor molecules, the probability of transfer for the entire distribution can then be measured through the summation of the product of the slice transfer probability (P_i) and the volume fraction of donor molecules present within the slice (ν_i) which is given as

$$P = \sum_{i=1}^{n} P_i \cdot \nu_i \tag{4.5.3}$$

Because symmetry has been imposed on the distribution profiles of the donor and acceptor molecules, the calculation can be simplified to consider only the transfer from one side of the donor distribution to the adjacent acceptor distribution.

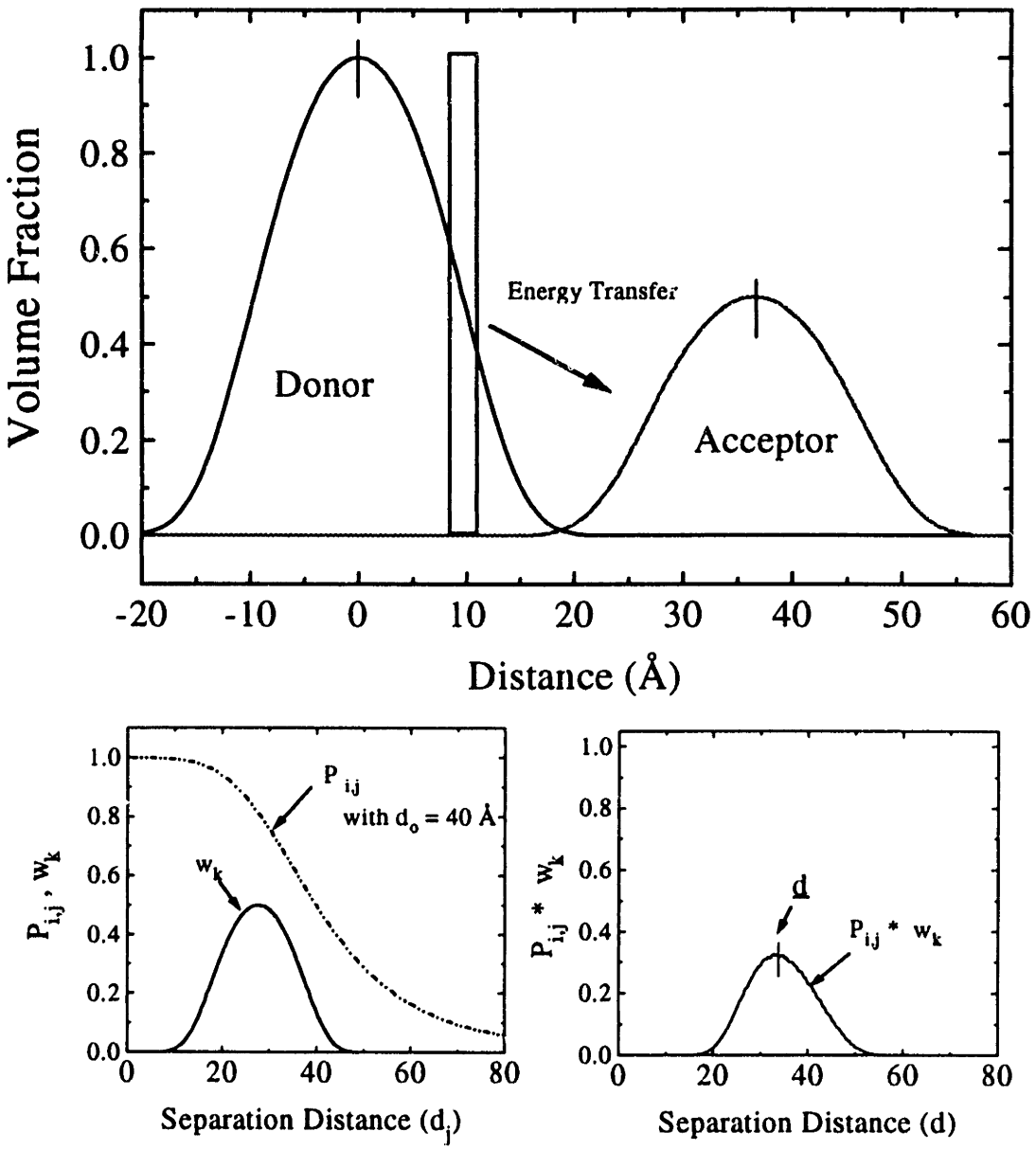

Figure 4.5.1 Calculation of $\underline{d}$ for a specific section of donor molecules through multiplication of the probability of transfer at a given distance d_j and a weighting function, w_k, which is proportional to the distibution of acceptor molecules.

By using the above equations, a molecular distribution profile can be adjusted for a given separation to result in the same amount of donor fluorescence quenching as is observed experimentally and, therefore, provides an estimate of the depth of penetration of the profile tail into the adjacent layers. For example, in Figure 4.5.1 one can observe that the experimental data denoted by the squares are more heavily quenched in comparison to what is predicted by theory for discrete (non-interpenetrated) layers with a predicted critical energy transfer distance of between 40 and 53Å (denoted by the dashed lines). This discrepancy is again an indication that there is some "diffuseness" to the assembled layers.

In an attempt to quantify the range of penetration, a lower bound and upper bound fitting of the data was performed using the above model. The lower bound fitting should represent the most heavily interpenetrated layers and involves simply assuming the lower extreme value for d_o of 40Å and then trying to determine the profile which will produce a lower bound fitting of the data. Similarly, the upper bound fitting should represent the least interpenetrated layers and be calculated using the upper extreme value for d_o of 53Å. The profiles obtained in this manner are gaussian distributions which have tails which effectively go to zero at distances from the center of the distribution of approximately 55Å and 25 Å, respectively. Because the typical discrete layer thickness would be about 19Å for the dPPP and 6Å for the PPV, this corresponds to a interpenetration over the discrete layer model of about 45-52Å for the upper bound and 15-22Å for the lower bound for an overall range of 15-52Å, or 1 to 2.5 bilayers. As can be observed in Figure 4.5.2, these upper and lower bound estimates (denoted by the solid lines) effectively bound the experiment data points. More emphasis should be placed on the data points below 0.4 because of the observed large standard deviation in non-quenched films which can be attributed to the presence of other quenching mechanisms. Volume fraction distribution profiles corresponding to an intermediate degree of penetration using d_o = 46.5 Å (the average of 40 and 53Å) are shown in Figure 4.5.3 along with the profiles predicted for discrete layers of dPPP and PPV. The spacer layers make up the remaining amount of volume and are made to correspond with experimentally determined thickness values.

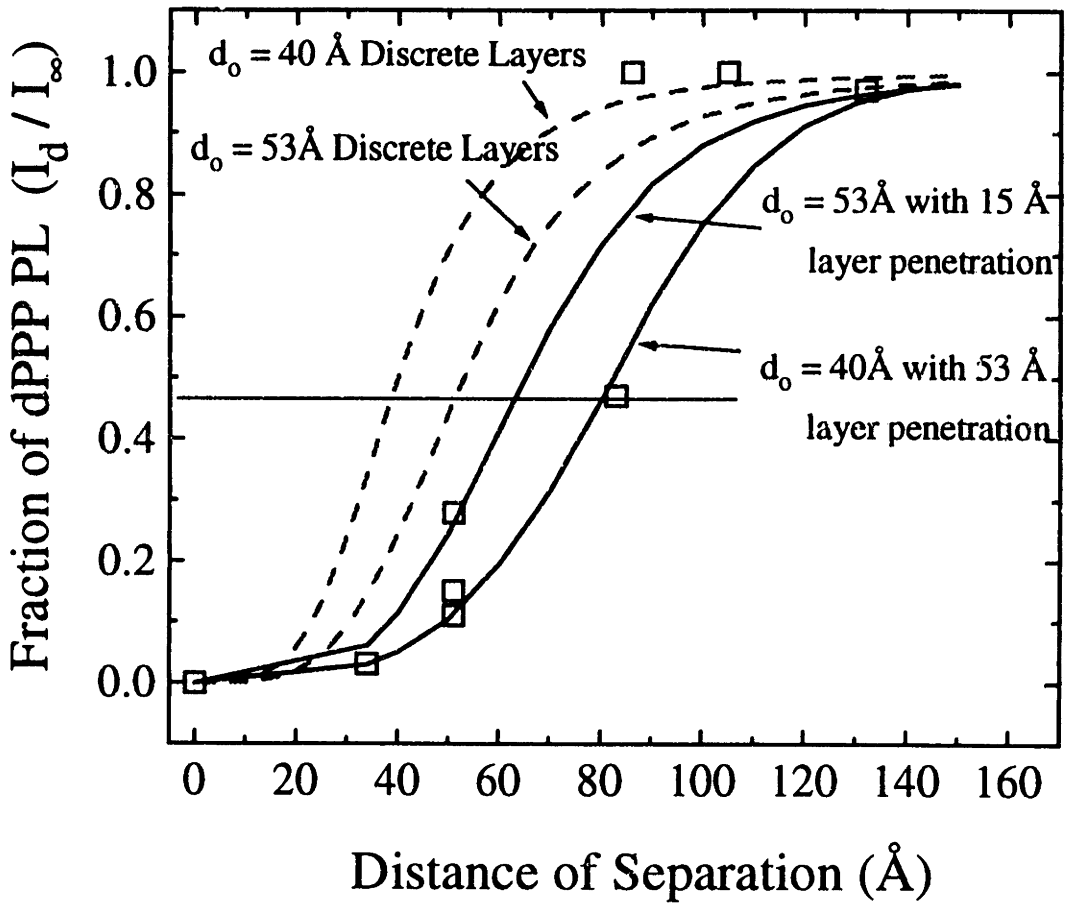

Figure 4.5.2 Comparison of the re-emergence of the photoluminescence as a function of the distance separating the centers of the dPPP and PPV layer distributions for discrete non-interpenetrated layers (dashed lines) and for interpenetrated layers (solid lines - upper and lower estimates).

In comparison to the other values reported for the level of interpenetration of assembled films, the results for PMA/PAH given here (segment penetration of 1 to 2.5 bilayers) agrees with those experiments on SPS/PAH which used the Surface Force Apparatus (SFA) and viologen mediated electron transfer which suggest that segments could penetrate 1.5 to 2.5 bilayers. However, if the energy migration through either dipole-dipole coupling or exciton migration is considered to be significant, the results described here actually represent an upper estimation to the level of interpenetration of layers. Considering that exciton migration in conjugated polymers can be quite high [174] and that donor-donor energy transfer has been estimated to extend over 200Å at high donor concentrations [175], we conclude that the level of penetration of dPPP or PPV into the PMA/PAH spacer bilayers is less than 2.5 bilayers.

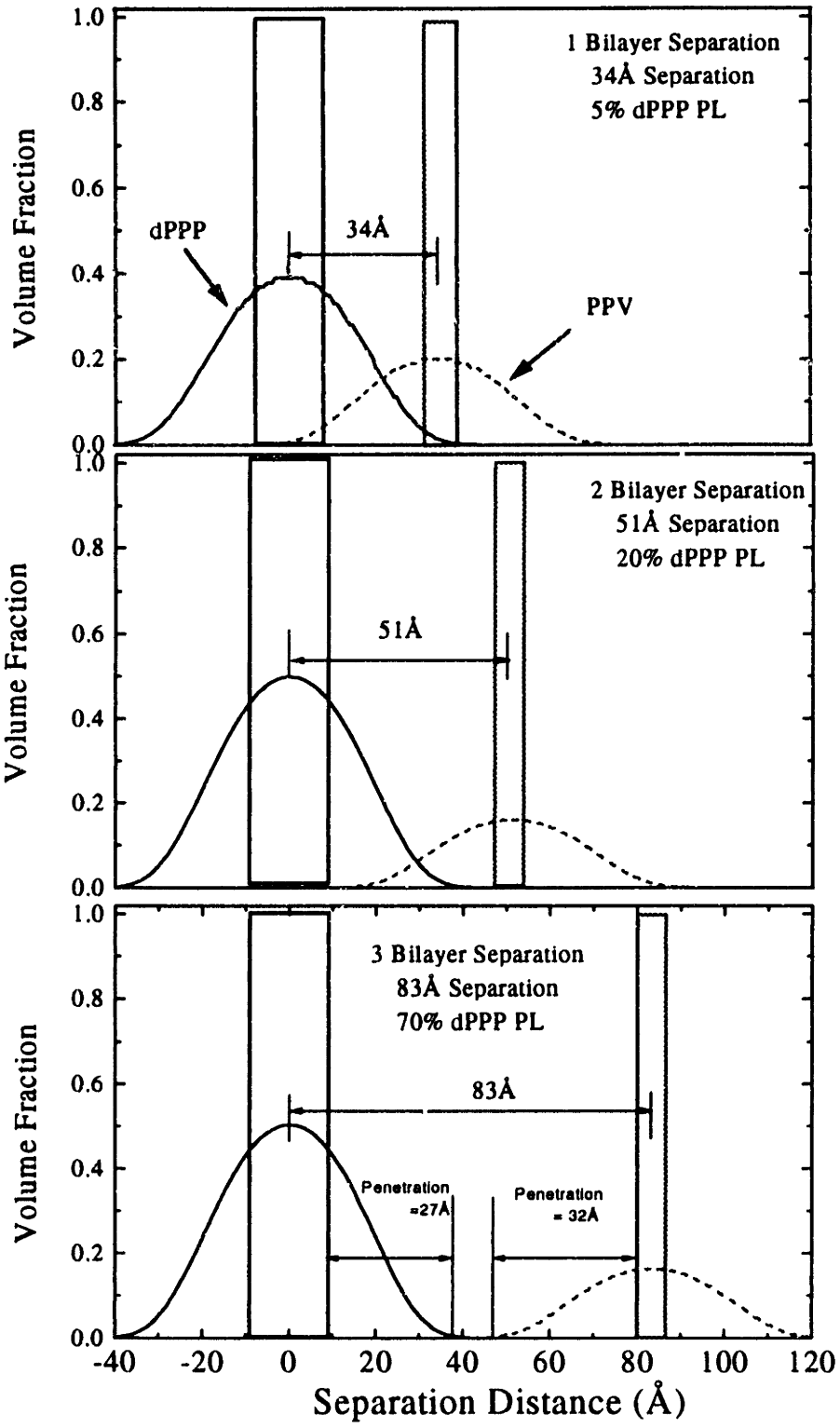

Figure 4.5.3 The dPPP and PPV volume fraction profiles for heterostructures with 1 to 3 PMA/PAH bilayers of separation calculated using an intermediate value for d_o of 46.5Å. For comparison the profiles for discrete layers of dPPP and pPPV are shown.

4.6 Results of SPS/PAH and PAA/PAH Heterostructure Separation Studies

Because sequential adsorption is applicable to a wide variety of polyelectrolytes, the ability to build heterostructures in order to estimate the level of penetration between the layers is not limited to the materials described above. In fact, other quenching studies have been made with different donor and acceptor molecules, as well as with different types of bilayer spacers. Here we briefly describe two additional separation studies which use the same dPPP donor and PPV acceptor with different types of spacer bilayers. The first spacer bilayer considered will be SPS/PAH assembled under low ionic strength conditions. This bilayer represents one of the thinnest bilayers which can be consistently assembled (~5-6Å on silicon by ellipsometry) and the incorporation of it into a heterostructure with pPPV and dPPP represents a heterostructure which consists entirely of highly charged polyelectrolytes which should have relatively flat conformations. The second bilayer considered is PAA/PAH assembled under pH conditions which give a thick bilayer characterized by long loops and tails.

4.6.A. SPS/PAH Separation Study

The solution conditions used for the fabrication of the heterostructure repeat unit of $[PPV/(SPS/PAH)_x/dPPP/(PAH/SPS)_x]_y$ are given in Table 1 of the Experimental section above. Heterostructures with 1 to 8 bilayers (x = 1,2,3,4,5,6,7,8) of separation were assembled to a varying number of heterostructures of up to 12 and monitored by UV-visible spectroscopy on hydrophilic glass and by ellipsometry on silicon with two prep layers of PMA/PAH. Linear build-up was achieved for heterostructures with up to 120 bilayers with an average SPS/PAH measured bilayer thickness of 6Å and a dPPP absorbance which was roughly one eighth of that observed for the heterostructures made with PMA/PAH. Following a thermal conversion of the films at 210°C for 11 hours, the deconvoluted absorbance of the PPV was shown to roughly one half of what was obtained for the PMA/PAH heterostructures. Film thickness values were confirmed by profilometry and the amount of dPPP photoluminescence quenching was measured as discussed in the previous section.

By combining all of this structural and photophysical data, the amount of dPPP quenching as a function of the estimated separation distance from PPV was determined and is summarized in Figure 4.6.1. It should be noted that instead of using a range of values for the quantum yield, the quantum yield of each heterostructure was estimated based on the film absorbance and experimental derived curves of quantum yield as a function of sample absorbance. As can be observed from Figure 4.6.1, the dPPP was significantly more interpenetrated than theoretically predicted for the previous case of PMA/PAH spacer layers. Because the data seemed to fluctuate below 0.2, no adequate fitting of the experimental data could be performed. However, through comparison with the data obtained for PMA/PAH, it can be concluded that the level of penetration is greater than 53Å. Even with 8 bilayers of separation (over 50Å) the photoluminescence of the dPPP is not regained. It is believed that this high level of interpenetration is due to the formation of incomplete surface coverage which gives a highly mixed film structure.

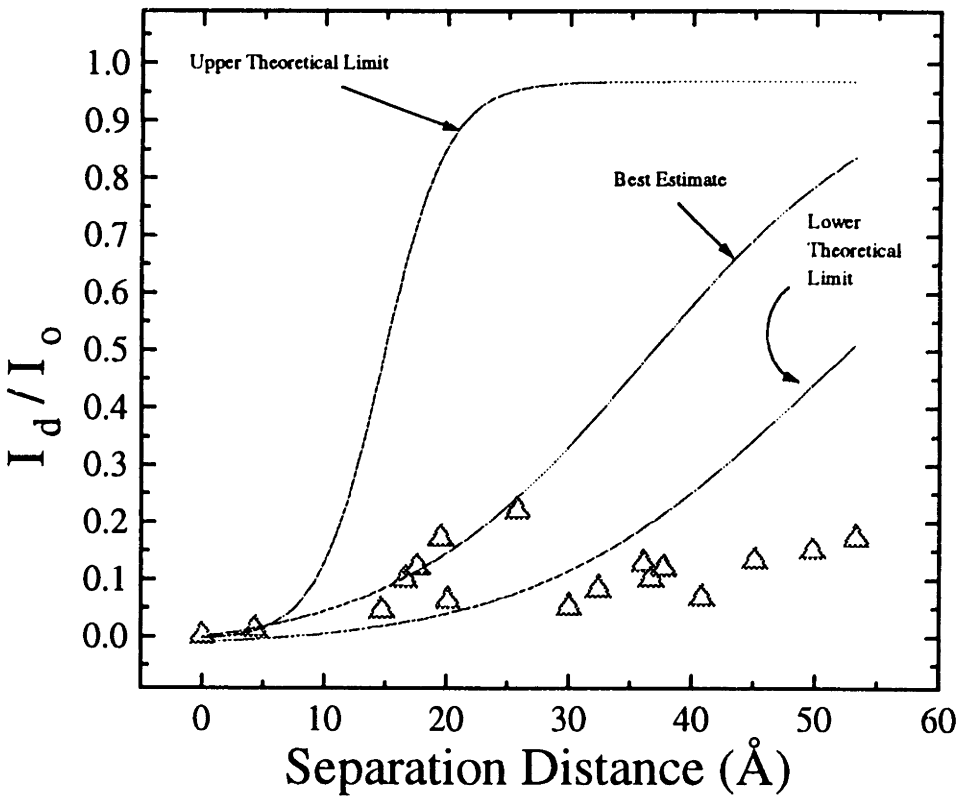

Figure 4.6.1 Relative amount of quenching of the dPPP photoluminescence by PPV as a function of the separation distance made with SPS/PAH bilayers. The lines represent the theoretical estimations made for discrete layers with a range of values for d_o of 12-53Å.

4.6.B. PAA/PAH Separation Study

The solution conditions used for the fabrication of the heterostructure repeat unit of $[PPV/(PAA/PAH)_x/dPPP/(PAH/PAA)_x]_y$ are given in Table 4.3.1 of the Experimental section above. Optically clear heterostructures with 1 to 3 bilayers (x =1,2,3) of separation were assembled to a varying number of heterostructures of up to 5 and monitored by UV-visible spectroscopy on hydrophilic glass and by ellipsometry on silicon with 1 to 3 prep layers of PAA/PAH. Based on ellipsometry data, each heterostructure had approximately 12Å of PPV separated from over 60Å of dPPP by PAA/PAH bilayers which fluctuate in thickness from 57 to 131 Å with the bilayers adsorbed onto layers of pPPV giving spacer bilayer thickness values roughly twice the thickness of those assembled onto dPPP. The thickness of the layers within the three heterostructures examined are summarized in Figure 4.6.2. The expected PAA/PAH bilayer thickness obtained for films assembled on silicon under identical conditions was 65Å/bilayer. Profilometry measurements of the total heterostructure assemblies on glass gave values for the film thickness which were roughly 30% thinner than those measured on silicon by ellipsometry. While more work will be needed to completely understand all of these thickness changes in the heterostructure, the fact that no significant quenching of the dPPP photoluminescence was observed for any of these heterostructure films when the pPPV was converted to PPV indicates that one sufficiently large bilayer is enough to completely prevent energy transfer from dPPP to PPV.

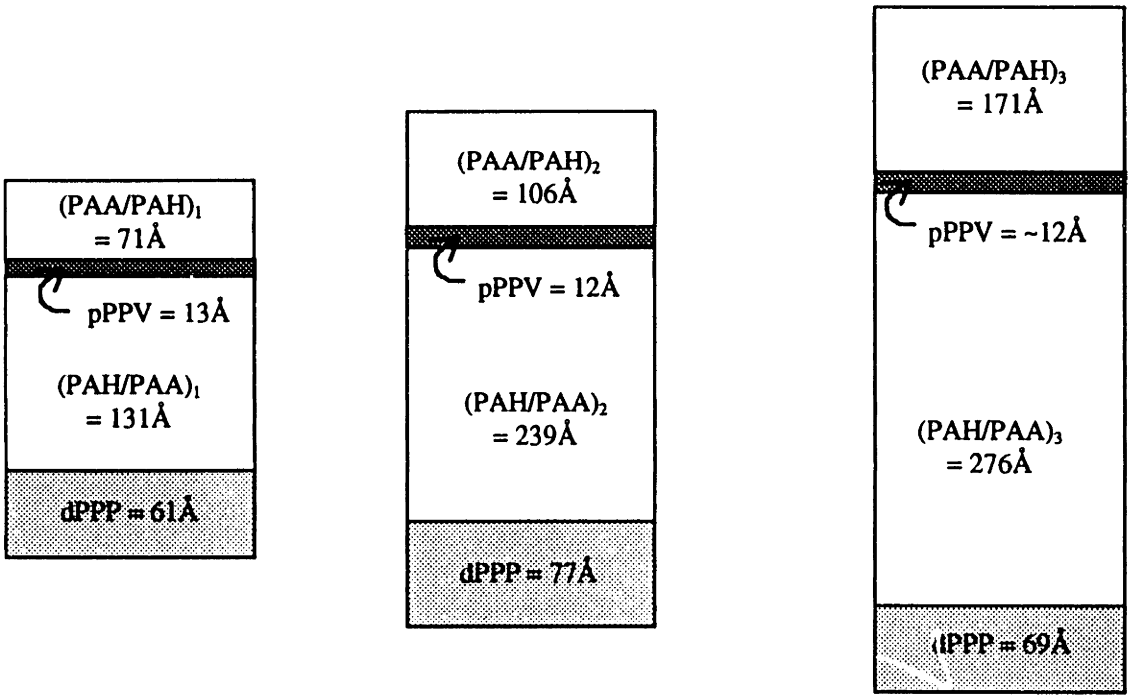

Figure 4.6.2 Schematic representation of the layer thickness values measured by ellipsometry (before conversion) for heterostructures containing 1 to 3 spacer bilayers of PAA/PAH. Note that the spacer bilayers deposited on dPPP layers are much thicker than those deposited on the pPPV.

4.7 Concluding Remarks

When the three separation studies are considered together, it appears that a range of penetration behavior can be obtained which is highly dependent on the system assembled and not on a specific number of bilayers. If it is assumed that the highly penetrated SPS/PAH bilayers are a result of sub-monolayer build-up which causes additional mixing of the adsorbed layers, then the conclusion can be made that the level of penetration of segments from one layer into an adjacent layer which consists of at least a monolayer, is less than 50Å. Though, in general, more heterostructure studies should be made to determine under what condition this conclusion holds, the applicability of it to systems which use salt to increase the bilayer thickness of the spacer bilayers would be of particular interest.

Chapter 5. - Sequentially Adsorbed Films for Organic Light Emitting Devices

5.1 Introductory Remarks

Though the uses for electrostatic self-assembled films have been varied, one of the most promising applications for these films is in light emitting diodes (LEDs). LEDs are semiconducting or electrochemical devices which emit radiation (electroluminesce) in the visible wavelength region with the application of a voltage [176]. The recent discovery that organic semiconducting polymers and organic dyes can be used in these devices [177] has created a flurry of research effort in this field. Current efforts have achieved high quantum efficiencies (~4%) [178], light output intensities of 1000 [179] to 70,000 Cd/m^2 [180] under normal operation and up to 5 x 10^6 Cd/m^2 with short voltage pulses [181], lifetimes of over 10,000 hours [182], and a broad spectrum of colors [183,184], including white light [185]. By blending electroluminescent polymers which emit in different regions of the visible spectrum, it has also been possible to tune the color of some LEDs by simply controlling the voltage applied [186].

Even though brightness and efficiency levels have been competitive with traditional materials, the lack of long-term device stability for most of the organic LED's has been the major stumbling block to their commercialization in the past [187]. However, recent advances in long term device performance have lowered the barrier to commercialization of these organic LEDs [179]. Current research efforts have even focused on the fabrication of microcavity devices [188] for lasing in these polymer films [189] in the hope of making thin film organic lasers which are electrically pumped.

Usually, simple organic LEDs consist of an active organic thin film sandwiched between a transparent indium tin oxide (ITO) electrode deposited on glass and a vacuum deposited metal electrode such as aluminum. Figure 5.1.1 illustrates a typical LED construction. One theory on the operation of organic LEDs, put forth by I. D. Parker, involves the tunneling of electrons and holes through interfacial barriers, caused by the band offset between the polymer and the electrode [190], which form negatively and positively charged polarons within the polymer [191,192]. The polarons migrate under the

influence of an applied electric field, combine to form a polaron exciton which then undergoes radiative recombination [193,194]. The height of the injection barrier can be controlled by selecting an electrode with the desired work function which can in turn affect the observed device turn-on voltage as well as the device efficiency. The lower of the two interfacial barriers will control the flow of majority carriers and thus the current-voltage (I-V) behavior. The higher barrier will control the flow of minority carriers and thus the device efficiency. Because the level of injection will depend on the electric field, a field dependent light output should also be observed. The optimum device performance comes about when both barriers are low, the injection of electron and holes are balanced, and the emitting material has few non-radiative pathways for excited state decay.

While Parker gives experimental evidence on derivatized poly(p-phenylene vinylene) which confirms his claims of controlling device characteristics through selection of the appropriate electrodes, others have seen that device characteristics are often more sensitive to surface preparation than to the work function of the deposited materials [195]. This discrepancy has been accounted for with a band bending modified tunneling theory (BBMT) in which barrier formation occurs through the generation of interface states caused by impurities or polymer-metal interactions [196]. In this case, the carrier injection becomes more sensitive to the nature of the barrier than to the work function of the metal. Band bending by surface states will continue to be a source of further research but should, in the mean time, emphasize the importance of sample preparation and of the polymer-metal interactions in the fabrication of polymeric LED's. This can also be seen as a unique opportunity for self-assembly because of its ability to control the composition of the polymer surface to within tens of angstroms by varying the last deposited layer.

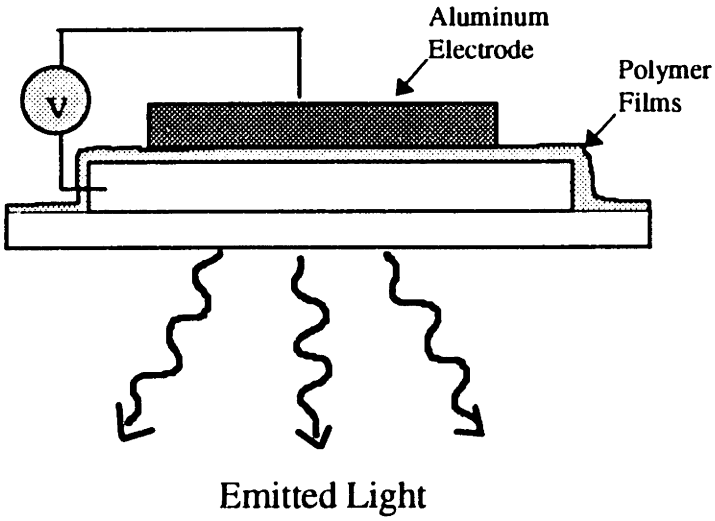

Figure 5.1.1 Schematic representation of a polymeric based light emitting device composed of a bottom ITO transparent electrode and a top electrode of thermally evaporated aluminum.

Another advantage that self-assembly has in device fabrication is the ability to readily form heterostructure devices. Heterostructure devices have been one means by which a more balanced injection of holes and electrons, and thus eight fold increases in efficiency, have been achieved [108]. In the case of PPV which has positively charged polarons as the majority carrier, an electron transport layer (ETL) can be placed between it and the metal electrode. This layer not only helps to transport negatively charged polarons away from the negative electrode and into the emissive PPV layer, but also provides a barrier to the migration of positively charged polarons. Therefore, they accumulate at the interface. The intended result is that the negative and positive polarons will efficiently combine into a polaron exciton near the PPV-ETL interface and decay radiatively. Similarly, if needed, a hole transport layer (HTL) could also be placed between the ITO and the emitting layer to restrict the migration of the negatively charged polarons and increase that of the positively charged polarons. Devices having an emitting layer sandwiched between both a ETL and a HTL have been produced using sublimed dyes and have shown that it is possible to confine charge carriers and molecular excitons to an emitter layers as thin as 50Å [197]. With self-assembly, thin film structures can be

fabricated with both polyelectrolytes and charged dyes. This fine level of control would be difficult, if not impossible, using tradition fabrication techniques such as spin-coating.

Another proposed mechanism for the operation of organic LEDs which is different from the tunneling theory discussed above is the formation of a light emitting electrochemical cell (LEC). The operation of this device is based on the in-situ formation of a p-n junction from the oxidation of the materials at one electrode and reduction at the other electrode [198]. The net result of this mechanism on device performance is that, for thin film devices, one should observe a turn-on voltage which is independent of the electrode type and the device thickness. The device should also give symmetric plots for both the light versus applied voltage and current versus applied voltage. Slow kinetics for the formation of the p-n junction can lead to an observable "charging" time which can be lowered with the addition of electrolyte counterions and ion-transporting materials. Within this chapter, the device performance of LEDs made from films of sequentially adsorbed layers of derivatized poly(p-phenylene) will be discussion in the context of these two theories of device operation.

5.2 Sequential Adsorption of dPPP with Various Polycations

While poly(phenylenevinylene) and its derivatives are the most well studied polymers in the literature for use in LEDs [177-179,181,187,189,193-196,198,199], poly(phenylene) (PPP) based molecules have also received attention as emitting materials [183,184,200,201,202,203,204]. Due to its large band gap, PPP has the desired quality of emitting in the blue region of the spectrum, which is not easily achieved by other conjugated polymers. However, because of PPP's low processibility in its underivatized form, most of the above works use PPP-ladder type molecules which have chemical bridging units between phenylene units to promote planarity, and functional groups substituted on both the bridging unit and the phenylene unit to promote solubility. These planar structures often have to be synthetically manipulated to avoid the formation of molecular aggregates, which can lead to a red-shifted component of the photoluminescence [205]. In contrast, Reynolds and coworkers have synthesized a polyanionic version of PPP (dPPP) which is soluble in water, does not contain bridging units, and does not exhibit significant shifting from its blue photoluminescence [170]. Because this molecule is a polyelectrolyte, it is ideally suited for sequential adsorption and subsequent incorporation into an organic LED. In order to fully understand the device characteristics of such a film, the properties of the sequentially adsorbed film must first be characterized. Therefore, this section will summarize the characterization of the sequentially adsorbed films and the following section will discuss their device properties once the film is incorporated into an LED. The chemical structures of dPPP and the polycations with which it is assembled can be viewed in Figure 5.2.1.

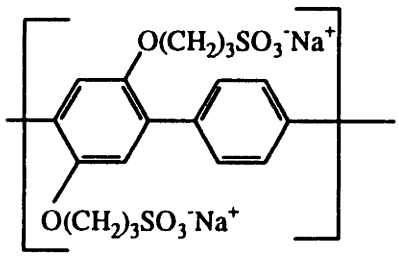

dPPP

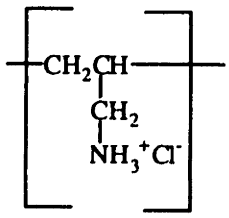

PAH

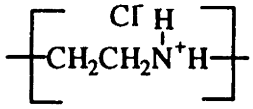

PEI

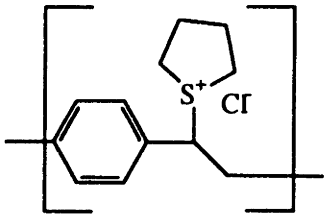

pPPV

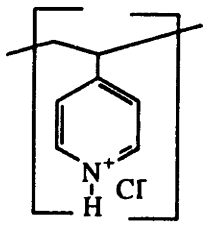

PYR

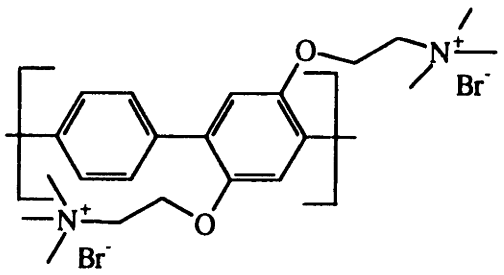

(+)PPP

Figure 5.2.1 Chemical structures of the polycations assembled with derivatized poly(p-phenylene) [dPPP] - Poly(allylamine hydrochloride) [PAH], Poly(ethylene imine) [PEI], sulfonium precursor to poly(phenylenevinylene) [pPPV], Poly(vinylpyridine) [PYR], and polycationic derivatized poly(p-phenylene) [(+)PPP].

The polycations assembled with dPPP include poly(allylamine hydrochloride) [PAH], poly(ethylene imine) [PEI], the sulfonium precursor to poly(phenylenevinylene) [pPPV], poly(vinylpyridine) [PYR], and a polycationic derivatized poly(p-phenylene) [(+)PPP]. The experimental conditions and the resultant film characteristics are summarized in Table 5.2.1 for the sequentially adsorbed films of dPPP/PAH, in Table 5.2.2 for films of dPPP/PEI, in Table 5.2.3 for films of dPPP/pPPV, and in Table 5.2.4 for the sequentially adsorbed films of dPPP/PYR and dPPP/(+)PPP. For all of these films, dPPP was adsorbed from a solution with a concentration of approximately 0.001M and no salt was added to any of the polycation solutions. With the exception of the films of dPPP/PEI, all of the films exhibited a linear build-up. The dPPP/PEI films typically exhibited a two regime build-up involving a very thin layer for the first 5 bilayers assembled followed by thicker layers for subsequent bilayers. This has been previously observed for PEI and is believed to be linked to the highly branched nature of the molecule [90]. The dPPP absorbance per bilayer of these two regimes is denoted in Table 5.2.2 for all dPPP/PEI films except those assembled with dPPP and PEI solution pH's of 7, which showed linear growth. The displayed bilayer thickness was calculated by dividing the total film thickness by the number of bilayers assembled and does not take into account this non-linearity in growth. The conditions for which the dPPP/PEI films turned cloudy during build-up are also noted in Table 5.2.2. Overall, it appears that the dPPP films assembled with PEI behave very differently from the other polycations.

For each dPPP/polycation combination, except (+)PPP, a rough estimate was made of the volume percent of dPPP contained within each sequentially adsorbed film using an absorbance /thickness ratio for dPPP of 1875 Å/absorbance unit. This value was derived from a correlation of the dPPP layer absorbance and layer thickness as measured by UV-visible spectroscopy and ellipsometry for substrates of glass and silicon, respectively, dipped under the same solution conditions. The average measured dPPP solution extinction coefficient of 9670 (Abs. unit l cm^{-1} $moles^{-1}$) was not used because it gave estimates of greater than 100% dPPP for all of the films. An estimate for the amount of dPPP in dPPP/(+)PPP films was not made because both PPP derivative absorb in the same region.

Table 5.2.1 Properties of Sequentially Adsorbed Films of dPPP/PAH

[PAH] (M)	PAH pH	dPPP pH	[NaCl] in dPPP (M)	Peak Abs. /bilayer	Thickness /bilayer	% dPPP (estimated)
0.001	2.5	7	-------	0.001 ^{sg}	--------	--------
0.001	2.5	3.5	-------	0.002 ^{sg}	6 Å ^{p}	60%
0.01	2.5	3.5	-------	0.003 ^{hg}	7 Å $^{p/hg}$, 5Å $^{e/si}$	80% 100%
0.01	3.0	4.5	-------	0.003 ^{hg,sg}	5 Å $^{p/hg,\ e/si}$	100%
0.01	3.0	5.0	-------	0.003 ^{hg}	5 Å $^{p/hg\ ito,\ e/si}$	100%
0.01	2.5	3.5	0.1 M	0.007 ^{hg}	16 Å $^{e/si}$	80%

sg - silanized glass substrate, hg - hydrophilic glass substrate, si - silicon substrate, ito - patterned ITO glass substrate, p - profilometry thickness measurement, e - ellipsometry thickness measurement

Table 5.2.2 Properties of Sequentially Adsorbed Films of dPPP/PEI

(All PEI concentrations = 0.001M)

PAH pH	dPPP pH	[NaCl] in dPPP (M)	Peak Abs. /bi. (<5 bi.)	Peak Abs. /bi (>5 bi.)	Thickness /bilayer	% dPPP (estimated)
7	7	-------	--------	0.003 ^{sg}	--------	--------
7	3.5	-------	0.007 $^{sg,\ ito}$	0.030 $^{sg,\ ito}$	94 Å $^{p/\ sg}$ (Cloudy)	60%
3.5	3.5	-------	0.004 $^{hg,\ sg,\ ito}$	0.009 $^{hg,\ sg,\ ito}$	20 Å $^{p/hg}$	80%
7	7	0.1 M	0.007 ^{ito}	0.015 ^{ito}	-------	-------
3.5	3.5	0.1 M	0.007 ^{hg,sg}	0.009 ^{hg}	23-43 Å $^{e/si}$ (Cloudy)	70% -40%

sg - silanized glass substrate, hg - hydrophilic glass substrate, si - silicon substrate, ito - patterned ITO glass substrate, p - profilometry thickness measurement, e - ellipsometry thickness measurement

Table 5.2.3 Properties of Sequentially Adsorbed Films of dPPP/pPPV

[pPPV] (M)	pPPV pH	dPPP pH	[NaCl] in dPPP (M)	Peak Abs. /bilayer	Thickness /bilayer	% dPPP (Estimated)
0.0002	~5	3.5	-------	0.001 ^{hg} 0.002 ^{prep,ito}	3-5 Å $^{p/hg,\ e/si}$ 5-8 Å $^{p/prep}$	60% - 40% 70%-50%
0.001	~5	3.5	-------	0.004 ^{sg,hg}	10 Å $^{p/sg\ hg}$	70%
0.0002	~5	3.5	0.1 M	0.005 ^{hg} 0.006 ^{prep}	14 Å $^{p/hg}$ 15 Å $^{p/prep}$	70% 70%
0.0002	~5	3.5	0.4 M	0.007 ^{hg} 0.009 ^{prep}	23 Å $^{p/hg}$ 25 Å $^{p/prep}$	60% 70%

sg - silanized glass substrate, hg - hydrophilic glass substrate, si - silicon substrate, ito - patterned ITO glass substrate, p - profilometry thickness measurement, e - ellipsometry thickness measurement

Table 5.2.4 Properties of Sequentially Adsorbed Films of dPPP/PYR and dPPP/(+)PPP

Polyion	[Polyion] (M)	[Polyion] pH	dPPP pH	[NaCl] in dPPP (M)	Peak Abs. /bilayer	Thk /bilayer	% dPPP (estimated)
PYR	0.001	2.5	3.5	-------	0.005 ^{hg}	16Å $^{p/hg}$	60%
PYR	0.001	2.5	3.0	0.1 M	0.007 ^{hg}	23 Å $^{p/hg}$	60%
(+)PPP	0.001	3.5	3.5	-------	0.003 ^{hg} 0.002 ^{ito}	6 Å $^{e/si}$	--------
(+) PPP	0.001	3.5	3.5	0.1 M	0.004 ^{ito}	23Å $^{e/si}$	--------

sg - silanized glass substrate, hg - hydrophilic glass substrate, si - silicon substrate, ito - patterned ITO glass substrate, p - profilometry thickness measurement, e - ellipsometry thickness measurement

It can be observed from the above data that, with the exception of the dPPP/PEI films, under low ionic strength solution conditions, all of the bilayers are relatively thin. It can also be observed that the bilayer thickness is increased with the addition of salt to the dPPP solution. Of the films which gave thin bilayers, the films of dPPP/PAH appeared to be the most dPPP rich, followed by the films of dPPP/pPPV and then the dPPP/PYR. Of course, the dPPP/(+)PPP films, which contain only PPP-type polymers, are the films which have the largest amount of conjugated polymer. In fact, this combination of a polycationic and polyanionic derivatized PPP represents the first time that an all-conjugated film of the same polymer has been made using sequential adsorption.

5.3 Device Properties of dPPP based LEDs

Devices were constructed through sequential adsorption onto cleaned indium tin oxide (ITO) patterned substrates followed by thermal evaporation of aluminum . The resultant device consisted of 16 - 2 mm x 2mm pixels spaced 2 mm apart from each other. Though occasionally several pixels were illuminated when only one was specifically addressed ("cross-talk"), the emitted light was collected only from the pixels being addressed. Therefore, the actual quantum efficiencies may be higher than those recorded. In nearly all cases, little to no light was observed in reverse bias [(-) ITO, (+) Al] and uniformly lit pixels were obtained in forward bias [(+) ITO, (-)Al].

The overall results are summarized in Table 5.3.1. It can be that all of the estimated external quantum efficiencies are below the 1% reported value for PPP-ladder type polymers [205] and the 4% reported value for the ethylene oxide substituted derivatized PPP which operates in LEC type device [206]. It can also be observed that the turn-on voltage of each type of device scales with the device thickness which implies that the dPPP containing films operate by a tunneling mechanism rather than an electrochemical mechanism. Therefore, the lower quantum efficiencies obtained here are likely caused from the unbalanced injection of holes and electrons. Evidence supporting this assertion can be obtained from the dPPP films built on top of a PPV heterostructure consisting of 10 bilayers of SPS/PPV and 20 bilayers of PMA/PPV. Though more efficient device performance has been obtained for this PPV heterostructure alone [107],

for the series of experiments discussed here, the PPV heterostructure gives approximately 300 nW of green light and an efficiency of 0.001%. However, when 10 bilayers of dPPP/PPV are placed on the anode (ITO) side of the films, both the amount of light and the device efficiency decrease to 34 nW and 0.0002%, respectively. This can be understood in terms of taking a PPV heterostructure, which is known to be a good hole transporting platform, and making it into an even more efficient hole transporting film with the addition of a few bilayers of dPPP/PPV. Now, the charge injection of the holes and electrons is even more unbalanced. This causes the current to increase (not shown) and both the amount of light emitted (still green) and the efficiency to decrease as the only remaining recombination occurs in the vicinity of quenching surface states near the aluminum electrode. It appears from the much higher currents observed for devices of dPPP/PPV over those of dPPP/PAH, dPPP/PEI, and dPPP/PYR that the combination of dPPP and PPV makes for a particularly good hole transport layer.

When the PPV heterostructure is put next to the ITO anode and films of dPPP/PAH and dPPP/PYR are near the aluminum cathode, the efficiency of the emission is observed to increase. This efficiency increase suggests that holes are impeded either by the interface between the PPV heterostructure and the dPPP containing layers, or by the slower transport of holes through the PPV heterostructure. The fact that blue light is still observed for these devices indicates that the recombination zone is still within the dPPP containing layers and that the emission is primarily limited by the injection of electrons from the aluminum. It is believed that using a top electrode with a lower work function, or an electron transporting layer between the electrode and the dPPP film would greatly increase the efficiencies of all the dPPP devices. Based on their higher light output (95 nW) and the fact that, despite their thinness, they are electrically more robust than the other devices considered here, the films of dPPP/(+)PPP hold the most promise for such an increase. A plot of the light output and current as a function of applied voltage for such a device can be viewed in Figure 5.3.1. It is believed that their better device characteristics are in some way linked to the presence of only conjugated polymer.

Table 5.3.1 Summary of ITO/(dPPP Film)/Al Devices Assembled

Film	dPPP pH	Polyion pH	[NaCl] in dPPP	Film Thickness	Light Turn-on Voltage	Max. Light (nW)	External Quantum Efficiency
$(dPPP/\ PAH)_{20}$	2.5	3.5	-------	100 Å	5 V	1.3	5×10^{-5} % (blue light)
$(dPPP/\ PAH)_{10}$	2.5	3.5	0.1 M	175 Å	6 V	10	5×10^{-6} % (blue light)
$(dPPP/\ PAH)_{20}$ on IS10M20	2.5	3.5	0.1 M	480 Å	5 V	12	3×10^{-4} % (blue light)
$(dPPP/PEI)_{40}$	3.5	3.5	-------	500 Å	6 V	24	3×10^{-5} % (blue light)
$(dPPP/PEI)_{20}$	3.5	3.5	0.1 M	860 Å	10 V	30	2×10^{-3} % (blue light)
$(dPPP/PEI)_{30}$	7.0	7.0	0.1 M	1000 Å	12 V	15	1×10^{-2} % (blue light)
$(dPPP/PEI)_{31}$	3.5	3.5	0.1 M	1250 Å	14 V	1.3	2×10^{-3} % (blue light)
$(dPPP/PPV)_{30}$	~5	3.5	------	200 Å	4-5 V	30	2×10^{-6} % (green light)
$(dPPP/PPV)_{20}$	~5	3.5	0.1 M	340 Å	5-6 V	4	3×10^{-5} % (green light)
IS10M20 on $(dPPP/PPV)_{20}$	~5	3.5	0.1 M	460 Å	4 V	34	2×10^{-4} % (green light)
$(dPPP/PYR)_{10}$	2.5	3.0	0.1 M	270 Å	4 V	1	3×10^{-6} % (blue light)
$(dPPP/PYR)_{20}$	2.5	3.0	0.1 M	540 Å	8 V	3	2×10^{-5} % (blue light)
$(dPPP/PYR)_{10}$ on IS10M20	2.5	3.0	0.1 M	750 Å	4 V	2.5	2×10^{-5} % (blue light)
$(dPPP/(+)PPP)_{35}$	3.5	3.5	------	210 Å	7 V	95	2×10^{-3} %
IS10M20 (green)			------	480 Å	5-6V	300	1×10^{-3} %

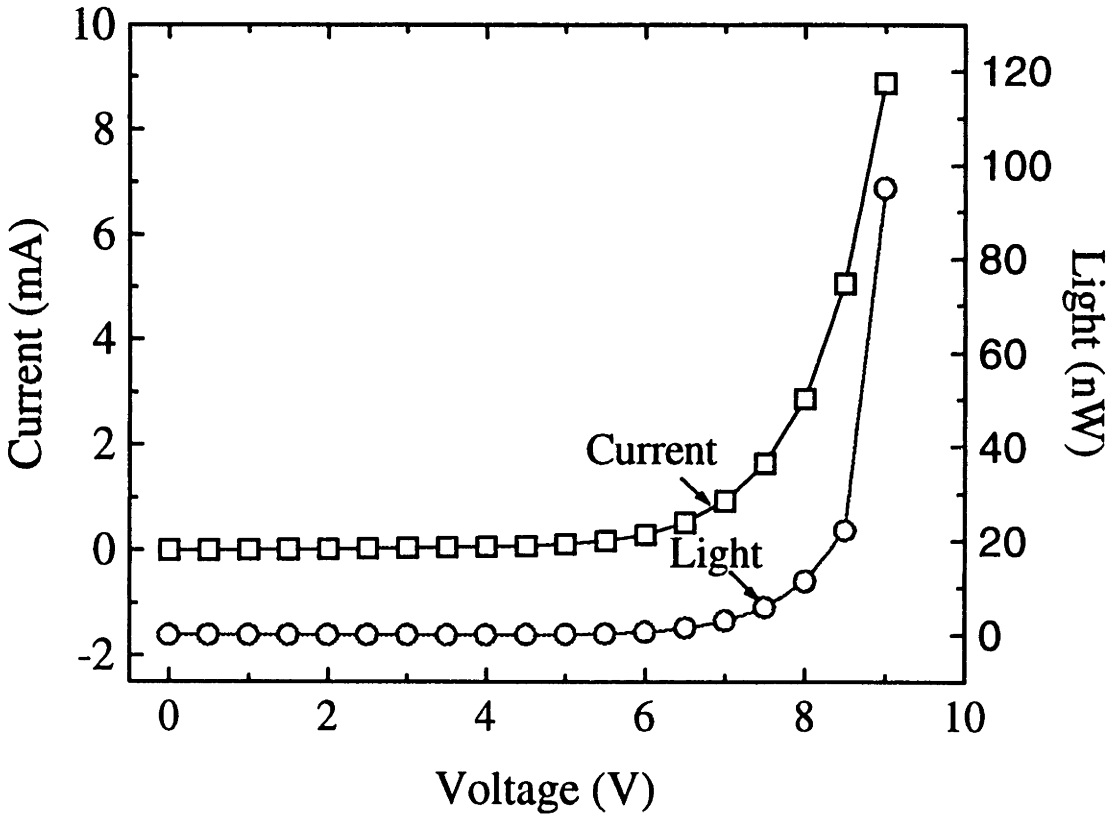

Figure 5.3.1 A plot of current versus voltage and light versus voltage for a 35 bilayer film of dPPP/(+)PPP.

5.4 Concluding Remarks

It has been shown in this chapter that sequentially adsorbed films containing dPPP can be incorporated into blue light emitting devices which give characteristics consistent with a tunneling mechanism. The devices appear to be dominated by the transport of holes and give quantum efficiencies much lower than those reported in the literature. However, it is believed that with the use of either a lower work function metal or an electron transporting layer, the device efficiency could be greatly enhanced. The dPPP films which are believed to hold the most promise for such an enhancement are those assembled from solutions of polycationic and polyanionic derivatized PPP. This combination represents the first time that a film composed of single conjugated polymer has been fabricated using the process of sequential adsorption.

Chapter 6. - Conclusions, Summary, and Future Work

6.1 Summary and Conclusions

This thesis has sought to understand the process of sequential adsorption of polyelectrolytes in terms of the effects that processing parameters have on the resultant film structure, to extend this technique's capability to include novel materials which have not previously been assembled, and to use sequentially adsorbed films in potentially useful applications such as light emitting devices (LEDs). First, an attempt was made to put the process of sequential adsorption in context with what is already known about the adsorption of a single layer onto a substrate through an extensive literature review of polyelectrolyte adsorption. Surface charge dominated and contact-ion pair dominated sequential adsorption were put forth as two possible limiting behaviors.

Fundamental studies relating the processing parameters of sequential adsorption to the resultant film structure were undertaken for the polycationic poly(allylamine hydrochloride) (PAH) sequentially adsorbed with highly charged sulfonated polystyrene (SPS) and weakly charged poly(methacrylic acid) (PMA). Based on results obtained for SPS/PAH films assembled with low polydispersity SPS (M_w/M_n =1.10) of varying molecular weight under varying SPS solution ionic strength conditions, it was concluded that under low ionic strength conditions (≤0.1M NaCl) the bilayer thickness was not dependent of the SPS molecular weight (bi. thk. ~ M^0) . However, under high ionic strength conditions (≥1.0 M NaCl), the bilayer thickness was significantly dependent on the molecular weight (bi. thk. ~ $M^{0.2 \cdot 0.3}$) and could be more than doubled when the molecular weight of the SPS was varied between 35K and 400K. This molecular weight dependence was consistent with the transition of the conformations of the adsorbed molecules from being relatively flat (molecular weight independent) at low ionic conditions to being very loopy (molecular weight dependent) at high ionic strength due to the electrostatic screening of the segment-segment repulsion by the salt ions.

Analysis of the bilayer thickness increase for a given molecular weight as a function of the ionic strength of the SPS solution showed that for SPS molecular weights above 35K and NaCl concentrations of 1.0 M or less, the bilayer thickness scales with the square root of the ionic strength as predicted from single layer adsorption theory. Considering that this same behavior has been observed for several other systems, this relationship may represent a common characteristic of sequentially adsorbed polyelectrolyte films.

Films of PMA and PAH assembled under low ionic strength conditions (no added salt) showed no significant increase in bilayer thickness as the molecular weight of the PMA was varied from 15K to 100K. Changing the solution concentrations of both PAH and PMA from 0.005 M (moles of monomer / liter) to 0.01M gave the same thickness for the PMA layer, but a 4Å increase in thickness for the PAH layer as measured by ellipsometry. This seems to indicate that the PAH was sensitive to the concentration of the polyelectrolyte solution, while the PMA was not.

Measurements of the individual PMA and PAH layer thickness values taken as the pH of the PMA and PAH was varied independently from 2.5 to 4.5 showed three trends; (1) an increase in PAH layer thickness with an increase in the pH of the PAH solution, (2) an increase in PMA layer thickness with a decrease in the pH of the PMA solution, and (3) an increase in the thickness of the PMA layer with increased thickness of the PAH layer. The increase in PAH layer thickness with increased PAH solution pH was attributed to the increased dissociation of the carboxylic acid groups of the adsorbed PMA molecules at higher pH. The increased PMA layer thickness with a decrease in the solution pH of the PMA is attributed to a reduction in the repulsion of negatively charged carboxylate groups due to lower dissociation of the carboxylic acid. The increase in layer thickness of the PMA with an increase in the thickness of the PAH layer is consistent with contact-ion pair dominated sequential adsorption in which an increase in the thickness of the underlying adsorbed layer causes an increase in the amount adsorbed due to an increase in the number of sites available to form contact-ion pairs. Films of other highly charged polycations assembled with weak polyacids have given similar results

with the exception that for films of poly(acrylic acid) (PAA) and PAH, the amount of PAA adsorbed is independent of the thickness of the underlying PAH layer [207]. Overall, changing the solution pH was shown to be a powerful tool to manipulate the thickness of the individual layers of sequentially adsorbed films.

Sessile water drop contact angle measurements and methylene blue adsorption studies on the PMA/PAH films made with varying solution pH conditions indicated that at a low number of bilayers the penetration of an underlying layer into the outermost surface layer is primarily determined by the thickness of the outermost layer with thin layers being more easily penetrated by underlying layers. Despite the film's continued linear growth, contact angle measurements made at higher numbers of bilayers ($\geq$10 bilayers) indicate that the outermost surface layers of all of films become heavily penetrated by the underlying layers to the extent that surfaces which had either PMA or PAH as the last layer adsorbed were nearly indistinguishable from one other. Yet, the oscillation in the surface charge with the adsorption of either PMA or PAH, as measured by methylene blue adsorption, is maintained. It is believed that this observation is linked to the increase in roughness with an increasing number of bilayers which has been substantiated by Small Angle X-ray Reflectivity. Cross-sectional TEM has likewise observed an increase in roughness with an increasing number of bilayers for a heterostructure system consisting of alternating blocks of PMA/PAH and ruthenium containing molecules. Though the contrast of the blocks were the opposite of what was initially expected (PMA/PAH blocks = dark, ruthenium containing layers = light), the images did show layering which was consistent with the expected structure. This marks the first time this technique has been used for sequentially adsorbed films and will be the subject of further research.

In Chapter 3 of this thesis, the technique of sequential adsorption was extended to include the assembly of a polyimide precursor with PAH, p-type doped polyaniline (PAni), and a precursor to poly(p-phenylenevinylene) (pPPV). It was demonstrated by infrared spectroscopy that, once assembled, the polyimide precursor could be converted to the polyimide either chemically or thermally. For films built with pPPV, it was

demonstrated that the polyimide precursor could be selectively converted chemically or that both precursors could be converted simultaneously using thermal means. This particular system demonstrated that it was also possible to obtain films composed of two non-ionic polymers through sequential adsorption and conversion of their precursor polymers.

Förster energy transfer studies between layers of poly(p-phenylenevinylene) (PPV) and a derivatized poly(p-phenylene) (dPPP) were undertaken as a means to estimate the level of penetration into spacer bilayers of PMA/PAH, SPS/PAH, and PAA/PAH. By monitoring the re-emergence of the photoluminescence of the dPPP as it was separated from the PPV by increasing numbers of spacer bilayers and fitting the experimental results to a model which assumed a certain level of layer penetration, estimations for the level of penetration of the dPPP and PPV segments into the spacer bilayers were made. The penetration of the PMA/PAH spacer bilayers was estimated to be 15-53Å (1 to 2.5 bilayers) based on the complete re-emergence of the dPPP photoluminescence with 3 spacer bilayers. The penetration of the thin (~6Å) SPS/PAH spacer bilayers was estimated to be over 53Å due to the fact that less than 25% of the dPPP photoluminescence was regained with 8 spacer bilayers. The penetration of the thick PAA/PAH spacer bilayers was estimated to be less than 80Å based on the complete re-emergence of the dPPP photoluminescence with a single spacer bilayer. Therefore, it appears that the level of penetration of one layer into adjacent layers is system dependent rather than universally limited to a certain number of bilayers.

In Chapter 5, it was shown that sequentially adsorbed films of dPPP with a variety of different polycations could be incorporated into a light emitting device (LED) to give blue light. The device characteristics are consistent with a tunneling charge injection mechanism and appear to be dominated by the transport of holes. It is believed that with further optimization using an electron transporting layer and a lower work function metal electrode, device performance can be significantly enhanced. One of the best candidates for optimization based on light output and electronic robustness are films based on the sequential adsorption of the polyanionic derivatized poly(p-phenylene) (dPPP) and a

polycationic derivatized poly(p-phenylene) [(+)PPP]. This represents the first time that a sequentially adsorbed film consisting of the same derivatized conjugated polymer has been assembled and subsequently incorporated into an organic light emitting device.

6.2 Future Work

6.2.1 Theory of Sequential Adsorption

While it is the hope of the author that the main issues regarding sequential adsorption of polyelectrolytes have been discussed in this thesis, there are still many tasks which need to be accomplished in the field of sequential adsorption. Probably most significantly of these is the need for a rigorous theoretical foundation for the process of sequential adsorption similar to that developed for single layer adsorption. Given the rapid growth of this field, there is now sufficient experimental data to begin to form a predictive theory of sequential adsorption. At the core of this new theory will be the repetition of adsorption to a non-planar surface. Within this thesis two limiting behaviors of sequential adsorption (surface charge dominated and contact-ion dominated) were put forth as a means to interpret experimental data. One of these behaviors was based on an extension of the results of the Self-Consistent Field (SCF) theory of Fleer and co-workers to the case of sequential adsorption. Considering this theory appears to be the best developed of the single layer adsorption theories, a first attempt at obtaining a theory of sequential adsorption might involve using the predicted results (in terms of the fraction and the length of loops, tails, and trains) for the adsorption of a polyelectrolyte to a planar surface as the surface for the first sequential adsorption step.

6.2.2 Fundamental Studies

Even though several fundamental studies of sequential adsorption were discussed in this thesis, there are several additional studies which are logical extensions of the work presented here and would aid in understanding of the process of sequential adsorption. First, a study involving the characterization of the substrate surface and its effect on film build-up should be undertaken. It has been shown in this thesis and in the literature [74-

79] that the use of preparatory bilayers can enhance the build-up of films and give thicker bilayers. It is believed that this occurs through both an increase in the surface charge and the surface roughness (loopiness). This can easily be proven using Atomic Force Microscopy (AFM) and the methylene blue adsorption technique discussed in Chapter 2.

A comprehensive study on the PMA molecular weight dependence of the PMA/PAH bilayer thickness for films assembled under varying pH conditions would show that, as was concluded in the SPS/PAH molecular weight study discussed in Chapter 2, a more loopy conformation leads to a more significant molecular weight dependence of the bilayer thickness. Furthermore, molecular weight exchange experiments in which the degree of adsorption reversibility is gauged by the ability of higher molecular weight chains to displace lower molecular weight chains could be performed for films of both SPS/PAH and PMA/PAH. Other studies which would be of fundamental interest includes determining if the trend that the bilayer thickness scales with the square root of the ionic strength at low ionic strengths ($\leq$1.0 M of monovalent salt) is common for a large number of sequentially adsorbed systems and if it can be attributed to the thickness increase of one or both materials within the bilayer. It would also be interesting to know if there is a corresponding relationship between bilayer thickness and solution ionic strength when the ionic strength of both solutions are increased by the same amount.

For most of the work on precursor polymers, it was assumed that large scale phase separation did not occur with the thermal conversion of the precursor polymer to their non-ionic form. This assumption could be checked by performing transmission and scanning electron microscopy on film sections (planar and cross-sectional) before and after conversion. Since both of the precursor polymers examined in this thesis (precursor polyimides and precursor PPV) have aromatic groups, RuO_4 can be used to selectively stain the precursor polymers both before and after conversion. However, this would limit the examination to sequentially adsorbed films of the precursor polymers with oppositely charge polymers which did not contain aromatic groups. Additionally, techniques such as depth profiling with Secondary Ion Mass Spectroscopy (SIMS) and Small Angle Neutron

Reflectivity (SANR) could be used to confirm results observed by electron microscopy for properly selected systems. Förster energy transfer studies on molecules tagged with well studied donor and acceptor groups (i.e. phenanthrene and anthracene) could also provide structural information for both precursor and non-precursor polymers without making assumptions regarding the extent of energy migration between donors and between acceptors. In fact, using time resolved photoluminescence spectroscopy, it should be possible to calculate the distribution of distances between layers of donor-tagged and acceptor-tagged molecules

6.2.3 Application of Sequentially Adsorbed Films

While the use of sequentially adsorbed films of dPPP in LEDs was shown in Chapter 5 of this thesis to give modest light outputs and external quantum efficiencies without the use of electron transport layer or low work function metal electrode, results for LEDs based on sequentially adsorbed films of other emitters have given light outputs of over 1000 cd/m^2 [208] and efficiencies approaching 2% [209] for two separate emitters. Further optimization of all of these devices using multilayered heterostructures should bring increased device performance. Other potentially useful devices which make use of the multilayered nature of sequentially adsorbed films include organic photovoltaic devices, organic transistors, and graded index optical waveguides. While preliminary work has been accomplished on sequentially adsorbed photovoltaic devices, no one has currently applied this technique to the production of organic transistors or graded index waveguides. The Hammond research group is currently attempting to produce patterned optical waveguides based upon the selective adsorption of polyelectrolytes to charged regions of surfaces patterned by self-assembled monolayers of thiols on gold [92]. By controlling the multilayered build-up such that a material with a high index of refraction is incorporated into layers which make up the center of the waveguide, it is believed that relatively inexpensive graded-index patterned optical waveguides can be made with extremely low optical loss.

Recent works [123,210] have implied that sequentially adsorbed films of polyelectrolytes have swelling properties similar to cross-linked gels. This observation may open up a whole new area of application for this technique and include biological applications such as controlled drug delivery. Other applications of sequentially adsorbed films such as second order nonlinear optics (NLO) rely on the ability to achieve some level of orientation in the typically planar isotropic films. Such ordering has been observed at low number of bilayers [94], but has yet to be substantiated for films with thickness values closed to those required for the construction of optical waveguides.

Several ways to achieve such orientation can be envisioned in addition to the typical procedure of electrical poling of the resultant film. Some of these include electrical poling during assembly, orientation through crystallization of the converted precursor films, and phase separation of a polyelectrolyte block copolymer consisting of unit with high, pH independent charge density and units with pH dependent charge density. It has been shown for single layer adsorption of SPS on a platinum substrate that the conformation of the molecule can be changed with the application of an electric field [16]. For sequential adsorption, the use of an electric field to control the conformations of the adsorbed molecules becomes more complicated due to the alternating charge of the adsorbing molecules and the fact that the substrate electrode becomes coated with material during film build-up. Yet, it may still be possible to actively control the conformations of the adsorbing polymers molecules with the use of an electric field. It has been shown for films of precursor PPV that orientation via crystallization can occur through the anisotropic weight loss which occurs during the conversion of the precursor PPV to PPV [211]. It may be possible to realize such orientation in sequentially adsorbed films of PPV and to subsequently use this orientation to fabricate polarized LEDs.

The assembly of a block copolymer composed of a block of highly charged sulfonic acid functionalized segments and a block of segments functionalized with carboxylic acid groups whose dissociation can be controlled with solution pH may also provide a means to control the conformations of the adsorbing polymer molecules. For example, under low ionic strength conditions the sulfonic acid functionalized block will

adsorb to the surface in a relatively flat conformation independent of solution pH. However, the adsorption conformation of the carboxylic acid functionalized block will be both constrained by the sulfonic acid functionalized block and dependent on the solution pH. A whole range of conformations would therefore be possible through the variation of solution pH and the relative lengths of the different blocks. These conformations could then be varied further with the addition of salt to the polyelectrolyte solution.

6.2.4 Concluding Remarks

Overall, the field of sequential adsorption of polyelectrolytes has been shown to offer a means to fabricate thin films with controllable film thickness. Fundamental studies of the influence of processing parameters such as polyelectrolyte molecular weight, solution pH, solution concentration, and solution ionic strength on the resultant film structure have been undertaken. However, a rigorous theory of sequential adsorption still needs to be developed and to be further supported by the results of additional fundamental studies. Though sequentially adsorbed films have already been used in many diverse applications, understanding of the underlying structural considerations should provide a means to many new future applications.

Chapter 1 References

1 G. Decher, J. D. Hong, and J. Schmitt, *Thin Solid Films*, **210/211**, 831, (1992).
2 M. Mandel, "Polyelectrolytes" in Encyclopedia of Polymer Science and Technology, second ed., **10**, 739, (1985).
3 P.J. Flory, Principles of Polymer Chemistry, Cornell University Press, Ithaca, N.Y., (1953).
4 Th. Odijk, *J. Poly. Sci. Poly. Phys. Ed.*, **15**, 477, (1977).
5 G. J. Gouy, *Physique*, **9** (4), 497, (1910).
6 G. J. Gouy, *Ann. Phys.* **7** (9), 129, (1917).
7 D. L. Chapman, *Phil. Mag.*, **25** (6), 475, (1913)
8 G.S. Manning, *Quart. Rev., Biophys.*, **11**, 179, (1978).
9 Th. Odijk, *Chem. Phys. Lett.*, **100**, 145, (1983).
10 M. Fixman, *J. Chem. Phys.*, **70**, 4995, (1979).
11 D. Stigter, *J. Colloid Interface Sci.*, **53**, 296, (1975)
12 E. Nordmeier, "Polyelectrolytes (Special Properties in Solution)" in The Polymeric Materials Encyclopedia: Synthesis, Properties, and Applications, J. C. Salamone ed., **7**, 5816, CRC Press Inc., Boca Raton (1995)
13 M. Satoh and J. Komiyama, "Polyelectrolytes (Counterion Binding and Hydration)" in The Polymeric Materials Encyclopedia: Synthesis, Properties, and Applications, J. C. Salamone ed., **7**, 5807, CRC Press Inc., Boca Raton (1995)
14 J.-L. Barrat and H. Löwen, "Report on the CECAM Planning Meeting", Lyon, March 27-29, (1995) [as received from the Internet]
15 S. Sugai, "Hydrophobic Polyelectrolytes" in The Polymeric Materials Encyclopedia: Synthesis, Properties, and Applications, 4, 3123, J. C. Salamone ed., CRC Press Inc., Boca Raton (1995)
16 M Kawaguchi, K. Hayashi, and A, Tahakashi, *Macromolecules*, **17**, 2066, (1984).
17 G. J. Fleer, M. A. Cohen Stuart, J. M. H. M. Scheutjens, T. Cosgrove, B. Vincent, Polymers at Interfaces, Chapmann & Hall, London, (1993)
18 E. A. Bekturov, L. A. Bimendina, and S. E. Kudaibergenov, "Polyelectrolytes (Chain Models of Polyions" in The Polymeric Materials Encyclopedia: Synthesis, Properties, and Applications, **7**, 5800, J. C. Salamone ed., CRC Press Inc., Boca Raton (1995)
19 J. C. Leyte and M. Mandel, *J. Poly. Sci. Pt. A*, **2**, 1879, (1964).
20 A. Silberberg, "Adsorption" in Encyclopedia of Polmer Science and Technology, 2nd ed., **1**, 5511, (1985).
21 H. M. Schneider, P. Frantz, and S. Granick, *Langmuir*, **12**, 994, (1996).
22 N. G. Hoogeveen, M. A. Cohen Stuart, and G. J. Fleer, *J. Colloid Interface Sci.* **182**, 133, (1996).
23 M. A. Cohen Stuart and G. J. Fleer, *Annu. Rev. Mater. Sci.*, **26**, 263, (1996).
24 M. Cohen-Stuart in "Short and Long Chains at Interfaces", Proceeding of the XXXth Rencontres de Moriond, J. Daillant, P. Guenoun, C. Marques, P. Muller, and J. T. T. Van, Ed., Editions Frontiéres:Gif- sur-Yvette, France, 1-12, (1996).
25 J. Meadows, P. A. Williams, M. J. Garvey, and R. A. Harrop, *J. Colloid Interface Sci.*, **139**, 260, (1990).

26 J. M.H. M. Scheutjens and G. J. Fleer, The Effect of Polymers on Dispersion Properties, ed. T. F. Tadros, 145, Academic Publishing, London, (1982).
27 N. G. Hoogeveen, M. A. Cohen Stuart, and G. J. Fleer, *J. Colloid Interface Sci.* **182**, 146, (1996).
28 M. A. Cohen-Stuart, T. Cosgrove, B. Vincent, *Adv. Colloid and Interface Sci.*, **24**, 143, (1986).
29 S. Beltrán, H. H. Hooper, H. W. Blanch, and J. M. Prausnitz, *Macromolecules*, **24**, 3178, (1991).
30 S. L. S. Stipp, *Langmuir*, **12**, 1884, (1996).
31 V. V. Tsukruk, V. N. Bliznyuk, D. Visser, A. L. Campbell, T. J. Bunning, W. W. Adams, *Macromolecules*, (1997).
32 M. Schneider, P. Frantz, and S. Granick, *Langmuir*, **12**, 994, (1996).
33 J. Meadows, P. A. Williams, M. J. Garvey, R. A. Harrop, and G. O. Phillips, *Colloids Surf.*, **32**, 275, (1988).
34 F. Th. Hesselink, "Adsorption of Polyelectrolytes from Dilute Solution" in Adsorption from Solution at the Solid/Liquid Interface, G. D. Parfitt and C.H. Rochester, Academic Press, Inc., (1983).
35 M. C. Cafe and I. D. Robb, *J. Colloid Interface Sci.*, **86**, p. 411, (1982).
36 J. Meadows, P. A. Williams, M. J. Garvey, R. A. Harrop, and G. O. Phillips, *Colloids Surf.* **32**, 275 (1988).
37 J. Meadows, P. A. Williams, M. J. Garvey, R. A. Harrop, and G. O. Phillips, *J. Colloid Interface Sci.*, **148**, 160, (1992).
38 P. Berndt, K. Kurihara, and T. Kunitake, *Langmuir*, **8** (10), 2486, (1992).
39 R. Ramaachandran and P. Somasundaran, *J. Colloid Interface Sci.*, **120**, 184, (1987).
40 J. B. Schlenoff and M. Li, *Ber. Bunsenges. Phys. Chem.*, **100**, 943, (1996).
41 H. Tanaka, L Ödberg, T. Lindström, and R Aksberg, *J. Colloid Interface Sci.*, **134**, 229, (1990).
42 A. W. M. De Laat, G. L. T. Van der Heuvel, *Colloids Surfaces A: Physicochem. Eng. Aspects*, **98**, 53, (1995).
43 T. Cosgrove, T. M. Obey, and B. Vincent, *J. Colloid Interface Sci.*, **111**, 409, (1986).
44 P. Chong and G. Curthoys, *J. Appl. Poly. Sci.*, **23**, 1565, (1979).
45 B. W. Greene, J. *Colloid Interface Sci.*, **37** (1), (1971).
46 A. Foissy , A. El Attar, and J. m. Lamarche, *J. Colloid Interface Sci.*, **96** (1), (1983).
47 J. Papenhuijzen, G. J. Fleer, and B. H. Bijsterbosch, *J. Colloid Interface Sci.*, **104** (2), 553, (1985).
48 F. Th., Hesselink, *J. Colloid Interface Sci.* **60**, 488, (1977).
49 M. J. Muthukumar, *J. Chem. Phys.* **86**, 7230, (1987).
50 T. Åkesson, C. Woodward, and B. Jönsson, *J. Chem. Phys.*, **91**, 2461, (1989)
51 M. K. Granfeldt, B. Jönsson, C. E. Woodward, *J. Phys. Chem.* , **95**, 4819, (1991).
52 M. A. G. Dahlgren, Å. Waltermo, E. Blomberg, P. M. Claessen, L. Sjöström, T. Akesson, B. Jönsson, *J. Chem. Phys.*, **97**, 11769, (1993).
53 M. R. Böhmer, O. A. Evers, and J. M. H. M. Scheutjens, *Macromolecules*, **23**, 2288, (1990).

54 O. V. Borisov, E. B. Zhulina, and T. M. Birshtein, *J. Phys. II (Fr.)*, **4**, 913, (1994).
55 H. G. M. van der Steeg, M. A. Cohen Stuart, A. de Keizer, and B. Bijsterbosch, *Langmuir*, **8**, 2538, (1992).
56 J. M. H. M. Scheutjens and G. J. Fleer, *J. Phys. Chem.*, **83** (12), 1619, (1979).
57 H. A. Van der Schee and J. Lyklema, *J. Phys. Chem.*, **88** (26), 6661, (1984).
58 H. G. M. van de Steeg, M. A. Cohen Stuart, A. de Keizer, and B. H. Bijsterbosch, *Langmuir*, **8** (10), 2538, (1992).
59 M. Muthukumar, *J. Chem. Phys.*, **86**, 7230, (1987).
60 A. Takahashi, *Poly. J.* , **23** (5), 715, (1991).
61 J. Blaakmeer, M. R. Bohmer, M. A. Cohen Stuart, and G. J. Fleer, *Macromolecules*, **23**, p. 2305, (1990).
62 H. C. Yang, D. L. Dermody, C. Xu, A. J. Ricco, and R. M. Crooks, *Langmuir*, **12**, 726, (1996).
63 T. A. Vilgris and G. Heinrich, *Macromolecules*, **27** (26), 7846 (1994).
64 H. Tanaka, L Ödberg, L. Wågberg, and T. Lindström, *J. Colloid Interface Sci.*, **134** (1), 219, (1990).
65 P. Linse, *Macromolecules*, **29** (1), 326, (1996).
66 R. K. Iler, *J. Colloid Interface Sci.*, **21**, 569, (1966).
67 W. B. Stockton, and M. F. Rubner, *Polymer Preprints*, **35** (1), 319, (1994).
68 G. Decher, B. Lehr, K. Lowack, Y. Lvov, and J. Schmitt, *Biosensors and Bioelectronics*, **9**, 677, (1994).
69 J.-D. Hong, K. Lowack, J. Schmitt, and G. Decher, *Progr. Colloid Polym. Sci.*, **93**, 98, (1993).
70 P. Berndt, K. Kurihara, and T. Kunitake, *Langmuir*, **9**, 481, (1993).
71 K. Lowack and C. A. Helm, *Macromolecules*, to be published.
72 Y. Lvov, G. Decher, and H. Möhwald, *Langmuir*, **9**, 481, (1993).
73 G. Decher and J. Schmitt, *Prog. Colloid Polym. Sci.*, **89**, 160, (1992).
74 J. Schmitt, T. Grünewald, G. Decher, P. S. Pershan, K. Kjaer, and M. Losche, *Macromolecules*, **26**, (1993).
75 G. Decher and J. D. Hong, *Ber. Bunsenges. Phys. Chem.*, **95** (11), (1991).
76 G. Decher and J. Hong, *Makromol. Chem. Macromol. Symp.*, **46**, 321, (1991).
77 Y. Lvov, K. Ariga, and T. Kunitake, *J. Am. Chem. Soc.*, **117** (22), 6117, (1995).
78 Y. Lvov, G. Decher, and G. Sukhorukov, *Macromolecules*, **26**, 5396, (1993).
79 T. M. Cooper, A. L. Campbell, and R. L. Crane, *Langmuir*, **11** (7), 2713, (1995).
80 Y. Lvov, F. Essler, and G. Decher, *J. Phys. Chem.*, **97**, 13773, (1993).
81 S. Wantanabe and S. L. Regen, *J. Am. Chem. Soc.*, **116**, 8855, (1994).
82 N. A. Kotov, I. Dekany, and J. H. Fendler, *J. Phys. Chem.*, **99**, 13065, (1995).
83 M. Gao, M. Gao, X. Zhang, Y. Yang, B. Yang, and J. Shen, *J Chem. Soc., Chem. Commun.*, 2777, (1994).
84 E. R. Kleinfeld and G. S. Ferguson, *Science*, **265**, 370, (1994).
85 S. W. Keller, H. - N. Kim, and T. E. Mallouk, **116** (19), 8817, (1994).
86 R. G. Freeman, K. C. Graber, K. J. Allison, R. M. Bright, J. A. Davis, A. P. Gunthrie, M. B. Hommer, M. A. Jackson, P. C. Smith, D. G. walter, and N. J. Natan, *Science*, **267**, 1629, (1995).

87 F. Saremi, E. Maassen, B. Tieke, G. Jordan, and W. Rammensee, *Langmuir*, **11**, 1068, (1995).
88 E. R. Kleinfeld and G. S. Feruson, *Chem. Mater.*, **7**, 2327, (1995).
89 W. Kong, L. P. Wang, M. L. Gao, H. Zhou, X. Zhang, W. Li, and J. C. Shen, *J. Chem. Soc., Chem. Commun.*, 1297, (1994).
90 Y. Lvov, K. Ariga, and T. Kunitake, *Chem. Lett.*, 2323, (1994).
91 S. L. Clark, M. Montague, and P. T. Hammond, *Supramol. Sci.*, **4**, 141, (1997).
92 E. R. Kleinfeld and G. S. Feruson, *Chem. Mater.* **7**, 2327, (1995).
93 J.-M. Leväsalmi, and T. J. McCarthy, Polym. Preprints - Polym. Chem., **37** (1), 457, (1996).
94 S. Tripathy, private communication.
95 J. H. Cheung, A. C. Fou, M. Ferreira, and M. F. Rubner, *Polymer Preprints*, **34** (2), 757, (1993).
96 J. H. Cheung, A. C. Fou, and M. F. Rubner, *Thin Solid Films*, **244**, 985, (1994).
97 Private Communication - M. F. Rubner
98 M. Ferriera, J. H. Cheung, and M. F. Rubner, *Thin Solid Films*, **244**, 806, (1994).
99 M. Ferreira, J. H. Cheung, W. Scruggs, and M. F. Rubner, *SPE - Antec '93 conference Proceedings*, **39**(3), New Orleans, (1993).
100 M. Ferreira and M. F. Rubner, *Macromolecules*, **28** (21), 7107, (1995).
101 J. W. Baur and M. F. Rubner, to be Published.
102 D. Yoo, J. Lee, and M. F. Rubner, *Mat. Res. Soc. Symp. Proc.*, **413**, 395, (1996).
103 A. C. Fou, D. Ellis, M. F. Rubner, *MRS Proceedings - Optical and Magnetic Properties of Organic Solid State Materials*, eds. A.F. Garito, A. Jen. C. Lee, and L. Dalton, **328**, p. 113, (1994).
104 A. C. Fou, D. Ellis, , M. Ferreira, and M. F. Rubner, *Polymer Preprints*, **35** (1), 221, (1994).
105 A. C. Fou and M. F. Rubner, *Macromolecules*, **28** (21), 7115, (1995).
106 A. C. Fou, O. Onitsuka, and M. F. Rubner, SPE Proceedings of ANTEC - '95 Boston Mtg., **II** (Materials), p. 1594, (1995).
107 A. C. Fou, O. Onitsuka, M. Ferriera, D. Howie, and M. F. Rubner, *Proceedings of Spring ACS Mtg. - Anaeim*, to be published, (1995).
108 A .C. Fou, O. Onitsuka, M. Ferreira, B. Hsieh, and M. F. Rubner, *J. Appl. Phys.*, **79** (10),7501, (1996).
109 M. Ferriera, M. F. Rubner, and B. R. Hsieh, *MRS Proceedings - Optical and Magnetic Properties of Organic Solid State Materials*, eds. A.F. Garito, A. Jen. C. Lee, and L. Dalton, **328**, 119, (1994).
110 D. Yoo and M. F. Rubner, SPE Proceedings of ANTEC - '95 Boston Mtg., II (Materials), 2568, (1995).

Chapter 2 References

111 Y. M Lvov and G. Decher, *Crystallography Reports*, **39**(4), 628, 1994.
112 W. B. Stockton, Ph.D. Thesis, M. I. T. (1995).
113 A. Takahashi, Polym. J., **23**, 100, (1991).
114 J. Marra, H. A. van der Schee, G. J. Fleer, and J. Lyklema, in Adsorption from Solution, eds. R. H. Ottewill, C. H. rochester, and A. L. Smith, Academic Press, 245, (1983).
115 J. Papenhuijzen, G. J. Fleer, and B. H. Bijsterboch, J. Colloid Interface Sci., **104**, 530, (1985).
116 W.Chen and T. J. McCarthy, *Macromolecules*, **30**, 78, 1997.
117 N. G. Hoogeveen, M. A. Cohen Stuart, G. J. Fleer, *Langmuir*, **12**, 3675, 1996.
118 C. Loucheux and J. Francois, "Polyelectrolytes, Cationic" in The Polymer Materials Encyclopedia: Synthesis, Properties, and Applications, J. C. Salamone ed., CRC Press, Inc. Boca Raton, (1995).
119 K. Sumaru, H. Matsuoka, and H. Yamaoka, *J. Phys. Chem.*, **100**, 790, (1996).
120 T. S. Chen and J. K. Thomas, *J. Polym. Sci.*,**17**, 1103, (1979).
121 M. Mandel, J. C. Leyte, and M. G. Stadhouder, *J. Phys. Chem.*, **71** (3), 603, (1967).
122 J. Horsky and H. Morawetz, *Makromol. Chem.*, **189**, 2475, (1988).
123 G. B. Sukhorukov, G. Decher, and J. Schmitt, to be published.
124 D. Yoo, Ph.D. Thesis, (1997).
125 T. Young, *Phil. Trans.*, **95**, 65, (1805).
126 R. J. Good in Contact Angle, Wettability, and Adhesion, p. 3, ed. K. L. Mittal, VSP, The Netherlands, (1993).
127 R. D. Hazlett in Contact Angle, Wettability, and Adhesion, p. 173, ed. K. L. Mittal, VSP, The Netherlands, (1993).
128 The Williams and Wilkins Co., **Biological Stains,** 9th ed., Baltimore, MD, 424, (1977).
129 U. S. Patent, 3M Company, 'Methylene Blue as a Quality Control Test', (1970).
130 SAXR work performed in collaboration with Greg Kellog and Michael Fasolka and cross-sectional TEM performed in collaboration Len Radzilowski and Aiping Wu (M. I. T. - Materials Engineering and Science Department)

Chapter 3 References

131 B. R. Hsieh, *Polym. Bull.*, **33**, 414, (1991).

132 J.-C. Chiang and A. G. MacDiarmid, *Synth. Met.* , **13**, 195, (1986).

133 J. H. Cheung, Ph.D. Thesis , Massachusetts Institute of Technology, (1993).

134 E. J. Oh, Y. Min, J. M. Wiesinger, S. K. Manohar, E. M. Scherr, P. J. Prest, A. G. MacDiarmid, and A. J. Epstein, *Synth. Met.*, **55-57**, 977, (1993).

135 C. H. Hsu, P.M. Peacock, R. B. Flippen, S. K. Manohar, and A. G. MacDiarmid, *Synth. Met.*, **60**, 232, (1993).

136 A. G. MacDiarmid, J.-C. Chiang, M. Halpern, W. S. Huang, S. L. Mu, N. L. D. Somasiri, W. Wu, and S. I. Yaniger, *Mol. Cryst. Liq. Crst.*, **121**, 173, (1985).

137 L. J. van der Pauw, *Philips Res. Repts.*, **13**, 1 (1958).

138 G. J. Fleer, M. A. Cohen Stuart, J. M. H. M. Scheutjens, T. Cosgrove, and B. Vincent, **Polymers at Interfaces**, Chapman and Hill, London, 350, (1993).

139 J. A. Kruez, A. L. Endrey, F. P. Gay and C. E. Stroog, *J. Polym. Sci.* **A-1,4**, p. 2607, (1966).

140 L. A. Laius, M. I. Bessonov, Ye. V. Kallistova, N. A. Adrove, and F. S. Florinskii, *Polym. Sci. USSR*, **A9**, 2470, (1967).

141 M. M. Koton, T. K. Meleshko, V.V. Kudryavtsev, P.P. Nechayev, Ye. V. Kamzolkina, and N. N. Bogorad. *Polym. Sci. USSR* **A24**, 791, (1982).

142 D. Wilson, H. D. Stenzenberger, and P.M. Hergenrother, Polyimides, Chapman and Hall, New York, (1990).

143 W. B. Stockton and M. F. Rubner, *Mat. Res. Soc. Symp. Proc.*, **328**, 257, (1994).

144 W. B. Stockton and M. F. Rubner, accepted *Macromolecules.*

Chapter 4 References

145 D. Laurent and J. B. Schlenoff, submitted to *Langmuir*.

146 J. H. Burroughes, D. D. C. Bradley, A. R. Brown, R. N. Marks, K. Mackey, R. H. Friend, P. L. Burn, and A. B. Holmes, *Nature*, **347**, 539,(1990).

147 M. Ferreira, O. Onitsuka, A. C. Fou, B. Hsieh, and M. F. Rubner, *Mat. Res. Soc. Symp. Proc.*, **413**, 49, (1996).

148 J. W. Baur, S. Kim, A. D. Child, K. R. Williams, J. R. Reynolds, and M. F. Rubner, to be published

149 See for example: Th. Förster in *Modern Quantum Chemistry: Istanbul Lectures Pt. 3*, O. Sinanöglu, Ed., Academic Press, New York, 1965.

150 M. A. Winnik, Chapter 2: Study of Complex Polymer Materials in *Photophysics of Polymers*, Eds. C. E. Hoyle and J. M. Torkelson, ACS Symposium Series **358**, Washington, DC (1987).

151 L. Stryer and R. P. Haugland, Proc. Natl. Acad. Sci. US, **58**, 719, (1967).

152 J. P. S. Farinha, J. M. G. Martinho, A. Yekta, and M. A. Winnik, *Macromolecules*, **28**, 6084, (1995).

153 H. Bücher, K. H. Drexhage, M. Fleck, H. Kuhn, D. Möbius, F.-P. Schäfer, J. Sondermann, W. Sperling, P. Tillmann, and J. Wiegand, *Mol. Cryst.*, **2**, 199, (1967).

154 H. Kuhn and M. Möbius, *Angew. Chem. Internat. Edit.*, **10** (9), 620, (1971).

155 D. R. Haynes, A. Tokmakoff, and S. M. George, *J. Chem. Phys.*, **100** (3), 1968, (1994).

156 H. Nakahara, K. Fukuda, D. Möbius, and H. Kuhn, *J. Phys. Chem.*, **90**, 6144, (1986).

157 H. Kuhn, *J. Chem. Phys.*, 53 (1), 101, (1970).

158 T. Ueno, S. Ito, S. Ohmori, Y. Onogi, and Masahide Yamamoto, *Macromolecules* , **25**, 7150, (1992).

159 A. Murphy, F. Grieser, D. N. Furlong, *Thin Solid Films*, **227**, 211, (1993).

160 A. Murphy, F. Grieser, D. Y. C. Chan, D. N. Furlong, and B. Matthews, *Colloids Surfaces A: Physicochem. Eng. Aspects*, **102**, 1, (1995).

161 H. Möhwald and R. v. Klitzing, TRIP, (1996).

162 G. Liu, *Macromolecules*, **26**, 1144, (1993).

163 T. Hayashi, T. Okuyama, S. Ito, and M. Yamamoto, *Macromolecules*, **27**, 2270, (1994).

164 J. W. Baur, P. Besson, S. A. O'Connor, and M. F. Rubner, *Mat. Res. Soc. Symp. Proc.- Electrical, Optical, and Magnetic Properties of Organic Solid State Materials III*, **413**, 583, (1996).

165 D. Yoo, J. Lee, and M. F. Rubner, *Mat. Res. Soc. Symp. Proc.- Electrical, Optical, and Magnetic Properties of Organic Solid State Materials III*, **413**, 395, (1996).

166 M. Ferreira, O. Onitsuka, A. C. Fou, B. Hsieh, and M. F. Rubner, *Mat. Res. Soc. Symp. Proc.*, **413**, 49, (1996).

167 J. W. Baur, S. Kim, A. D. Child, K. R. Williams, J. R. Reynolds, and M. F. Rubner, to be published

168 J. W. Baur, M. Hamilton, and M. F. Rubner, to be published

169 B. R. Hsieh, H. Antoniadis, M. A. Abkowitz, and M. Stolka, *Polymer Preprints*, **33** (2), 985, (1992).

170 A. D. Child and J. R. Reynolds, *Macromolecules*, **27** (7), 1975, (1994).
171G. Gauglitz, A. Lorch, and D. Oelkrug, *Z. Naturforsch*, **37a**, 219, (1982).
172 G. Decher, B. Lehr, M. Seufert, and G. Wenz, *Supramolecular Science* (1995).
173 M. F. Durstock and M. F. Rubner, to be published.
174 U. Lemmer, A. Ochse, M. Deussen, R. F. Mahrt, E. O. Göbel, H. Bassler, P. Haring Bolivar, G. Wegmann, H. Kurz, *Synth. Met.*, **78**, 289, (1996).
175 G. E. Johnson, *Macromolecules*, **13**, 145, (1980).

Chapter 5 References

176 C. H. Gooch, Injection Electroluminescent Devices, Wiley, N.Y., (1973).

177 J. H. Burroughs, D. D. C. Bradley, A. R. Brown, R. N. Marks, K. Mackay, R.H. Friend, and A.B. Holmes, *Nature*, **347**, 539, (199).

178 N. C. Greenham, S. C. Moratti, D. D. C. Bradley, R. H. Friend, and A. B. Holmes, *Nature*, **365**, 628, (1993).

179 A.R. Brown, D.D.C. Bradley, P. L. Burn, J. H. Burroughs, R. H. Friend, N. C. Greenham, A. B. Holmes, and A. Kraft, *Appl. Phys. Lett.*, submitted for publication.

180 S. Saito, T. Tsutsui, M. Era, N. Takado, C. Adachi, and T. Wakimoto, SPIE Proc.,1910, 212, (1993).

181 R.H Friend, N, Tessler, N. T. Harrison, G. J. Denton, *Mat. Res. Soc. Symp. Proc.* - Electrical, Optical, and Magnetic Properties of Organic Solid State Materials IV, to be published (1996)

182 Y. Shirota, , Y. Kuwabara, H. Inada, T. Wakimoto, H. Nakada, Y. Yonemoto, S. Kawami, and K. Imai, *Appl. Phys. Lett.*, **65**, p.807, (1994).

183 G. Grem, G. Leising, *Synth. Met.*, **55-57**, p. 4105, (1993).

184 G. Grem, G. Leditzky, B. Ullrich, and G. Leising, *Adv. Mater.*, **4**, p. 36, (1992).

185 J. Kido, M. Kohda, K. Okuyama, and K. Nagai, *Appl. Phys. Lett.*, **61**, p.761, (1992).

186 M. Berggren, O. Inganäs, G. Gustafsson, M. R. Andersson, T. Hjertberg, and O. Wennerström, *Synth. Met.*, **71**, p. 2185, (1995).

187 D. Braun, A. Brown, E. Staring, and E. W. Meijer, *Synth. Met.*, **65**, p. 85, (1994).

188 L. J. Rothberg, R. H. Jordan, A. Dodabalapur, and R. E. Slusher, *Polymer Preprint*, **38** (1), 327, (1997).

189 B. J. Schwartz, M. A. Diaz-Garcia, F. Hide, M. R. Anderson, Q. Pei, A. J. Heeger, *Polymer Preprint*, **38** (1), 325, (1997).

190 I. D. Parker, *J. Appl. Phys.*, **75** (3), p. 1656, (1994).

191 S. A. Brazovskii and N. N. Korova, *JETP Lett.*, **33** (4), (1981).

192 K. Fesser, , A. R. Bishop, and D. K. Campbell, *Phys. Rev. B*, **27**, p.4808, (1983).

193 T. W. Hagler, K. Pakbaz, K. Voss, and A. J. Heeger, *Phys. Rev. B*, **44**, p.8652, (1991).

194 D. D. C. Bradley and R. H. Friend, *J. Phys. Condensed Matter*, **1**, p.3671, (1989).

195 B. R. Hsieh, E. Ettedgui, K. T. Park, and Y. Gao, *Mol. Cryst. Liq. Cryst.*, **256**, p. 71, (1994).

196 E. Ettedgui, H. Razafitrimo, Y. Gao, and B. R. Hsieh, submitted to *Appl. Phys. Let.* (1996).

197 C. Adachi, T. Tsutsui, and S. Saito, *Appl. Phys. Lett.*, **57** (6), (1990).

198 Q. Pei, G. Yu, C. Zhang, Y Yang, A. J. Heeger, *Science*, **269**, 1086, (1995).

199 D. Braun, A. Brown, E. Starting, E. W. Meijer, *Synth. Met.*, **65**, 85, (1994)

200 J. Stampfl, S. Tasch, G. Leising, and U. Scherf, *Syn. Met.*, **71**, p. 2125, (1995).

201 G. Grem, V. Martin, F. Meghdadi, C. Paar, J. Stampfl, J. Strun, S. Tasch, and G. Leising, *Syn. Met.* **71**, 2193, (1995).

202 J. Huber, K. Müllen, J. Salbeck, H. Schenk, U. Scherf, T. Stehlin, R.Stern, *Acta Polymer*, **45**, 244 (1994).

203 J. F. Grüner, P. Hamer, R. H. Friend, J. Huber, U. Scherf, A. B. Holmes, *Adv. Mater.*, **6**, 748, (1994).

204 S. Kirstein, G. Cohen, D. Davidov, U. Scherf, M. Klapper, K. Chmil, and K. Müllen, *Synth. Met.*, **69**, 415, (1995).

205 Y. Geerts, U. Keller, U. Scherf, M. Schneider, and K. Müllen, *Polymer Preprint*, **38** (1), 315, (1997).

206 Y. Yang and Q. Pei, *Polymer Preprint*, **38** (1), 335, (1997).

Chapter 6 References

207 M. Durstock, D. Yoo, A. Wu, and M.F. Rubner, to be published.

208 M. Durstock and M. F. Rubner, to be published.

209 A. Wu and M. F. Rubner, to be published.

210 G. B. Sukhorukov, J. Schmitt, and G. Decher, *Ber. Bunsenges. Phys. Chem.*, **100**, 948, (1996).

211 Granier and E. L. Thomas, and F. Karasz, *J. Poly. Sci. B., Polym. Phys. Ed.*, **27**, 469 (1989).

APPENDIX A:
Solution Dissociation Properties of PMA and PAA

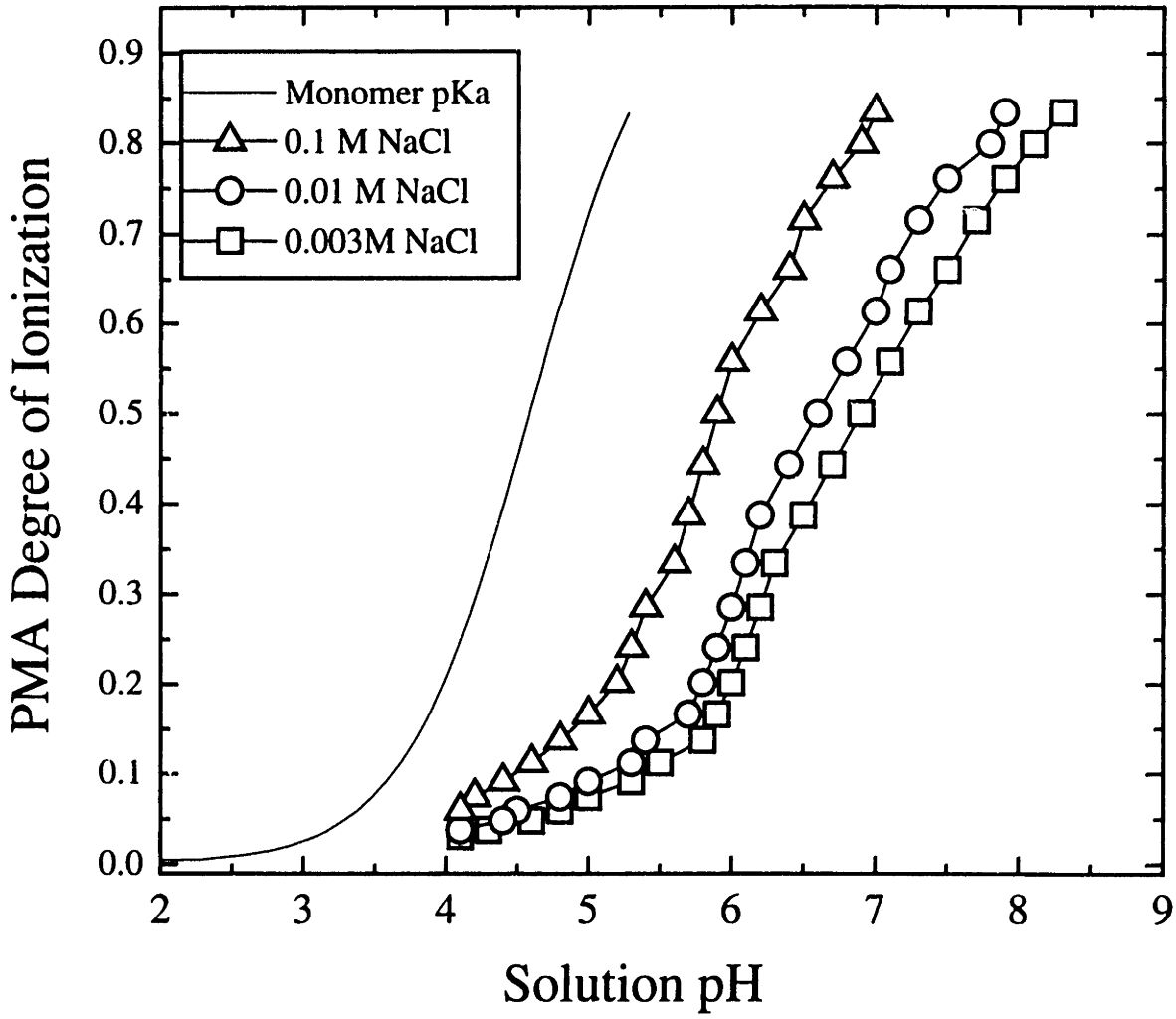

Figure 1 (Appendix A) Degree of Ionization of 0.005 M PMA in Solution as a function of solution pH with various amounts of NaCl as taken from Ref. [19]. Monomer dissociation based on pKa of 4.58.

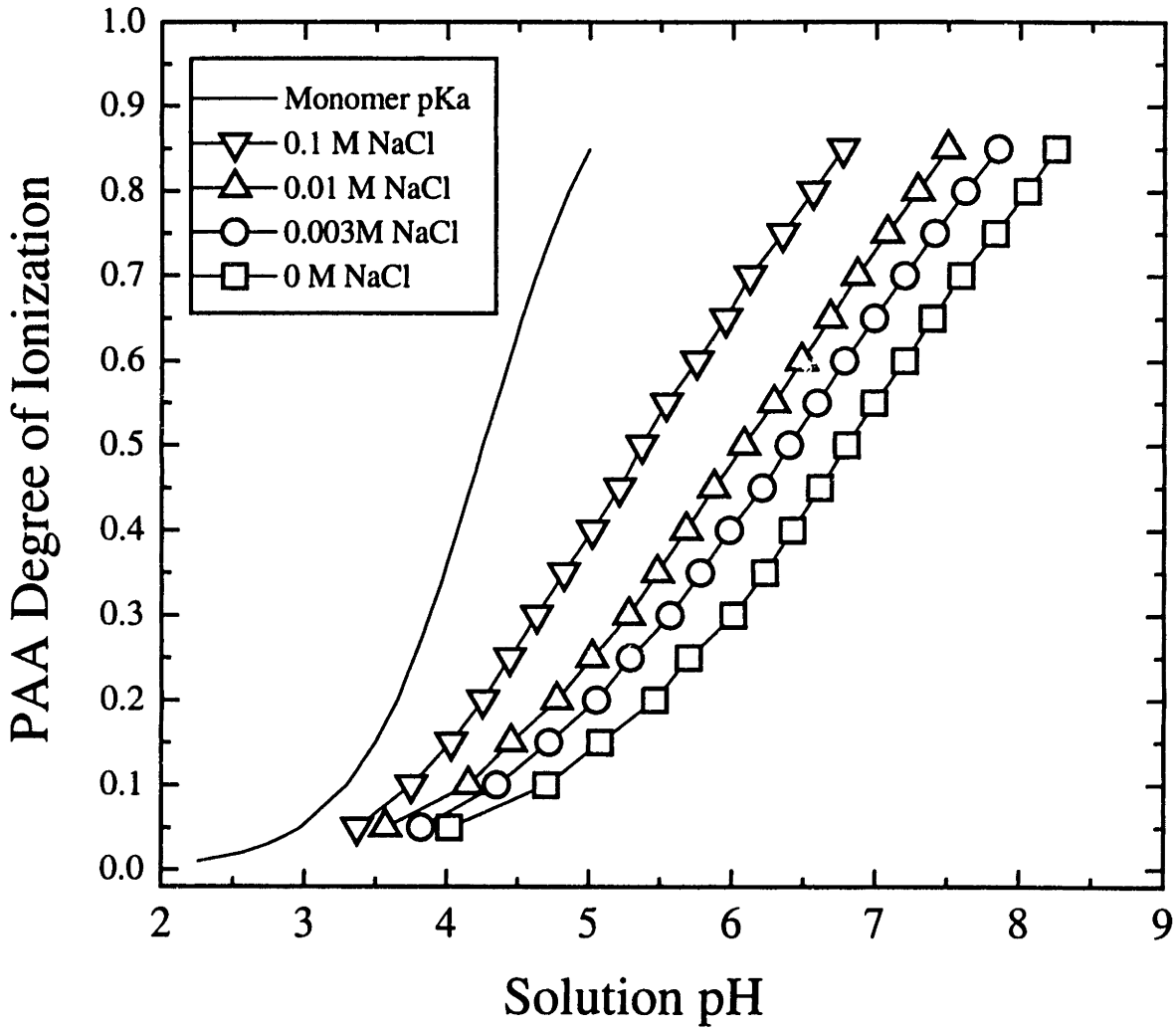

Figure 2 (Appendix A) Degree of Ionization of PAA in Solution as a function of solution pH with various amounts of NaCl as taken from Reference [2]. Monomer dissociation based on pKa of 4.25.